IMMUNOMODULATORY BIOMATERIALS TO PROMOTE EARLY TRANSPLANT INTEGRATION AND WOUND HEALING

A Dissertation
Presented to
The Academic Faculty

by

Mary Caitlin Powell Sok

In Partial Fulfillment
of the Requirements for the Degree
Doctor of Philosophy in the
Wallace H. Coulter Department of Biomedical Engineering

Georgia Institute of Technology and Emory University
December 2018

IMMUNOMODULATORY BIOMATERIALS TO PROMOTE EARLY TRANSPLANT INTEGRATION AND WOUND HEALING

Approved by:

Edward Botchwey, PhD, Advisor
Wallace H. Coulter Department of Biomedical Engineering
Georgia Institute of Technology

Krishnendu Roy, PhD
Wallace H. Coulter Department of Biomedical Engineering
Georgia Institute of Technology

Julia Babensee, PhD
Wallace H. Coulter Department of Biomedical Engineering
Georgia Institute of Technology

Andrew Neish, MD
Department of Laboratory Medicine and Pathology
Emory University

Andrew Adams, MD, PhD
Department of Surgery
Emory University

Date Approved: August 7, 2018

ACKNOWLEDGEMENTS

When I sat down to write my thesis, I knew I was going to cry when writing these acknowledgements. Here I am, months later, sitting down to write this section and I am already in tears after two sentences. There are so many people who have helped me and encouraged me to get to this point. When I started the MD/PhD program at Emory, the thought of defending my PhD thesis seemed too far away to even be fathomable. I first want to thank my advisor, Edward Botchwey, for all of his support and guidance over the past five years. Ed has been a constant source for inspiration and a fantastic sounding board, challenging me to expand my thought process and ideas. He has always been a "big picture" person, and every meeting that I had with him I left feeling inspired and ready to contribute to the scientific world, albeit at times overwhelmed. I feel that my ability to come up with new ideas and to talk competently about science has increased exponentially, sometimes to the point where I surprise myself. Ed has made me a better scientist and thinker, and in the future, his influence will make me a better physician to my patients.

I am extremely grateful for the expertise and insight my thesis committee has given me, which includes Drs. Andrew Adams, Julia Babensee, Andrew Neish, and Krishnendu Roy. Their constructive feedback and suggestions have helped to focus my thesis work and make it better. I am very lucky to have ended up in a program like Georgia Tech, where collaboration opportunities are unbelievably easy. In particular I would like to thank Dr. Andres Garcia and Dr. Gabe Kwong for their participation in helping me achieve the work presented in this thesis. Without their willingness to collaborate, this thesis would be a fragment of what it is. I would especially like to thank Jose Garcia for teaching me how to

make hydrogels and providing me with materials, and always being open to my many questions about materials characterization, and to Quoc Mac, who taught me the skin transplant model and was always interested in hearing how my experiments were going.

Next, I would like to thank the staff at BME, IBB, and in the PRL for their assistance in allowing the research community to operate smoothly and produce fantastic work. In particular, I would like to thank Nadia Boguslavsky, Sommer Durham, and Andrew Shaw for their training and support with the flow cytometry and microscopy core facilities. Thank you, Sommer, for putting up with my nocturnal flow cytometry habits and allowing me to run my samples until well into the night. I would not have been able to finish without your support.

I next want to thank my labmates for their constant support, conversations, and advice. I've had many deskmates in my time in the Botchwey lab, and I want to thank them all for being such good friends and colleagues. First, to Dr. Claire Olingy. Watching you work and listening to your ideas was truly inspirational. You are one of my science role models and I hope to continue to try to emulate you in the work that I do. Next, to Dr. Cheryl San Emeterio. I always felt like we had the best conversations, both about science and everyday life. It was a joy to come into lab to interact with you. Finally, Thomas Turner. Thank you for being a source of laughter and stress relief during these last few months of my PhD work. I owe an extreme debt of gratitude to Dr. Molly Ogle for her patience and guidance over the last five years. I truly don't know how you do it. Thank you for teaching me pretty much everything that I know about doing good science. Thank you for always answering my millions of questions about minutiae like protocols or techniques to the big questions like how to talk about my research within the greater framework of the

field. This thesis would not be finished without your invaluable assistance. Thank you also to Nathan Chiappa, Jada Selma, and Dr. Hannah Song, as well as alums Tiffany Wang, Dr. Tony Awojoodu, Dr. Jack Kreiger, and my former undergraduate students Krithik Srithar, Xianne Tria, Gabrielle Clarke, and Asha Scott for making my time in the Botchwey lab better than I ever imagined it would be.

I have so many friends and family who I am forever grateful for who have given me love and support through these long years of school. First, to my friends in medical school and graduate school – thank you for the laughs, the experiences, and for putting my with my complaints about school. In particular, I can't thank Chris Johnson enough for his friendship. It was nice always having someone who understood the ups and downs of MD/PhD life work in the lab next door. Thanks for always stopping to talk with me when I saw you in the hall. I can't get through this without thanking Tabby Khan, my life wouldn't be the same without you. My parents have been my constant cheerleaders ever since I was young. Thank you for allowing me to pursue my dreams and for guiding me to pursue science. I am the person that I am today because of the love you have given me and how you raised me. Thanks to my brothers, Daniel and Andrew, for always making me laugh, and to Dana and Steve for always being in my corner even all the way in Texas. I am so grateful to my in-laws in Atlanta who have adopted me as their own daughter. Thank you for cooking me food, for always encouraging me, and for loving me like family.

Finally, I have to thank my husband, Daniel Sok and our dogs, Ivy and Daisy. Ivy and Daisy have been fantastic companions to Daniel and I and are always there when I need a laugh or dog snuggles. Daniel and I met when I first moved down to Atlanta, and I don't think he knew what he was getting into when he met me. Daniel gives me so much

love and support, peppered with a healthy dose of realism to always remind me that things are not as bad as they may seem. Thank you for always taking care of me through the ups and downs, especially these last few months. You have been so patient and caring. Thank you for buying me flowers and Twizzlers and cheese. We have built an amazing life together with Ivy and Daisy and I could not ask for anything more.

TABLE OF CONTENTS

LIST OF FIGURES

LIST OF SYMBOLS AND ABBREVIATIONS

ANOVA	Analysis of variance
BSA	Bovine serum albumin
CD	Cluster of differentiation
CO_2	Carbon dioxide
CXCL	C-X-C ligand
CXCR4	C-X-C chemokine receptor 4
DC	Dendritic cell
DMEM	Dulbecco's Modified Eagle Media
DWC	Dorsal skinfold window chamber
ECM	Extracellular matrix
FBS	Fetal bovine serum
FGF	Fibroblast growth factor
GM-CSF	Granulocyte-macrophage colony stimulating factor
IACUC	Institutional Animal Care and Use Committee
IGF	Insulin-like growth factor
IHC	Immunohistochemistry
IL	Interleukin
iNOS	Inducible nitric oxide synthase
IFN	interferon
i.p.	Intraperitoneally
LPS	Lipopolysaccharide
kDa	Kilodalton

MCP-1	Monocyte chemoattractant protein-1
M-CSF	Macrophage colony stimulating factor
MDP	Macrophage-dendritic cell precursor
MerTK	Mer receptor tyrosine kinase
mg/kg	Milogram per kilogram
MMP	Matrix metalloproteinase
M1	Classically activated inflammatory macrophage
M2	Alternatively activated macrophages
NIH	National Institutes of Health
PBS	Phosphate buffered saline
PCA	Principle component analysis
PEG	Poly(ethylene glycol)
PEG-MAL	4-arm poly(ethylene glycol)-maleimide
PLGA	Poly(lactic-co-glycolic acid)
RGD	(Arginine-glycine-aspartic acid) peptide
ROS	Radical oxygen species
SSC	Side scatter
SDF-1	Stromal cell-derived factor-1
S.E.M.	Standard error of the mean
TGF-ß	Transforming growth factor-beta
T_H	T helper
TNF- α	Tumor necrosis factor-alpha
VCAM-1	Vascular cell adhesion molecule 1
VEGF	Vascular endothelial growth factor
VPM	Valine-proline-methionine peptide

SUMMARY

A major challenge in the transplant field is achieving a fine balance between achieving sufficient immunosuppression to prevent donated tissue rejection while managing the many side effects that occur in both the acute and chronic timeframe after induction of immunosuppressive therapy. There have been great advances made in the field of post-organ transplant prevention of rejection, but acute wound healing complications following transplant surgery still occur at unacceptably high rates compared to analogous non-transplant surgeries. Patient factors including age, obesity, and pre-existing conditions such as diabetes can put patients at greater risk for wound healing complications after organ transplant. Organ transplant is currently the only treatment for end-stage organ failure, so therefore the need exists for therapies that are able to accelerate post-transplant surgical wound closure while subsequently allowing for acceptance and integration of the transplanted tissue.

Cells of the innate and adaptive branches of the immune system have emerged as critical cellular mediators that can play roles in modulating the immune response after tissue injury towards enhanced wound healing and tissue regeneration. Specifically, alternatively activated subsets of monocytes and macrophages, along with tolerogenic Interleukin-10 (IL-10)+ dendritic cells, and regulatory T cells have been shown to promote vascular remodeling, tissue repair, and return to homeostasis in numerous tissues. While therapies that are able to target a single pro-regenerative cell subset at a time have previously been developed, little work has been done attempting to recruit wound healing cells from both myeloid and lymphoid lineages. Recognizing the complex interplay that

exists between the innate and adaptive branches of the immune system, we developed and characterized a novel immunomodulatory hydrogel with the ability to promote the recruitment and accumulation of wound healing immune cells of varied lineage.

Using localized delivery of aspirin-triggered resolvin d1 (AT-RvD1) a lipid specialized proresolving mediator, we demonstrated that injured tissue can be enriched with anti-inflammatory, pro-angiogenic populations of neutrophils, monocytes and macrophages. Local delivery of AT-RvD1 modulates the local cytokine profile and enhances vascular remodeling at early timepoints following injury. We then expanded upon these findings and developed a hydrogel system capable of the dual delivery of AT-RvD1 and IL-10 with differing release kinetics. Dual delivery of IL-10+AT-RvD1 not only increases anti-inflammatory monocyte and macrophage recruitment as was seen with local delivery of AT-RvD1 alone, but also results in significant accumulation of IL-10+ dendritic cells and regulatory T cells while recapitulating the vascular remodeling processes observed previously. Finally, we delivered these immunomodulatory hydrogels following allogeneic and syngeneic skin transplant. We observed significant modulation in the local immune response with combination IL-10+AT-RvD1 treatment with little effect on the makeup of immune cells populating the blood or draining lymph nodes. We observed allograft rejection across all treatment groups by our final timepoint, however, indicating that local immunomodulation is not sufficient to provide acceptance signals to the host.

This research presents a novel immunomodulatory hydrogel system that may aid in soft tissue regeneration by recruiting pro-regenerative immune cell subpopulations and stimulating vascularization after injury. These findings represent an improved understanding of how we may target pro-regenerative cells from different branches of the

immune system, and this treatment has the potential to enhance tissue regeneration and prevent wound healing complications after skin tissue injury.

CHAPTER 1. INTRODUCTION AND SPECIFIC AIMS

1.1 Introduction

Ongoing advances in transplantation surgical techniques, together with improvements in immunosuppression regimens (IS), have led to an appreciable reduction in the rate of postoperative morbidity and graft loss. Despite these advances, wound complications due to systemic IS are a common post-transplant surgical complication. Therefore, there is a need for therapies that have the ability to allow for wound healing while also preventing rejection without the off-target side effects of systemic IS. One method that has the potential of mediating these complications is the delivery of immunomodulatory factors that are able to accelerate wound healing and tissue integration through the local recruitment and education of anti-inflammatory, pro-regenerative subsets of immune cells, such as regulatory T cells (Treg), macrophages (M2a/c), and dendritic cells (tolDCs), that work to enhance tissue regeneration and alloimmunity by dampening immune activation and cytokine production of factors involved in pathologic inflammation and rejection.

Resolvins, a class of endogenous small lipid molecules, play a multifocal role in the resolution of acute inflammation. Recently, resolvins have also been shown to promote transplant acceptance through actions on dendritic cells and Tregs and can reduce graft injury via reduction of neutrophil recruitment. Resolvins can also preferentially recruit Ly-6CLo anti-inflammatory monocytes, which are skewed toward long-term anti-inflamamtory fate. The cytokine IL-10 is necessary for Treg-mediated allotolerance and

can participate in the local education of DCs capable of promoting Treg activity and allograft acceptance. Combining the delivery of these factors using degradable polyethylene glycol-maleamide (PEG-MAL) hydrogels is a novel method has the potential to accelerate wound closure and allotransplant integration with the host by concentrating the presentation of cells vital to wound healing in a therapeutic window while reducing complications in wound healing associated with systemic immunosuppression regimens.

We will exploit endogenous mechanisms of proregenerative immune signaling within immune cell populations to improve transplant surgical wound healing and transplanted tissue integration. Our approach is to engineer a degradable, injectable biomaterial scaffold to spatially localize and induce defined leukocyte and lymphocyte subpopulations that are critically involved in inducing immune tolerance. We have shown that biomaterials-mediated delivery of AT-RvD1 or IL10 is able to modulate macrophage activity in vitro and in vivo. In addition, studies using AT-RvD1-loaded PLGA films have demonstrated superior anti-inflammatory monocyte recruitment compared to cutaneous infusion. The central hypothesis of this proposal is that local recruitment of subsets of macrophages, dendritic cells, and T cells via delivery of AT-RvD1 and on-site IL-10-mediated induction of alloimmunity-promoting phenotypes will promote wound healing associated with allograft transplantation.

1.2 Specific Aims

Aim 1. To evaluate the effects of enhancing the recruitment of anti-inflammatory and pro-regenerative cell subsets to areas of inflammation using locally delivered AT-RvD1 after injury. Aim 1 characterizes the changes in immune cell recruitment and

associated vascular remodeling after local treatment with AT-RvD1 following tissue injury. In Aim 1A, we will assess the kinetics of pro- and anti-inflammatory immune cell recruitment and cytokine profile modulation in the murine dorsal skinfold window chamber after biomaterial delivery of AT-RvD1 model by flow cytometry, whole mount immunohistochemistry (IHC), and multiplexed cytokine array. In Aim 1B, the effects of local delivery of AT-RvD1 on post-injury vascular remodeling will be assessed by intravital imaging analysis and whole mount IHC.

Aim 2. To develop an injectable, degradable, PEG hydrogel-based delivery system for AT-RvD1 and IL10 and quantify in vivo changes in the origin, recruitment dynamics, and differentiation fate of immune cell subsets after gel implantation. Aim 2 develops a PEG hydrogel system capable of releasing IL-10 and AT-RvD1 and characterizes the modulation in the local immune response in the dorsal skinfold window chamber. In Aim 2A, we will characterize the encapsulation and release of AT-RvD1 and IL-10 from PEG hydrogels in vitro. In Aim 2B, we will implant hydrogels into the dorsal skinfold window chamber injury model and assess cell phenotypes surrounding the implant by flow cytometry, whole mount immunohistochemistry (IHC), and multiplex cytokine and growth factor profiling analysis after 1, 3, and 7 days. Internally controlled studies will compare unloaded gels to gels releasing IL-10 and/or AT-RvD1.

Aim 3. To investigate how modulation of cell recruitment and activation via local immunomodulation with AT-RvD1 and IL10 from PEG hydrogels regulates the immune response to transplanted tissue and promotes early wound healing and integration. Aim 3 examines the kinetics of immune cell recruitment and associated enhancement of syngeneic or allogeneic skin transplant integration. In Aim 3A, we will characterize syngeneic skin

transplant wound healing and integration after transplantation with PEG hydrogels releasing IL-10 and AT-RvD1. In Aim 3B, we will characterize skin allograft healing and acceptance after transplantation with PEG hydrogels releasing IL-10 and AT-RvD1. We will identify the response kinetics of immune cells to transplanted grafts by flow cytometry and immunohistochemistry. We will also assess molecular signals of rejection by immunostaining for deposition of donor derived IgG and IgM and through multiplexed cytokine profiling.

1.3 Significance

The current standard for preventing allograft rejection consists of systemic immunosuppression utilizing multiple drugs that vary in their mechanisms of action. While the use of systemic IS has reduced the rates of transplanted organ rejection, complications related to IS are still unacceptably high[1-3]. One potentially successful approach is to induce graft tolerance by acting intrinsically on the myeloid cells that are recruited to allograft tissue after transplant with engineered immunomodulatory cues delivered locally via biomaterial by tuning the recruitment of anti-inflammatory cell progenitors and inducing polarization into tolerogenic cell subsets through on-site education[4, 5]. The use of biomaterials for the local delivery of immunosuppressive of immunomodulatory factors is an underexplored area that has the potential to reduce these complications while preventing allograft rejection[6, 7]. Our proposed research will show how selective recruitment of anti-inflammatory immune cell subsets within allografts by dual delivery of AT-RvD1 and IL-10 to enhance generation of intrinsic mononuclear subsets with suppressive activity in order to inhibit graft-reactive T cell immunity, facilitate induction of Tregs, and induce transplantation tolerance.

CHAPTER 2. BACKGROUND

2.1 Systemic immunosuppressive therapy after transplantation can cause significant complications.

Solid organ transplantations have increased 20% in the United States in the last 5 years to over 30,000 procedures in 2016, and organ transplant is the most effective treatment option for patients suffering from end-stage organ failure [2, 8]. Currently, the use of post-transplantation immunosuppressive regimens (IS) has resulted in significant increases in survival after solid organ allograft, with rates nearing 90% after one year[9]. Despite decreases in acute rejection of transplants with IS, significant complications stemming directly from systemic IS are still prevalent, in both the acute and chronic time frame after transplant. Chronic use of systemic IS is associated with an increased risk of opportunistic infection, particularly fungal infection, lymphoproliferative disorders, and wound toxicity including cardiovascular disease or renal failure[2, 3]. In the acute phase, surgical wound complications associated with transplantation procedures are reported at rates over ten times higher than similar surgical procedures that do not involve immunosuppression [3]. Because of the early post-surgical complications associated with immunosuppressive therapy, there is an opportunity for the development of alternative therapies that are able to exploit endogenous mechanisms of wound healing and tissue acceptance to prevent acute wound closure complications and promote early tissue integration.

Impaired wound healing after transplant surgery is one of the most common complications arising from high doses of systemic immunosuppression. Wound dehiscence

and other complications have been reported in the context of nearly every transplant procedure, including heart, kidney, and liver [3, 10]. For example rates of surgical wound complications including superficial or deep wound infection, lymphocele, and wound dehiscence have been reported in 8-15% and sometimes up to 40% of heart transplant recipients compared with 0.5-10% of patients after similar general cardiac surgery procedures that do not involve transplantation [3]. These complications can be exacerbated by a multitude of patient risk factors, including age, obesity, and diabetes [11]. Given the aging population and rising obesity rates, wound healing complications following transplant are at risk of becoming more and more common.

Many immunosuppressive drugs utilized after transplant have been shown to impair or interfere with wound healing. The use of mTOR inhibitors such as sirolimus and everolimus after transplant have been implicated in increases in wound complications, with one study demonstrating an incidence of complications of 47% in patients receiving sirolimus following kidney transplant, compared to 8% in patients not receiving sirolimus[1]. In animal models, animals receiving sirolimus had reduced tensile strength in regenerating abdominal wounds compared to control[12]. When combined with corticosteroids, this effect was amplified, and tensile wound strength was reduced even further. These findings are further corroborated in a study utilizing pigs that received rapamycin after ureteric anastomosis [13]. Another mTOR inhibitor, everolimus, has also been shown to reduce anastomotic breaking strength in the rat intestine, indicating adverse effects on wound healing [14]. Other common immunosuppressive drugs such as cyclosporine A, tacrolimus, and mycophenate motefil have been studied with regards to their roles in wound healing and have been shown to impair wound healing processes [15-

17]. These studies indicate that the common combinatorial approach of immunosuppression taken to prevent the rejection of transplanted organs may be compounding the impairment of processes necessary to ensure proper healing of surgical sites and prevent wound healing complications.

2.2 Roles of the innate immune system in wound healing

The innate immune system plays a vital role in the restoration of homeostasis following tissue injury. Because of this, there exists an opportunity to exploit the mechanisms of wound repair driven by the innate immune system to accelerate or enhance healing after injury in a variety of contexts, including cutaneous wound healing [18, 19], ischemic cardiac injury[20], and nervous tissue regeneration[21]. The immune response to traumatic injury is characterized by a cascade of repair processes that result in the rapid accumulation of neutrophils that act as first-line defenders against microorganisms and signal amplifiers to recruit other immune cells to the injured tissue[22]. Secondly, there is an infiltration of mononuclear phagocytes that serve to clear debris, remodel and expand vasculature, and signal to circulating and parenchymal cells that help restore cellular and matrix composition[23, 24]. Studies investigating the depletion of neutrophils or mononuclear phagocytes have demonstrated delayed wound closure in aged mice[25], or failure to regenerate amputated zebrafish tail fins [26] or salamander limbs [27], suggesting that there is a complex interaction of all of these cellular subsets that is necessary for tissue repair to proceed after injury.

2.2.1 Neutrophils act as first responders to tissue injuries

Neutrophils are innate immune cells of the myeloid lineage that develop from hematopoetic progenitors in the bone marrow. In humans, they are the most abundant immune cell in human blood, and their role in homeostasis is to patrol and protect the host from pathogens and other harmful reagents [28]. Neutrophils play a major role in the response to pathogens, and are vital to stemming the tide of infection, although while carrying out anti-infectious effector functions, neutrophils may cause collateral damage to tissues surrounding the infected area. In sterile inflammation, such as acute tissue damage that occurs as a result of surgery, damage-associated molecular patterns (DAMPs) released from injured and dying cells provide the initial recruitment signals to circulating neutrophils [29]. Many of these DAMPs can act as chemoattractants to neutrophils, while others can activate surrounding tissues and induce the production of strong inducers of neutrophil chemotaxis, such as C-X-C motif chemokine ligand 8 (CXCL8) and leukotriene B4 [30-32]. Neutrophils responding to DAMPs can contribute to and perpetuate sterile tissue injury through amplification of the inflammatory response and the release of toxic effectors, such as reactive oxygen species (ROS) and proteolytic enzymes capable of damaging tissue [33, 34]. Neutrophils can also release neutrophil extracellular traps (NETs) that can be injurious to tissue [35, 36] and even contribute to the development of diseases such as systemic lupus erythematous, rheumatoid arthritis, diabetes, and thrombosis [37]. NETs contain nuclear contents as well as granular and cytosolic proteins, which result in the potential presentation of auto-antigens to the host immune system and the release of DAMPs that could further amplify ongoing immune reactions and cause tissue injury, and there have been several strategies employed to interfere with NETs that have resulted in decreases in tissue damage [38].

Although neutrophil activation and activity can have a detrimental role on tissue during inflammation, there is evidence that neutrophils can also promote tissue repair processes and the resolution of inflammation. In the context of tissue repair, it has been demonstrated that neutrophils are important for efficient wound repair, as neutropenic individuals often have difficulty healing wounds [39]. Additionally, mice deficient in formyl peptide receptors FPR1 and FPR2 exhibit delayed wound closure [40] and mice whose leukocyte recruitment is impaired by deletion of CXCR2 displayed decreased epithelialization and neovascularization following tissue injury [41]. These studies highlight a direct role for neutrophils in wound healing, although specific effector functions that neutrophils possess that may contribute to wound healing remain unclear.

One possible mechanism of neutrophil participation in wound repair is through the emerging evidence of neutrophilic subsets. Heterogeneity of neutrophils, similar to monocyte or macrophage heterogeneity, has shown that there are several subsets of neutrophils that may contribute to wound healing and angiogenesis. Revascularization and formation of new blood vessels are a vital process to wound repair. Newly formed vessels participate in provisional granulation tissue formation and are able to provide oxygen and nutrients to growing tissues [42]. Growth factors, such as vascular endothelial growth factor (VEGF), fibroblast growth factor (FGF), and transforming growth factor-beta (TFGB) have been identified as potent mediators of vascular remodelling during wound repair. Both human and murine neutrophils have been demonstrated to be a source of VEGF. Recently, a subset of neutrophils has been described that is able to promote vascular remodelling after hypoxic injury [43, 44]. These neutrophils express high levels of CD49d, VEGFR1, and CXCR4 and are important in the initiation of angiogenesis following injury.

Neutralization of these neutrophils resulted in impaired integration and angiogenesis of implanted islets. Additionally, these pro-angiogenic neutrophils are an important source of matrix metalloproteinases (MMPs) that are responsible for the degradation of extracellular matrix components and the release of VEGF. These studies indicate a clear role for neutrophils in the larger wound repair process.

2.2.2 The mononuclear phagocyte system

The mononuclear phagocyte system is comprised of monocytes and macrophages. These cell subsets exhibit a wide phenotypic heterogeneity and can carry out a variety of effector functions, including the coordination of innate and adaptive immune responses[24, 45-47], the killing of microbial pathogens and parasites [48], and the promotion of tissue repair[20, 49-51]. Monocytes are also able to differentiate into macrophages and dendritic cells after extravasation[52-54]. In response to tissue injury, these cells traditionally secrete many factors, such as inflammatory cytokines and chemokines, matrix and protein degrading factors, and growth factors[53, 55]. *In vivo*, monocytes and macrophages exist on a spectrum ranging from "classical" or "inflammatory" to "alternatively activated" or "anti-inflammatory", respectively [56]. The subset heterogeneity present among both monocytes and macrophages presents an opportunity to develop therapies that are able to specifically target subsets and manipulate their activity for the promotion of tissue repair after injury.

Monocytes are myeloid leukocytes that traffic to the blood and spleen during homeostasis. They are immunophenotyped as $CD11b^{+}CD115^{+}SSC^{low}$ cells. Circulating blood monocytes are comprised of at least two functionally distinct subsets[47]. Classical

"inflammatory" monocytes are characteristically Ly6C^{hi} CCR2^{hi} CX3CR1^{lo} in mice and CD14^{+}CD16^{-} in humans. Non-classical "anti-inflammatory" monocytes are Ly6C^{lo} CCR2^{lo} CX3CR1^{hi} in mice and CD14^{lo}CD16^{+} in humans. Classical monocytes predominate the acute phases of injury and are recruited to injury following neutrophil infiltration by migrating towards gradients of inflammatory cytokines such as MCP-1[53, 57]. Classical monocytes secrete inflammatory cytokines such as IL-6, iNOS, and TNFα[58], produce high levels of matrix metalloproteinases and cathepsins, and phagocytose debris[20]. During homeostasis, non-classical monocytes patrol the endothelium and after injury they predominate in later phase inflammation, secrete higher levels of VEGF, TGFβ, and IL-10 and lower levels of TNFα and IL-1β, and promote angiogenesis and matrix deposition[20, 59]. While studies of toxin-induced muscle injury[51], acute liver injury[50], and autoimmune disease[60] show that classical monocytes are recruited from circulation and subsequently convert *in situ* into non-classical monocytes and M1 or M2 macrophages, other studies in myocardial infarction[20] and excisional skin injury[18] indicate that non-classical monocytes can be recruited directly from blood. Until recently, it was unknown whether non-classical versus classical monocytes give rise to distinct macrophage phenotypes. Our group is the first to show that non-classical monocytes recruited from blood may serve as biased progenitors of M2 "alternatively activated" macrophages[61].

Macrophage phenotype and function is described as spectrum of M1 "inflammatory" to M2 "alternatively-activated" or "regenerative" macrophages[24]. M1 polarization from naive macrophages *in vitro* is accomplished by stimulation with IFNγ, lipopolysaccharide, and/or TNFα[62]. These M1 macrophages produce reactive oxygen species and many inflammatory cytokines that support necrotic tissue clearance, and growth factors such as

VEGF and FGF2[63-66] upon stimulation. The release of these pro-inflammatory cytokines *in vivo* aids in pathogen and necrotic tissue clearance and sets off a signal cascade that allows for the recruitment of additional immune populations. While it has been found that an M1 response is necessary for normal wound healing to occur, over-activation or excessive persistence of M1 macrophages can propagate tissue damage and result in an unresolved inflammatory response [24].

M2 "alternatively activated" macrophages are differentiated *in vitro* via a mechanism separate from M1 macrophages. M2 macrophages can be further subdivided into M2a, M2b, and M2c subsets that all differ in their surface markers and effector functions. M2a polarization requires IL-4 and/or IL-13 *in vitro*, and these macrophages support extracellular matrix deposition and epithelial wound closure via high expression of arginase-1 (CD206), which allows them to generate precursors for collagen and fibroblast stimulating factor, [24, 62, 63, 66-68]. M2b polarization requires immune complexes combined with toll-like receptor (TLR) or IL-1R ligands, whereas M2c macrophages arise via IL-10 stimulation[62, 63, 67, 69]. M2b and M2c contribute to suppressing inflammation through secretion of IL-10. Due to macrophage plasticity *in vivo* and lack of distinguishing biomarkers, specific functions of M2a-c subtypes in tissue repair remain poorly understood. Nevertheless, the dominant presence of M2 versus M1 macrophages is associated with positive healing outcomes in numerous contexts[18, 23, 70-72].

2.3 The adaptive immune system and wound healing

In contrast to innate immunity, the adaptive immune provides more of a delayed and specific response. The innate immune system is comprised of the lymphocytes B cells

and T cells. Currently, there is little evidence for the role of B cells in tissue healing, although this is an area that has not received much study. On the other hand, there is growing evidence pointing towards T cells playing a crucial role in tissue repair and regeneration – however the exact function of T cell subsets and their level of accumulation at injury sites is largely unknown and seems to vary from tissue to tissue.

T cells are capable of secreting a diverse range of cytokines and growth factors, which can have detrimental of beneficial effects on tissue healing. For example, it has been shown that CD4+ T helper 1 (TH1) cells and cytotoxic CD8+ T cells inhibit bone regeneration via secretion of IFN-y and TNF- α [73]. On the other hand, biomaterials that promote CD4+ T helper 2 (TH2) cell activity have been shown to guide interleukin-4 dependent macrophage polarization after traumatic muscle injury, which is critical for muscle tissue regeneration [72]. Additionally, CD4+ regulatory T cells (Treg) are critical for the repair and regeneration of several tissues including skin, bone, lungs, kidney, skeletal muscle, and cardiac muscle [74-78]. Tregs are potent suppressors of the immune system and have recently been rediscovered as indirect and direct regulators of tissue healing. Tregs can modulate regeneration by controlling neutrophils, inducing macrophage polarization, regulating other subsets of helper T cells, and activating local tissue progenitor cells[79-84]. This growing body of evidence suggests that there is complex interplay between both the innate and adaptive immune systems in the processes of wound healing, and that these processes can be harnessed to direct tissue healing using a multifactorial approach that acts on multiple key regulators of wound healing.

2.4 Cells of the innate immune system are active mediators of transplant acceptance and rejection in concert with the adaptive immune system.

It has long been recognized that T cells play a major role in directing both transplant rejection and tolerance. Indeed, much of the research in the field of transplant immunology has focused on modulating the response of the adaptive immune system after allograft surgery. However, targeting of innate immune cells including mononuclear phagocytes and granulocytes has gained increasing interest due to their ability to play both detrimental and beneficial roles[4]. Neutrophils are recruited to graft tissue in response to ischemia reperfusion injury (IRI) inherent in all transplant procedures[85]. There they can exacerbate graft tissue damage through the release of metalloproteinases and neutrophil elastase, and actively mediate acute rejection through CD8+ cytotoxic T cell signaling[86-88]. Additionally, while the interaction of neutrophils and cells of humoral immunity is not well-understood, it has been found that neutrophils have the capacity to leave peripheral sites of injury and deliver antigen to lymph nodes[89]. On the other hand, there are subsets of neutrophils that may promote wound healing and tissue repair, and aid in the reperfusion of graft tissue[43]. Mononuclear cell infiltration, including monocytes (MO), dendritic cells (DCs) and macrophages, and the production of pro-inflammatory cytokines such as tumor necrosis factor-alpha (TNF-α), interleukin (IL)-1α, and IL-1β are inherent to the transplant milieu[5]. Macrophages of both donor and recipient origin infiltrate the allograft and proliferate in situ, and comprise 40-60% of cellular infiltrate in acute rejection[90]. Up-regulation of surface MHC class II and increased expression of T cell costimulatory molecules by activated DCs are also implicated in acute rejection. Upon functional maturation, “passenger” DCs in donor tissue migrate to recipient secondary lymphoid organs along chemokine gradients where they are key mediators in alloantigen presentation. Early activation of DCs also leads to allotransplant injury due to accumulation

of interferon-γ-producing neutrophils, infiltrating macrophages, CD4+ T cells, B cells, and invariant natural killer T (NKT) cells[91]. Conversely, the phenotypic plasticity of monocyte precursors and DCs in response to microenvironmental signals, the presence of tolerogenic mononuclear phagocyte subsets that coincide with allograft acceptance, and their roles in Treg expansion are evidence that MO and DC subsets are key targets in the quest for transplant acceptance[92, 93]. For example, we have shown that Ly6C^{Lo} anti-inflammatory monocytes (AMs) are skewed toward long-term anti-inflamamtory cell fate[61, 94]. These AMs can also promote Treg differentiation through PD-1 signaling[95]. Additionally, after differentiation into M2a/c macrophages, these cells can release cytokines that reduce inflammatory DC activity and suppress T cell activation[92, 93].

2.5 Endogenous biomolecules can promote wound healing and tissue acceptance

2.5.1 Resolvins play a multi-factorial role in modulating innate and adaptive immune responses.

Resolvins are a class of bioactive small molecule lipids derived from the omega-3 polyunsaturated fatty acids eicosapentaenoic acid (EPA) and docosahexaenoic acid (DHA)[96]. Resolvins are potent proresolving lipid mediators that act to drive cellular processes toward the resolution of inflammation and have been deemed "specialized proresolving mediators" (SPMs). Specifically, the D-series resolvins including resolvin D1 (RvD1) and Aspirin-triggered Resolvin D1 (AT-RvD1) are derived from DHA act as endogenous agonists of the cellular receptors GPR32 and ALX/FPR2, which are broadly expressed in immune cells, including neutrophils, monocytes, macrophages, dendritic cells, and lymphocytes, and in certain types of specialized epithelial cells[97-100]. These

SPMs have a multi-faceted role in modulating the cellular response to tissue injury and inflammation. Ligation to these receptors can decrease the transendothelial migration of neutrophils, enhance macrophage phagocytosis of apoptotic cells and microbes, modulate cytokine release from macrophages, and stimulate phagocyte efflux from inflamed tissues, all of which are considered hallmarks of active resolution of inflammation[100]. More recently, studies have shown that these SPMs are able to modulate the activity of cells in the adaptive immune system in ways that were previously unknown. Resolvins D1 and D2 are able to inhibit human T cell activation by various means, including reducing cytokine production by CD8+ and CD4+, reducing differentiation of naïve CD4+ T cells into T helper 1 and 17 (T_H1/T_H17) subsets, and concomitantly enhanced the de novo generation and function of FoxP3+ Tregs through GPR32 signaling[101]. Use of systemically-delivered resolvins in various transplant models have shown that resolvins can preserve allotransplant function by modulating the activity of neutrophils, DCs, and T cells[102-104].

2.5.2 IL-10 modulates dendritic cell activation and function to promote transplant acceptance

IL-10 is a cytokine which plays a critical role in the control of immune responses. It is expressed by both innate and adaptive immune cells including monocytes, macrophages, dendritic cells, and virtually all T cell subsets[105]. IL-10 signaling can have direct effects on both innate and adaptive immune cells. For example, IL-10 treatment of premature DCs prevents maturation, resulting in decreased MHC-II expression on the DC surface, and subsequently increases DC release of IL-10[106]. These IL-10 producing DCs have been termed “tolerogenic DCs” (tolDCs) and have the ability to induce functional

Tregs[107]. IL-10 also has the ability to block T cell costimulation and prevent proliferation in both T_H1 and T_H2 T cell subsets[108]. IL-10 signaling is also required for Tregs to mediate tolerance to alloantigens *in vivo*[109]. These studies highlight the role that IL-10 plays not only in the education of tolerogenic immune cells but also in the induction and maintenance of transplant tolerance.

CHAPTER 3. ASPIRIN-TRIGGERED RESOLVIN D1-MODIFIED MATERIALS PROMOTE THE ACCUMULATION OF PRO-REGENERATIVE IMMUNE CELL SUBSETS AND ENHANCE VASCULAR REMODELING[1]

3.1 Abstract

Many goals in tissue engineering rely on modulating cellular localization and polarization of cell signaling, including the inhibition of inflammatory infiltrate, facilitation of inflammatory cell egress, and clearance of apoptotic cells. Omega-3 polyunsaturated fatty acid-derived resolvins are gaining increasing recognition for their essential roles in inhibition of neutrophil invasion into inflamed tissue and promotion of macrophage phagocytosis of cellular debris as well as their egress to the lymphatics. Biomaterial-based release of lipid mediators is a largely under-explored approach that provides a method to manipulate local lipid signaling gradients in vivo and direct the recruitment and/or polarization of anti-inflammatory cell subsets to suppress inflammatory signaling and enhance angiogenesis and tissue regeneration. The goal of this study was to encapsulate Aspirin-Triggered Resolvin D1 (AT-RvD1) into a degradable biomaterial in order to elucidate the effects of sustained, localized delivery in a model of sterile inflammation. Flow cytometric and imaging analysis at both 1 and 3 days after injury showed that localized AT-RvD1 delivery was able significantly increase the accumulation

[1] Adapted from: M.C.P. Sok, M.C. Tria, C.E. Olingy, C.L. San Emeterio, E.A. Botchwey, Aspirin-Triggered Resolvin D1-modified materials promote the accumulation of pro-regenerative immune cell subsets and enhance vascular remodeling, Acta Biomater 53 (2017) 109-122. Reprinted with permission from Elsevier

of anti-inflammatory monocytes and M2 macrophages while limiting the infiltration of neutrophils. Additionally, cytokine profiling and longitudinal vascular analysis revealed a shift towards a pro-angiogenic profile with increased concentrations of VEGF and SDF-1α, and increased arteriolar diameter and tortuosity. These results demonstrate the ability of locally-delivered AT-RvD1 to increase pro-regenerative immune subpopulations and promote vascular remodeling.

3.2 Introduction

Resolvins are a class of bioactive small molecule lipids derived from the omega-3 polyunsaturated fatty acids eicosapentaenoic acid (EPA) and docosahexaenoic acid (DHA)[96]. Resolvins are potent proresolving lipid mediators that act to drive cellular processes toward the resolution of inflammation. Specifically, the D-series resolvins derived from DHA act as endogenous agonists of the cellular receptors GPR/32 and ALX/FPR2, which are broadly expressed in immune cells, including neutrophils, monocytes, macrophages, and lymphocytes, and in certain types of specialized epithelial cells[97, 98, 110]. Ligation to these receptors results in a number of different actions, including decreased transendothelial migration of neutrophils, enhancement of macrophage phagocytosis of apoptotic cells and microbes, modulation of cytokine release from macrophages, and stimulation of phagocyte efflux from inflamed tissues, all of which are considered hallmarks of active resolution of inflammation [100]. Treatment with resolvins can be used to promote the resolution of inflammation and healing in in many pathological conditions, including bacterial infection, peritonitis, and asthma [111-113]. Additionally, subcutaneous resolvin D2 injections have been shown to increase collateral circulation after ischemic injury [114]. While these studies have been promising, many

utilized systemic delivery of resolvins, which limits its bioavailability at the site of inflammation and can result in rapid degradation, requiring multiple injections at high dosages [115, 116].

Currently, biomaterial-based delivery systems for localized delivery of resolvins have not widely been developed [117, 118]. Others have shown that local delivery of resolvin D1 (RvD1) using a biomaterial wrap can reduce neointimal hyperplasia after vascular injury [119, 120], but more exploration is needed to fully characterize the effects of local resolvin delivery in other models. Utilization of biomaterial-mediated delivery of resolvins to areas of injured tissue has the potential to amplify the effect of resolvins produced endogenously during inflammation. Aspirin-triggered Resolvin D1 (AT-RvD1) is a D-series resolvin that can be produced physiologically when the enzyme cyclooxygenase-2 (COX-2) is acetylated in the presence of aspirin [115]. It possesses the same mechanism of action as RvD1, but due to a conformational change of a hydrogen molecule from (S) to (R) around the seventeenth carbon, can resist rapid degradation by oxidoreductases, resulting in a longer *in vivo* half-life [115, 121-123]. The longer activity of AT-RvD1 *in vivo* makes it an attractive small molecule for incorporation into biomaterials that seek to promote resolution of inflammation and enhance wound healing.

One strategy to promote resolution of inflammation is to modulate the profile and activities of cells involved in the inflammatory response [18, 124-126]. Neutrophils have classically been viewed as a largely homogeneous population of myeloid immune cells that do not possess the ability to polarize into subsets, unlike other leukocyte populations with multiple phenotypes, such as T lymphocytes or macrophages. It was long thought that neutrophils were only able to act as the immune system's short-lived "first responders" to infection or

injury and that these responses were well-defined and limited in scope. Classical neutrophils are able to carry out pro-inflammatory effector functions and these can exacerbate tissue injury under pathologic conditions [127]. Prevention of excessive neutrophil accumulation enhances wound healing in non-healing diabetic wounds and increases cardiac function after acute myocardial infarction due to reduced release of reactive oxygen species, proinflammatory mediators, and proteases - which resulted in a reduction in tissue damage [82, 128-130]. However, there is now significant evidence for the existence of heterogeneous subsets within the larger neutrophil population, and these subsets are able to carry out functions in both homeostatic and pathogenic immune responses.

One such subset of neutrophils that has been defined is able to promote vascular formation after hypoxic injury [44]. These circulating neutrophils express high levels of CD49d, VEGFR1, and CXCR4 and are able to extravasate into tissues in a mechanism independent from classical neutrophils and are recruited by VEGF-A [43]. These neutrophils are necessary for early angiogenic processes, and inhibition of these cells results in a significant decrease in new vessel formation *in vivo*. The existence of this pro-angiogenic neutrophil population presents a new cellular target whose recruitment or function may be manipulated to promote early vascular network expansion processes that are crucial to wound healing and tissue regeneration, but currently these strategies have not been explored.

Previously, we have shown that the preferential recruitment of non-classical "anti-inflammatory" monocytes ($CD45^{+}CD11b^{+}Ly6C^{low}$ in mice and $CD14^{low}CD16^{+}$ in humans) as opposed to classical "inflammatory" monocytes ($CD45^{+}CD11b^{+}Ly6C^{hi}$ in mice and

$CD14^{+}CD16^{-}$ in humans) promotes microvascular network expansion after sterile injury through modulation of the local inflammatory environment [18, 71, 131]. Following recruitment to inflamed tissue, monocytes may transiently persist in their undifferentiated state or differentiate into macrophages. In addition to tuning monocyte recruitment, modulation of macrophage phenotype has been utilized as a strategy to direct tissue regeneration [63, 64, 70, 132-134]. Macrophages exhibit different phenotypes based on their gene and protein expression profiles, and these phenotypes have distinct effector functions that can drive inflammatory processes or promote tissue regeneration[23, 24, 51]. Classically-activated (M1) macrophages that are activated in response to injurious or infectious stimuli are strongly microbicidal, produce reactive nitrogen and oxygen intermediates, and release pro-inflammatory cytokines such as tumor necrosis factor-α (TNF-α), interleukin (IL)-1β, and IL-12[45, 52, 66, 135]. M1 macrophages are implicated in initiating and sustaining inflammation, especially in the context of biomaterial implants, where persistent M1 activation can lead to chronic inflammation and fibrosis[136, 137]. In contrast, alternatively activated (M2) macrophages can be activated by canonical anti-inflammatory cytokines such as IL-4, IL-10, and IL-13, as well as in response to fungal cells, parasites, and apoptotic cells[45, 138]. M2 macrophages are in turn considered to generally possess anti-inflammatory actions through the release of cytokines such as IL-10, as well as support angiogenesis and tissue repair [70, 132, 133]. Therefore, dual-acting therapies that both suppress damaging inflammation via blockade of excessive neutrophil accumulation acutely and also promote the action of anti-inflammatory, proresolving monocytes and macrophages throughout the progression of inflammation represent a promising strategy to enhance tissue repair after injury.

In this study, we investigate how localized delivery of AT-RvD1 from polymer scaffolds modulates the accumulation of circulating neutrophils and monocytes after injury. We show that AT-RvD1 released from poly(lactic-co-glycolic acid) (PLGA) scaffolds retains the ability to inhibit neutrophil function and increase macrophage activity. Using the murine dorsal skinfold window chamber as a model of sterile inflammation and inflammatory vascular remodeling, we demonstrate that AT-RvD1-loaded PLGA scaffolds decrease the frequency of neutrophils and their infiltration into tissue while simultaneously increasing the frequency of anti-inflammatory $Ly6C^{lo}$ monocytes and CD206+ alternatively activated macrophages. Biomaterial delivery of AT-RvD1 resulted in significantly higher numbers of anti-inflammatory monocytes than a single topical dose of dissolved AT-RvD1 immediately following injury. In this work, we show that local delivery of aspirin-triggered resolvin D1 (AT-RvD1) via biomaterial scaffold is able to enrich injured tissue with pro-angiogenic neutrophils, presenting a novel small molecule-based strategy for enhancing early angiogenesis through neutrophil subsets. Additionally, we observed a shift in the peri-implant cytokine profile towards a pro-angiogenic microenvironment. AT-RvD1 materials increased microvascular arteriolar diameter and vascular tortuosity, and increased the density of CD31+ microvasculature. These results indicate that biomaterial delivery of AT-RvD1 can alter the tissue microenvironment after injury to one that supports resolution of inflammation and tissue regeneration.

3.3 Results

3.3.1 PLGA films release bioactive AT-RvD1

PLGA thin films were fabricated to encapsulate and rapidly release encapsulated AT-RvD1. The release of AT-RvD1 was measured through the use of a gradient method via HPLC using a UV-Vis detector at a wavelength of 301nm. Known concentrations of AT-RvD1 were tested using this method and the retention time was found to be centered around 8.6 minutes. To assess AT-RvD1 release kinetics, unloaded PLGA films or films loaded with AT-RvD1 were incubated in PBS. The AT-RvD1 peak was detected during analysis of the AT-RvD1 release samples, while no peaks were detected corresponding to this retention time when empty PLGA films were tested (Figure 1A-B). The AT-RvD1-loaded PLGA films released 1.2±0.2ng of the loaded AT-RvD1 after 1 hour, 7.2±0.3ng after 24 hours, 8.6±0.2ng after day 3, and 10.3±0.1ng after day 7 (Figure 1C-D). Release after 7 days was below the limits of detection. To further characterize the films, scanning electron microscopy was used to observe the surface of the films. No observed differences

were seen in the surface morphology of AT-RvD1-loaded or empty PLGA films (Figure 1E-F).

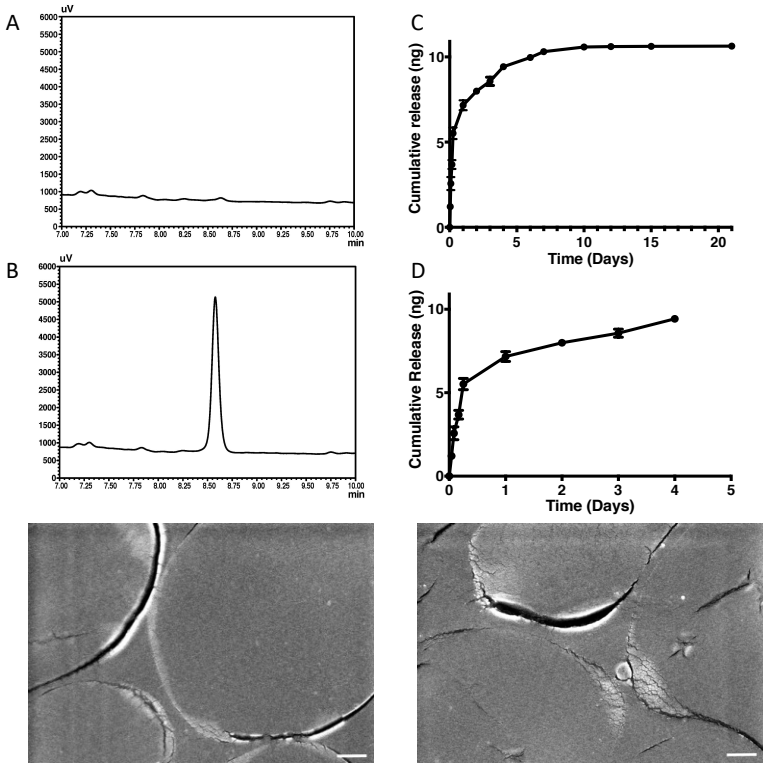

Figure 1 HPLC Measurements of AT-RvD1 Release. (A) HPLC chromatograph of unloaded PLGA scaffold. (B) HPLC chromatograph of PLGA scaffold loaded with AT-RvD1. Arrow demonstrates AT-RvD1 elution peak. (C) Release profile of AT-RvD1 loaded into PLGA scaffolds. (D) Early release of nearly 80% of AT-RvD1 is achieved over 3 days.

After we verified release of AT-RvD1 from PLGA films, the bioactivity of released AT-RvD1 was assessed. Previous studies have shown that exposure to resolvins increase macrophage phagocytic ability, therefore a phagocytosis assay was used to confirm AT-RvD1 bioactivity after release from PLGA films[139]. Cell culture media was incubated with AT-RvD1-loaded PLGA films or empty PLGA films AT-RvD1 for 24 hours and then used to treat RAW264.7 macrophages. Based on HPLC measurements, the films released an average of 7.5±0.6ng AT-RvD1 into RAW264.7 cell culture media over 24 hours. After

4 hours of treatment, phagocytic ability was measured using fluorescent latex beads. RAW264.7 macrophages that were treated with media containing released AT-RvD1 exhibited increased phagocytosis of latex beads, as visualized using fluorescence microscopy (Figure 2A-B). Quantification of the number of phagocytosed latex beds indicated increases in the overall phagocytic activity of macrophages treated with AT-RvD1 film release media (Figure 2C). As a secondary metric of bioactivity, we treated MPRO neutrophils with release media derived from AT-RvD1 films. Neutrophils treated with media incubated with AT-RvD1-loaded PLGA films exhibited significantly decreased MPO activity after both 30 and 60 minutes compared to neutrophils treated with media incubated with unloaded PLGA films (Figure 2D). Taken together, these results demonstrate that AT-RvD1 maintains its bioactivity after release from PLGA films and promotes myeloid cell functions induced by native AT-RvD1.

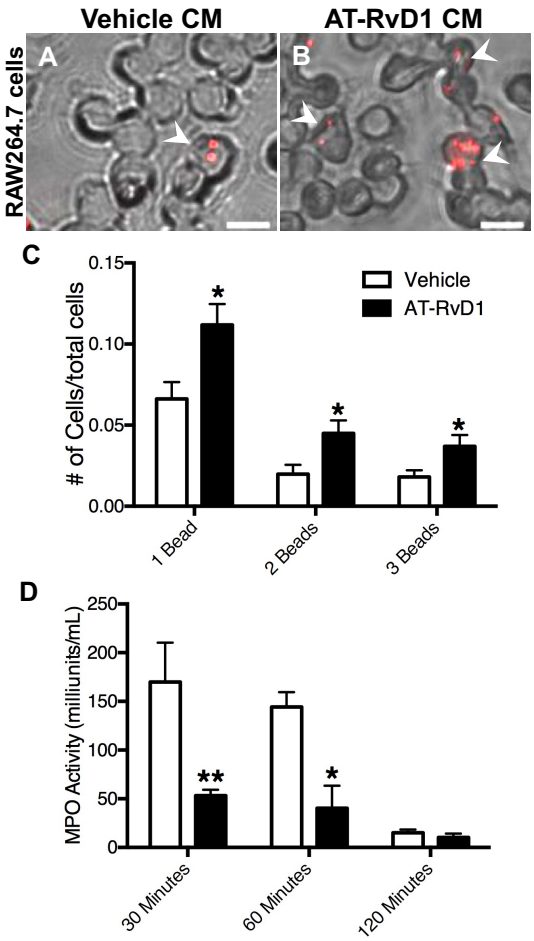

Figure 2. Released AT-RvD1 promotes macrophage phagocytosis and inhibits neutrophil myeloperoxidase (A-B) Brightfield and epifluorescence micrographs of RAW264.7 macrophages treated with PLGA film-conditioned media (Vehicle CM) or AT-RvD1 conditioned media (AT-RvD1 CM). White arrowheads indicate engulfed beads by macrophages. Scale bar, 5μm (C) Quantification of phagocytic activity of RAW264.7 macrophages. (D) Myeloperoxidase activity of MPRO-differentiated neutrophils decreases significantly after treatment with AT-RvD1 conditioned media. Data presented as mean ± S.E.M. Statistical analyses were performed using two-tailed t-tests *p<0.05, **p<0.01 n=3 samples per group.

3.3.2 AT-RvD1 delivery decreases neutrophil infiltration in the acute phases of inflammation

To explore myeloid cell influx during the inflammatory cascade, the murine dorsal skinfold window chamber model was used. This model allows for longitudinal intravital

imaging of host responses to biomaterial implants including remodeling of microvascular networks and changes to the innate immune response following injury and material implantation[18, 71, 131]. To evaluate the in vivo infiltration of circulating neutrophils, we utilized whole mount immunohistochemistry (IHC) and flow cytometry at days 1 and 3 after implantation of AT-RvD1-loaded PLGA or unloaded PLGA onto the dorsal tissue. For initial analysis, an additional group consisting of 100ng AT-RvD1dissolved in 200 μL sterile saline was added to compare the effects of one-time bolus delivery with biomaterial-mediated delivery. This dosage was chosen based on previous studies utilizing AT-RvD1[121]. Neutrophils were immunophenotyped as CD45+CD11b+Ly-6C+Ly-6G+[140]. At day 1, neutrophils were the dominating cell type present out of all CD45+CD11b+ myeloid cells. In the tissue, animals treated with AT-RvD1 scaffolds and saline-AT-RvD1 solution had a significantly lower frequency of neutrophils compared to animals that received unloaded PLGA scaffolds (Figure 3A). This decrease in neutrophils present in the tissue was accompanied by a significant increase in the neutrophil frequency within the blood of AT-RvD1-treated mice, but not in mice receiving the saline-AT-RvD1 solution (Figure 3B). All groups undergoing dorsal skinfold window chamber surgery demonstrated elevation of blood neutrophils relative to uninjured control animals; however, neutrophils were even further elevated in the AT-RvD1 scaffold group (Figure 3C). By day 3, there were no differences in tissue or blood neutrophils in either group, but the overall proportion of neutrophils out of all CD45+CD11b+ cells decreased greatly, likely due to the influx of CD45+CD11b+ monocytes (Figure 4A-B). After 1 day, the proportion of pro-angiogenic neutrophils expressing CD49d remained unchanged between animals given AT-RvD1-loaded implants and PLGA-only implants in both blood and

tissue (Figure 3D-E). However, after three days there were significantly more CD49d+ neutrophils present in the tissue of animals treated with AT-RvD1 scaffolds, but no differences were observed in the blood (Figure 3F-G).

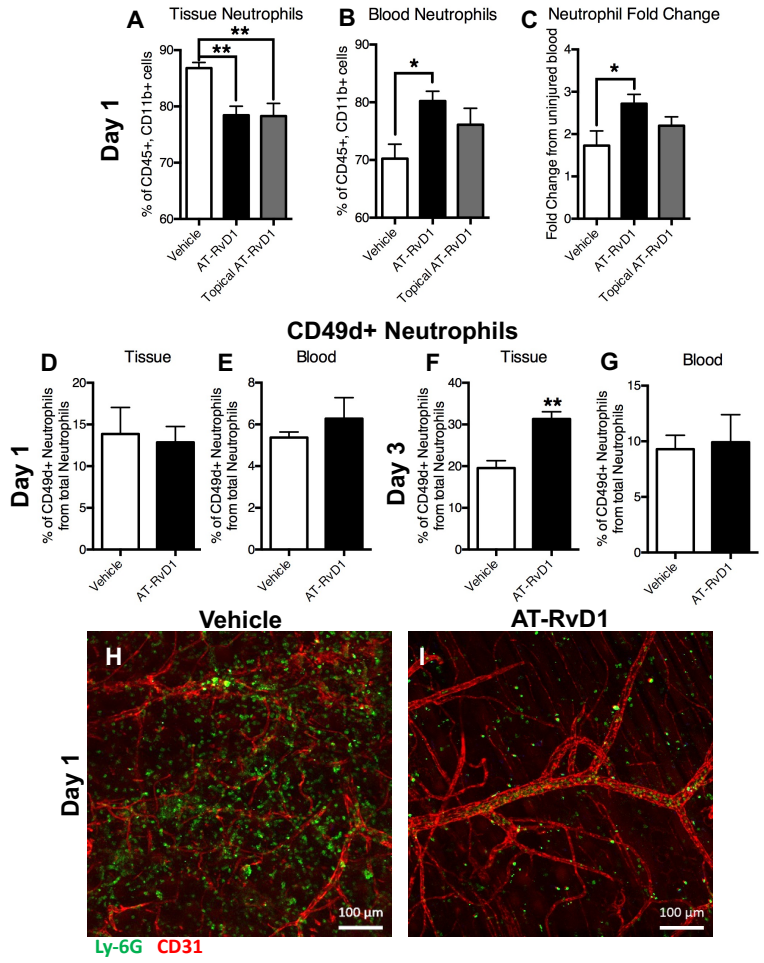

Figure 3. AT-RvD1 treatment sequesters neutrophils in the blood compartment after 1 day. Flow cytometric analysis of neutrophils after 1 day in the (A) blood and (B) tissue. (C) Fold change in blood neutrophils after 1 day compared to blood from an uninjured mouse. (D-G) Analysis of CD49d+ neutrophils in tissue and blood at 1 and 3 days after film implantation (H-I) Whole mount immunostaining of Ly-6G+ neutrophil infiltration into tissue one day after PLGA or AT-RvD1-loaded PLGA film implant. Scale bars, 100µm. Data presented as mean ± S.E.M. Statistical analyses were performed using one-way ANOVA with Tukey's post-hoc test *p<0.05, **p<0.01 n=4-6 animals per group.

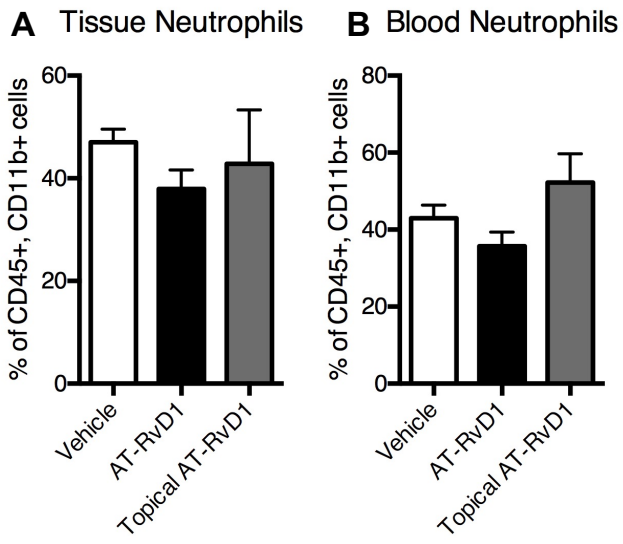

Figure 4 Tissue and Blood Neutrophils three days after PLGA film implant. The overall proportion of neutrophils out of CD45+ CD11b+ cells decreases after three days. Flow cytometric analysis of neutrophils in the (A) dorsal tissue and (B) blood three days after surgery.

Qualitative confocal micrographs taken 24 hours after surgery reveal a larger number of Ly-6G+ neutrophils in the tissue of mice treated with control PLGA films compared to AT-RvD1 film treated animals (Figure 3H-I). A 3D transformation representing the distance from CD31+ vasculature was overlaid onto Imaris-rendered images to analyze the distance that neutrophils had invaded into the extravascular tissue space (Figure 5A-D). Neutrophils in the peri-implant area of PLGA-only scaffolds were able to migrate significantly further into the interstitial tissue than neutrophils in the peri-implant area of AT-RvD1-loaded PLGA scaffolds after 1 day post-injury (Figure 5C). However, no difference was found in neutrophil migration through interstitial tissue after 3 days (Figure 5D). Additionally, 3D analysis of total cell numbers revealed that tissue surrounding AT-RvD1 implants have significantly fewer Ly-6G+ neutrophils at both days 1 and 3 after scaffold implantation (Figure 5E-F). Collectively, these data suggest that local

release of AT-RvD1 can suppress neutrophil infiltration and migration in the early stages of inflammation.

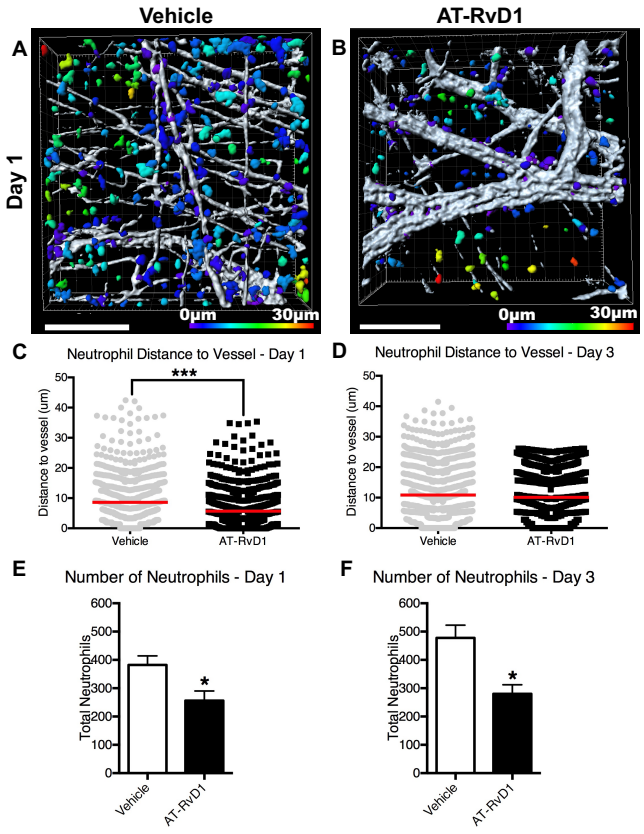

Figure 5. Localized AT-RvD1 delivery limits neutrophil migration through inflamed dorsal tissue. (A-B) Renderings of neutrophil distance from CD31+ vasculature one day after film implantation (representative Imaris renderings of Ly-6G+ cells, color-coded according to distance from the closest CD-31+ blood vessel: purple=0µm, red= 30µm) (C-D) Quantification of neutrophil distance to vessel at post-implant days 1 and 3. Imaris 3-d quantification of neutrophil numbers after (E) one day and (F) three days. Statistical analyses were conducted using two-tailed Mann-Whitney test (C-D) and two-tailed t-test (E-F) *$p<0.05$, ***$p<0.001$, $n>100$ cells, across 3-4 animals per group. Scale bars, 100µm

3.3.3 AT-RvD1 Delivery Increases the Proangiogenic Neutrophil Population After Injury

At one and three days following surgery and implantation of either AT-RvD1-loaded or empty PLGA (vehicle) biomaterial films onto dorsal tissue, the accumulation of neutrophils was assessed through flow cytometry and subsequent SPADE of the generated

data (Figure 6A). The resultant SPADE trees are displayed in Figure 6B and Figure 7A. The SPADE partitioning algorithm was first able to separate a cluster of CD49d+ cells from the greater Ly6G+ neutrophil tree (Figure 6B) and a smaller subset of neutrophils expressing high levels of VEGFR1, and CXCR4 from this CD49d+ branch (black box, Figure 6B). This second cluster of CD49d+ CXCR4+ VEGFR1+ cells was determined to be the pro-angiogenic neutrophils described by Massena et al, and the frequencies of cells within these clusters were measured compared to the rest of the SPADE tree[44].

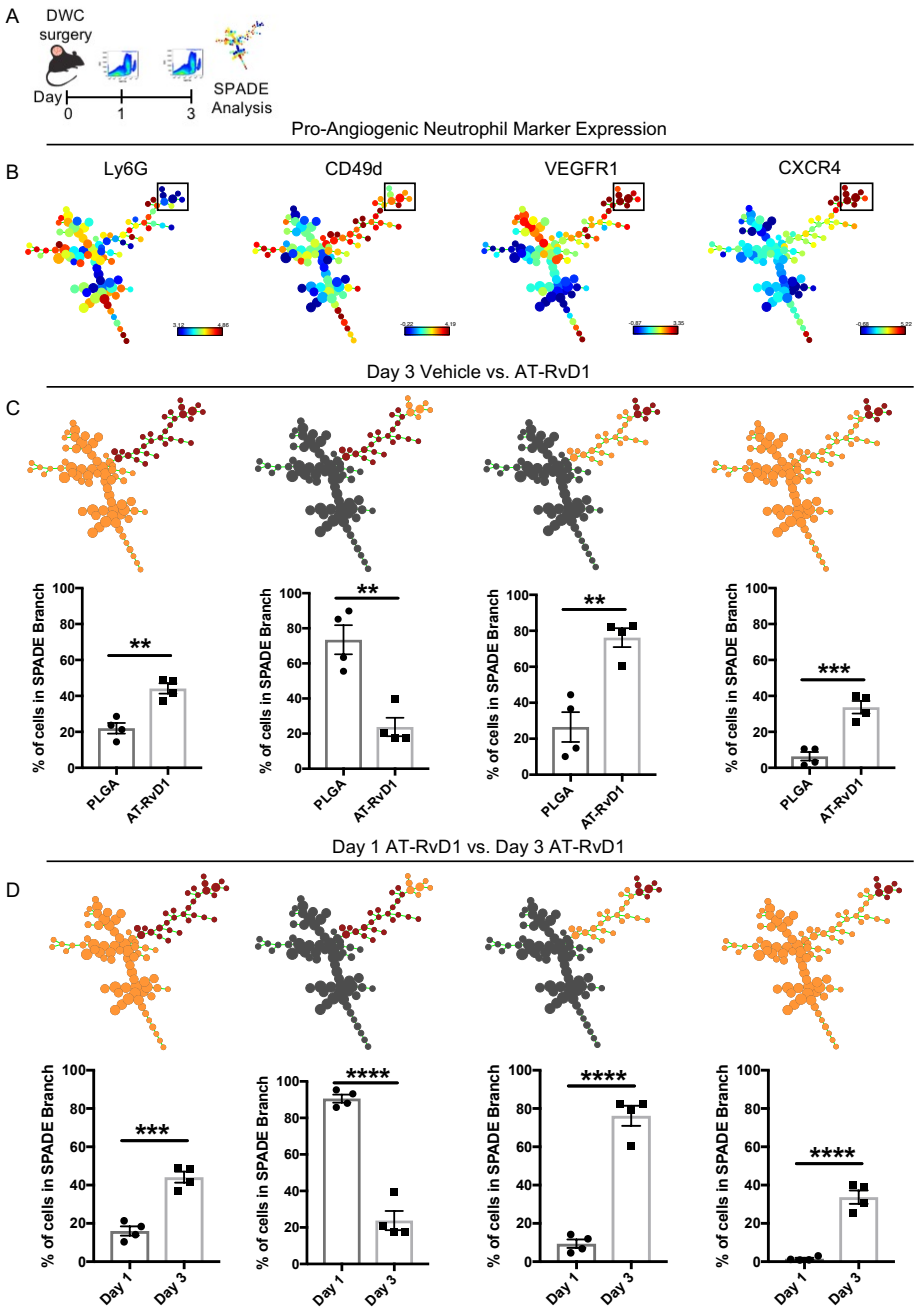

Figure 6. SPADE Analysis of Neutrophil Subsets. (A)Experimental schematic (B) SPADE trees colored by pro-angiogenic neutrophil marker expression. The black box indicates the population identified by SPADE as proangiogenic neutrophils. (C) Cell frequency within highlighted branches at day 3 in AT-RvD1 vs vehicle. (D) Cell frequency in the same branches comparing day 1 AT-RvD1 and day 3 AT-RvD1 Data presented as mean ± S.E.M. Statistical analyses were performed using two-tailed t-tests *p<0.05, **p<0.01, ***p<0.001, ****p<0.0001 n=4 samples per group When comparing the

frequencies of neutrophils in these clusters, no differences were found between vehicle and

AT-RvD1-loaded films at 1 day after biomaterial implant or when comparing groups receiving unloaded films at days 1 and 3 (Figure 7B-C). We then analyzed cell frequencies between vehicle and AT-RvD1-loaded films at day 3 and found that delivery of AT-RvD1 significantly increased CD49d+ neutrophils (Figure 6C). Additionally, we found that within the CD49d+ cluster, cells contained in the pro-angiogenic neutrophil cluster were significantly increased after AT-RvD1 treatment, comprising nearly 80% of the CD49d+ cluster and 40% of the total neutrophils (Figure 6C). Finally, we analyzed AT-RvD1-treated neutrophils at days 1 and 3 and saw significant increases in the pro-angiogenic neutrophil clusters at day 3 (Figure 6D). We also applied tSNE, another dimensionality reduction technique to the flow cytometry data and were able to visualize clusters of CD49d+ neutrophils at days 1 and 3, and we saw increased clustering of AT-RvD1-treated samples around the CD49d+ cluster, lending further support to our SPADE analysis (Figure 8). These results demonstrate that treatment of injured tissue with AT-RvD1, a proresolving lipid mediator, is able to increase CD49d+ pro-angiogenic neutrophils by day 3 after injury.

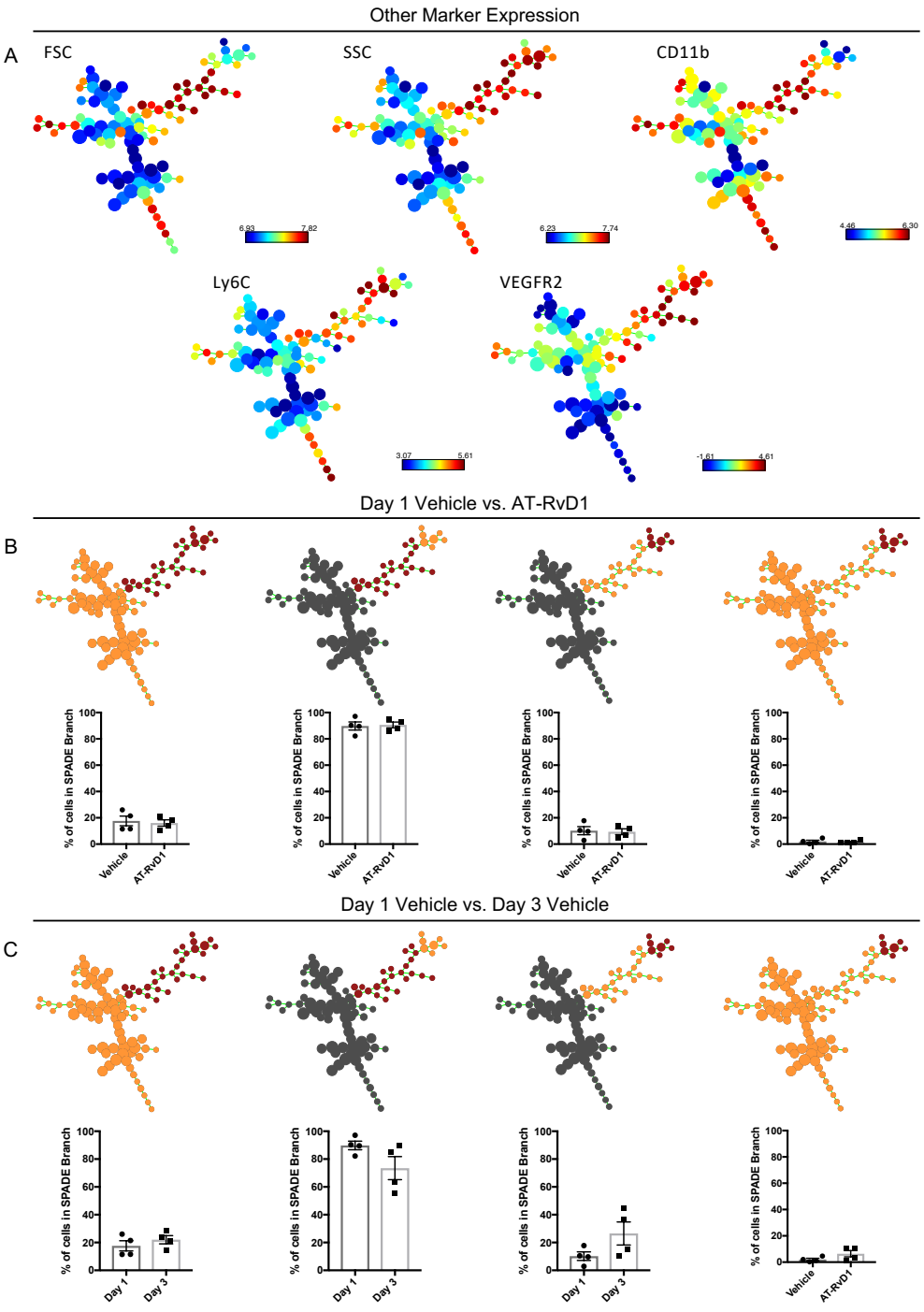

Figure 7. Additional Neutrophil SPADE Analysis.(A) SPADE trees colored by marker expression levels of remaining panel markers (B-C) Analysis of cell frequency in the highlighted SPADE branches comparing Day 1 vehicle vs AT-RvD1 and Day 1 vehicle vs Day 3 Vehicle. Data presented as mean ± S.E.M. Statistical analyses were performed using

two-tailed t-tests n=4 samples per group .

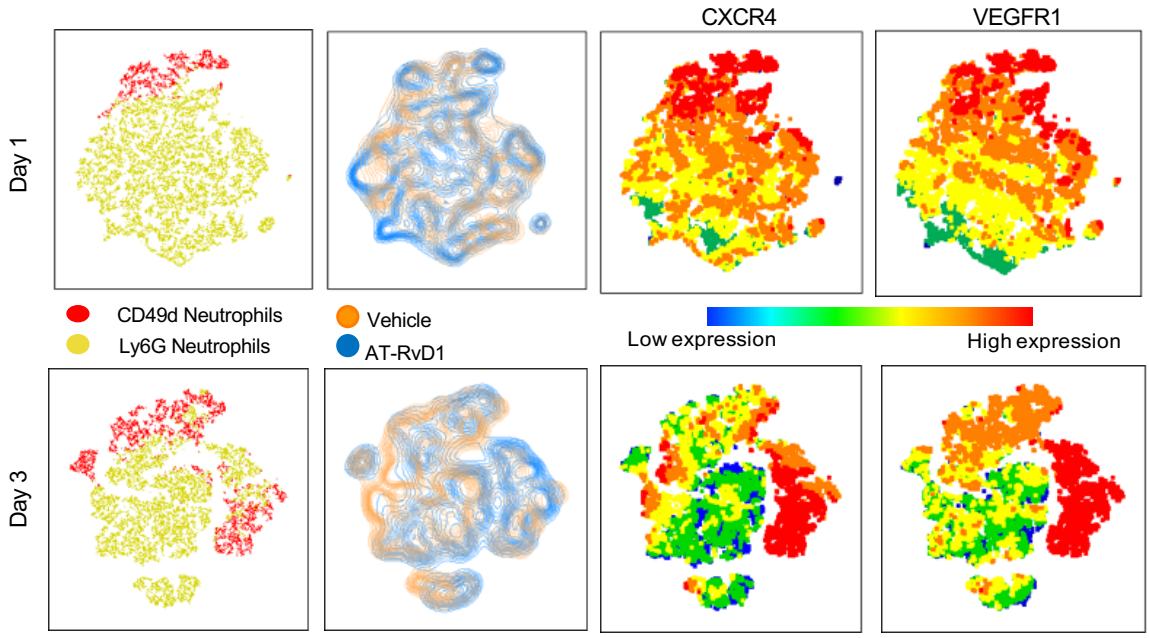

Figure 8. tSNE of Neutrophils at Days 1 and 3. tSNE analysis applied to Ly6G+ neutrophils at days 1 and 3 following PLGA film implantation. Plots show separation of CD49d+ neutrophils from total neutrophils by CXCR4 and VEGFR1 surface marker expression .

3.3.4 Proangiogenic Neutrophils Treated with AT-RvD1 Display Enhanced Perivascular Positioning

We then utilized while mount IHC and 3d rendering of confocal images to visualize the position of classical Ly6G+ CD49d- and pro-angiogenic neutrophils in peri-implant areas (Figure 9A-B). Contrary to SPADE analysis, we observed significant increases in the numbers of CD49d+ neutrophils in AT-RvD1-treated peri-implant tissue one day after surgery compared to vehicle (Figure 9C,E). This finding is most likely due to local changes near the implants that are too small in magnitude to affect the overall cellular profile assessed by SPADE. This significant increase in CD49d+ neutrophils was also observed at day 3 compared to vehicle (Figure 9G). These increases in CD49d+ neutrophil number

were accompanied by subsequent significant decreases in both CD49d- neutrophils but also total neutrophil numbers compared to vehicle at days 1 and 3 (Figure 10A-D). It has been established that AT-RvD1 is able to inhibit the extravasation of classical neutrophils into inflamed tissue. Due to the ability of pro-angiogenic neutrophils to migrate independently from classical neutrophils, their infiltration is not inhibited and even enhanced by AT-RvD1 treatment. In addition to observed increases in total CD49d+ numbers, the neutrophils exposed to local AT-RvD1 were significantly closer to CD31+ vasculature versus vehicle control at both days 1 and 3 (Figure 9 F,H and Figure 10). Given the importance of these CD49d+ pro-angiogenic neutrophils to the process of vascular remodeling, and recent findings that pro-angiogenic neutrophils migrate to areas of new vascular budding, their proximity to CD31+ vessels after injury may indicate their participation in forming new vessel networks.

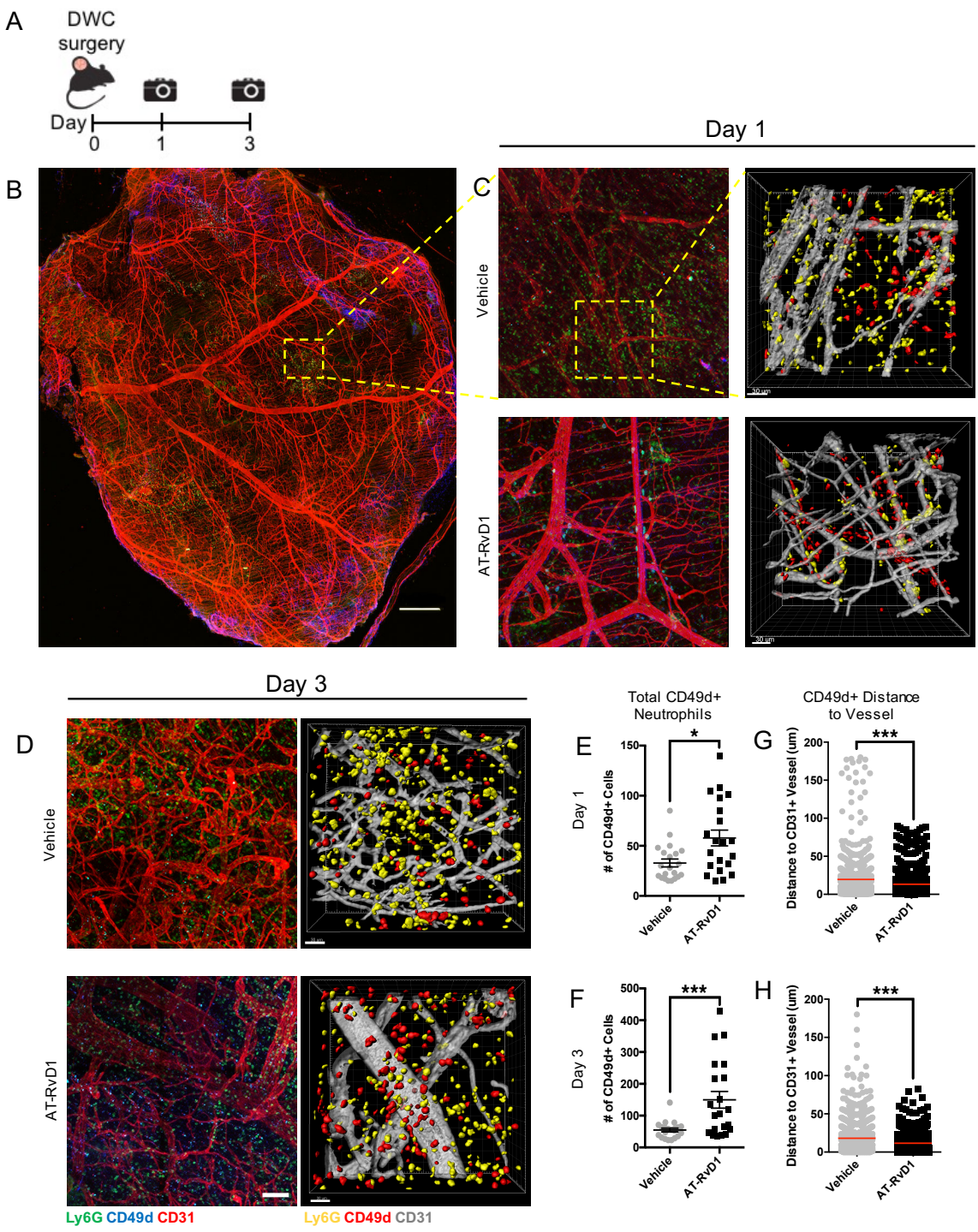

Figure 9. Recruitment and infiltration of CD49d+ neutrophils into dorsal tissue(A) Experimental schematic. (B) 10x image of the whole mount dorsal skin tissue (C) Confocal images and Imaris renderings of neutrophil infiltration into tissue at day 1 (D) Confocal images and Imaris renderings of neutrophil infiltration into tissue at day 3 (E-H) Quantification of Imaris renderings for total CD49d+ neutrophils and distance to CD31+

vessel at days 1 and 3. Statistical analyses were conducted using two-tailed Mann-Whitney test (G-H) and two-tailed t-test (E-F) *p<0.05, ***p<0.001, n>100 cells, across 3-4 animals per group. Scale bars, 500 µm for 10x confocal, 100µm for 20x confocal, and 30 µm for Imaris

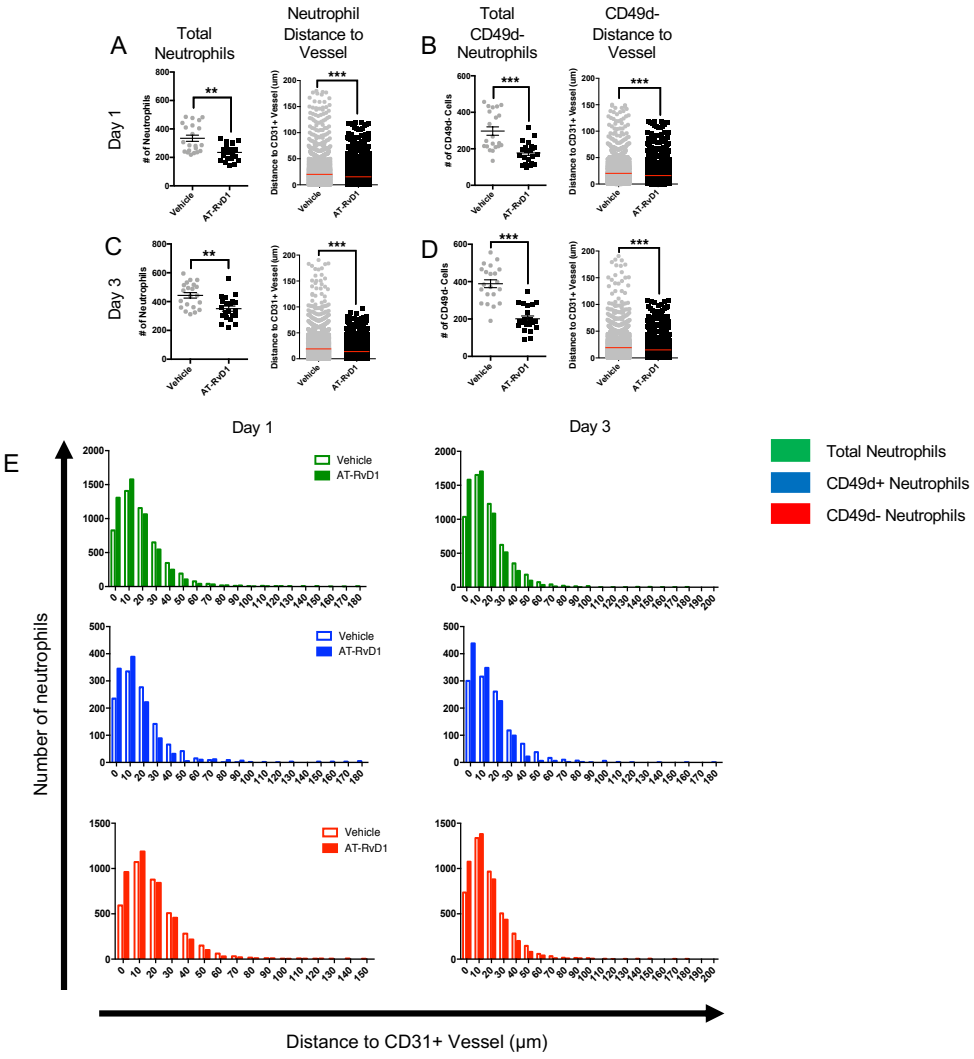

Figure 10. Neutrophil population distance to vessel measurements(A-D) Quantification of Imaris renderings for total neutrophils and CD49d- neutrophils. (E) Histograms showing number of neutrophils found within each distance to vessel measurement. Statistical analyses were conducted using two-tailed Mann-Whitney test (B,D) and two-tailed t-test (A,C) *p<0.05, **p<0.01, ***p<0.001, n>100 cells, across 3-4 animals per group .

These findings represent not only a previously unknown action of AT-RvD1, but also promotes the idea that specific subsets of neutrophils are able to be targeted. Angiogenesis is a complex process that is critical for wound healing and tissue regeneration

after injury. Previously, other immune subpopulations including monocytes and macrophages have been targeted for their roles in the angiogenic process but targeting the newly discovered pro-angiogenic neutrophil subset has not been explored until now. These exciting new findings have the potential to further our understanding of what mechanisms govern early angiogenesis and how we are able to direct the cells involved through exogenous factors to enhance vascular network expansion in many contexts.

3.3.5 AT-RvD1 increases anti-inflammatory monocyte and macrophage populations

In addition to exploring the effect of local AT-RvD1 on neutrophil infiltration, we examined the accumulation of monocyte and macrophage subsets after injury to the dorsal skin. After 3 days, 3D renderings show more CD68+ monocytes/macrophages in the peri-implant tissue of mice treated with AT-RvD1-loaded scaffolds (Figure 11A-B). Following quantification, AT-RvD1-treated animals were found to have significantly more CD68+ monocytes/macrophages than PLGA-only animals (Figure 11C). Further analysis of 3D renderings reveals a significantly lower neutrophil-to-monocyte/macrophage ratio in animals treated with AT-RvD1 scaffolds compared to animals that received unloaded PLGA scaffolds (Figure 11D). An increase in the ratios of neutrophils to other subsets of white blood cells have been associated with persistent inflammation and poor clinical outcomes in malignancy and wound healing[141-143].

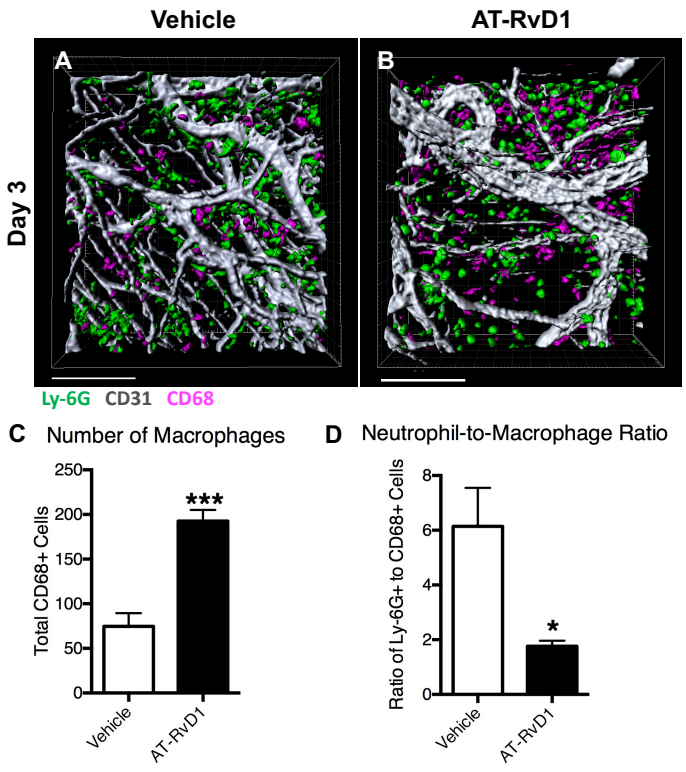

Figure 11. Local delivery of AT-RvD1 increases CD68+ monocytes and macrophages. (A-B) Imaris renderings of CD68+ macrophage and Ly-6G+ neutrophil accumulation. (C) Quantification of CD68+ cells found in each Imaris rendering after 3 days. (D) Neutrophil to monocyte/macrophage ratio. Scale bars, 100µm. Data presented as mean ± S.E.M. Statistical analyses were performed using two-tailed t-test *p<0.05, ***p<0.001, n>100 cells, across 3-4 animals per group.

In order to further examine the hypothesis that biomaterial-delivered AT-RvD1 can influence the accumulation of anti-inflammatory immune cells, we performed flow cytometry to further characterize myeloid cell subpopulations present in the inflamed dorsal tissue. Analysis 1 day after injury indicated that there were no differences in CD45+CD11b+Ly-6CLo anti-inflammatory monocytes (AM) or CD45+CD11b+Ly-6CHi inflammatory monocytes (IM) in the tissue for all groups (Figure 13A-B). After 3 days, there were significantly more AMs present in dorsal tissue that had received an AT-RvD1-loaded implant compared to the PLGA only group or a topical dose of AT-RvD1 in solution

immediately following surgery (Figure 12A). Conversely, there were significantly fewer IMs present in the AT-RvD1 treated dorsal tissue compared to PLGA-only and topical AT-RvD1 treatments (Figure 12B). The ratio of AM to IM in the dorsal tissue was significantly higher in the AT-RvD1 film-treated animals than in AT-RvD1 topical application or empty PLGA implant-treated animals (Figure 12C).

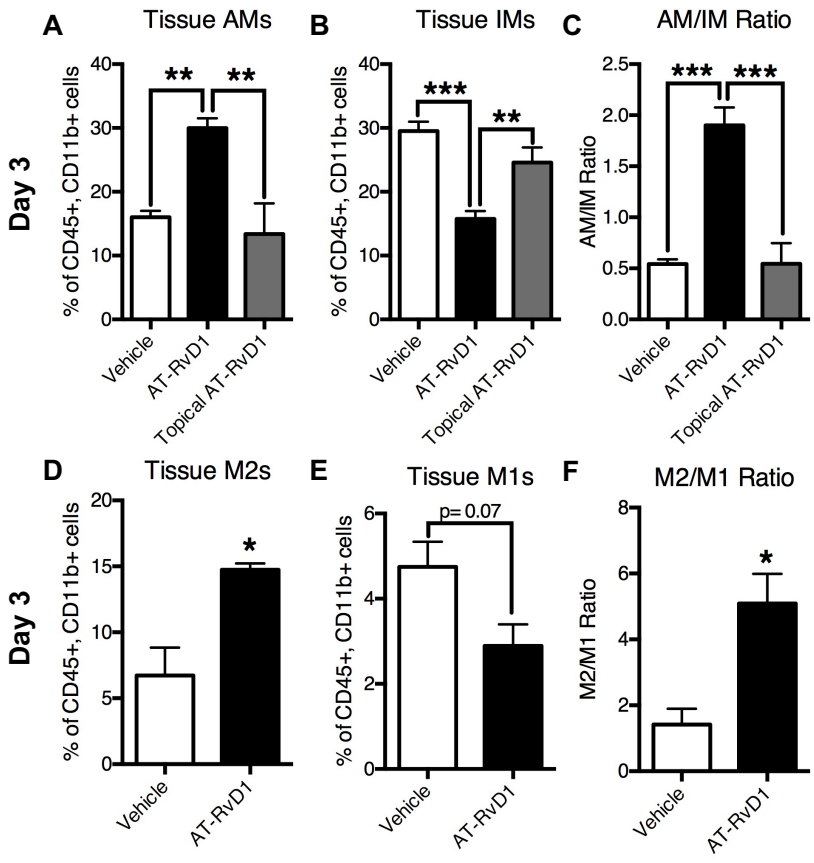

Figure 12. Biomaterial delivery of AT-RvD1 promotes AM and CD206+ macrophage accumulation. Flow cytometric analysis of (A) Ly-6CLo AMs and (B) Ly-6CHi IMs. (C) Tissue AM/IM ratio. Analysis of (D) M2 (F4/80+ CD206+ CD86-) macrophages and (E) M1 (F4/80+ CD206- CD86+) macrophages at day 3. (F) M2/M1 "regenerative ratio" analysis. Data presented as mean ± S.E.M. Statistical analyses were performed using one-way ANOVA with Tukey's post-hoc test or two-tailed t-test *p<0.05, **p<0.01, ***p<0.001 n=4-6 animals per group

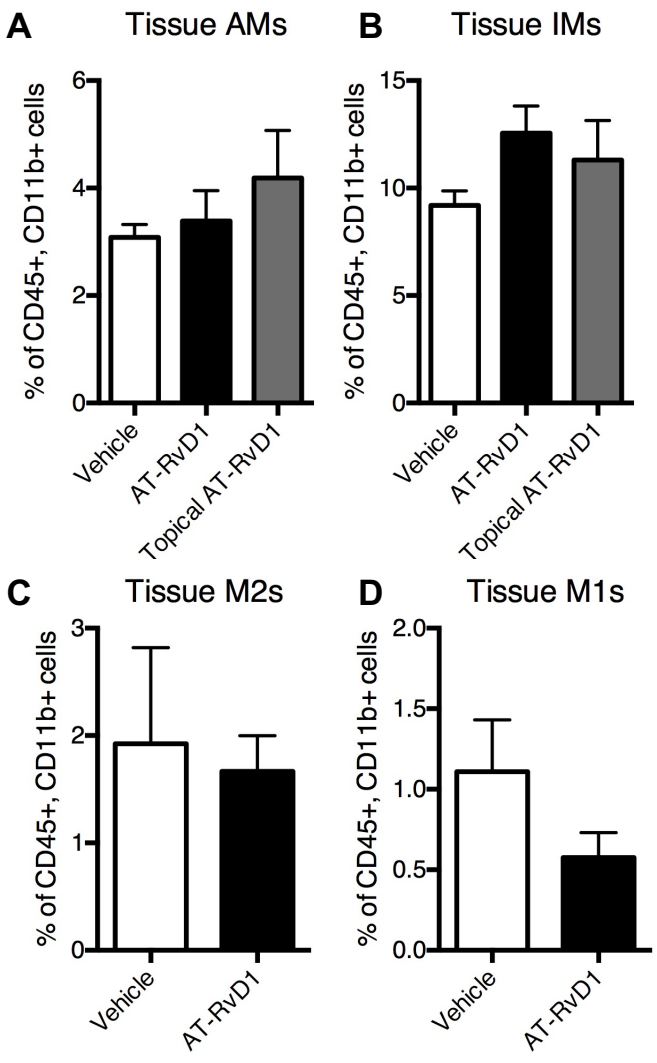

Figure 13. Tissue monocyte and macrophage levels are unchanged 1 day after surgery. Flow cytometric analysis of (A) AMs, (B) IMs, (C) M2s, and (D) M1s present in dorsal tissue

We next immunophenotyped subpopulations of macrophages to explore how AT-RvD1 delivery impacts macrophage accumulation. No differences were found in the frequency of total macrophages between AT-RvD1-loaded PLGA implants and PLGA-only implants after 1 day (Figure 13C-D). Analysis of digested dorsal tissue after 3 days showed that there was a significant increase in the presence of F4/80+CD86-CD206+ macrophages, an immunophenotype indicative of M2 or alternatively activated

macrophages[138], in the AT-RvD1 treated mice (Figure 12D). The proportion of M1 classically activated F4/80+CD86+CD206- macrophages showed a trend of decrease (Figure 12E); however, the ratio of M2 to M1 macrophages was significantly increased in animals treated with AT-RvD1-loaded implants. Increases in the ratio of M2 to M1 macrophages have been correlated with increased tissue healing and has consequently been called the "regenerative ratio" [70] (Figure 12F). Taken together, this data shows that local AT-RvD1 treatment both increases the overall frequency of macrophages present in inflamed dorsal tissue after 3 days and induces accumulation of monocyte and macrophage subsets that have been associated with tissue regeneration and wound healing.

3.3.6 AT-RvD1 modulates cytokine expression levels in dorsal tissue

To better understand how AT-RvD1 delivery impacts the production of inflammatory mediators, multiplexed protein analysis was performed on peri-implant dorsal tissue both 1 and 3 days post-surgery. The expression levels of known pro-angiogenic and anti-inflammatory cytokines were significantly increased both 1 and 3 days after surgery. There was an increase in the level of VEGF in the AT-RvD1 implant tissue after 1 day compared to PLGA implant tissue, which decreased for both groups by day 3 (Figure 14A). IL-4 expression levels were significantly increased at both day 1 and day 3 in AT-RvD1 implant tissue, but day 3 expression in AT-RvD1 treated animals was decreased compared to day 1 levels (Figure 14B) and the level of SDF-1α was significantly increased at day 3 in animals treated with AT-RvD1 implants (Figure 14C). Expression levels of other proteins such as MMP-9 and FGF-b were unchanged between AT-RvD1-implant and PLGA implant animals (Figure 15A-B). Levels of IL-10 were found to be no

different between AT-RvD1-implant and PLGA implant animals after 1 day, but all samples had IL-10 levels below the limit of detection at day 3 (Figure 15C).

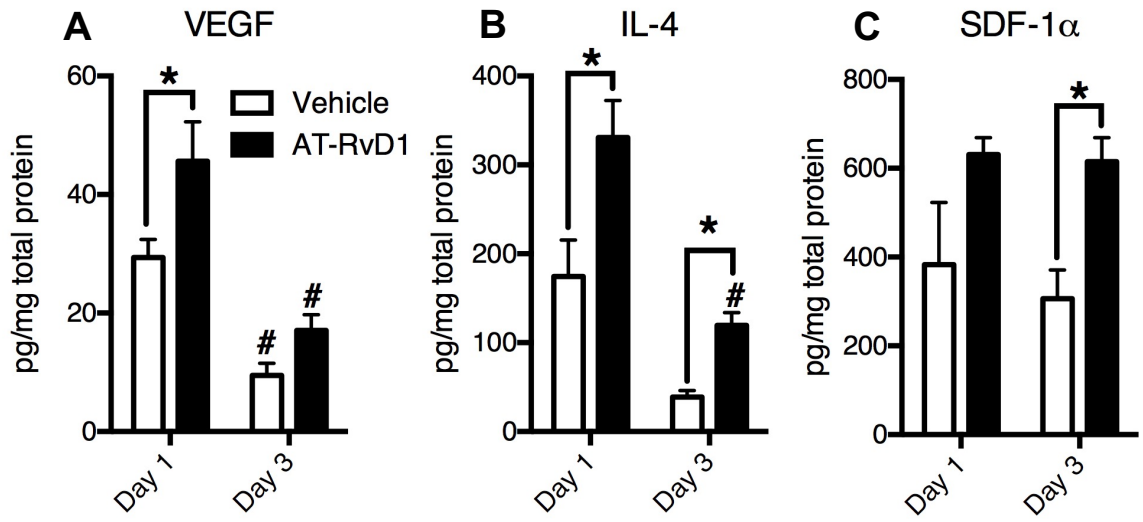

Figure 14. Local delivery of AT-RvD1 modulates the peri-implant cytokine profile towards regeneration and angiogenesis. (A) VEGF expression at 1 and 3 days post film implantation. (B) IL-4 expression at 1 and 3 days post film implantation. (C) SDF-1**α** expression at 1 and 3 days post film implantation. Data presented as mean ± S.E.M. Statistical analyses were performed using two-way ANOVA with Tukey's post-hoc test *$p<0.05$, #$p<0.05$ compared to day 1 expression levels n=3 animals per group.

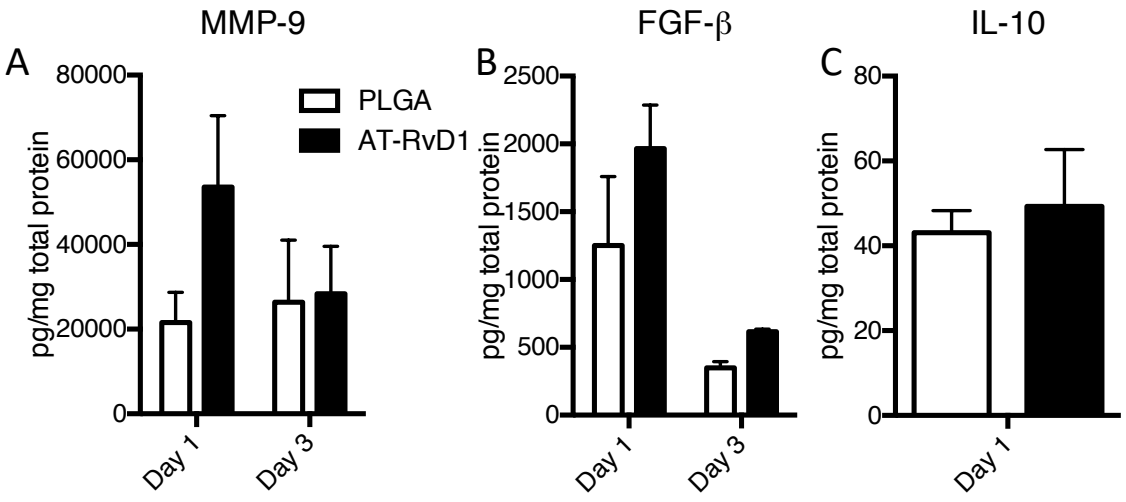

Figure 15. Cytokine levels in the dorsal skin tissue at 1 and 3 days post-surgery. Luminex multi-plex analysis of (A) MMP-9, (B) FGF-β, and (C) IL-10 expression is unchanged between groups after dorsal skinfold window chamber surgery.

3.3.7 AT-RvD1 enhances microvascular remodeling

In order to determine if the local delivery of AT-RvD1 to injured tissue promotes expansion and remodeling of microvascular networks, brightfield imaging of window chambers was conducted after material implantation (day 0) and again at day 3 after injury (Figure 16A-E). Micrographs were then assessed for changes in the vascular parameters of total length, arteriolar diameter, and vascular tortuosity, all of which are classic signs of microvascular remodeling[131]. The total length of vasculature normalized to the area of analysis (i.e. length density) was unchanged between groups after 3 days (Figure 16E). Conversely, a significant increase in both the arteriolar diameter and vascular tortuosity of AT-RvD1-treated animals was observed compared to animals receiving PLGA-only implants (Figure 16F-G). These changes to the vasculature can be observed in the micrographs of AT-RvD1 treatment (Figure 16D), and are absent in the peri-implant area of PLGA-only scaffolds (Figure 16B).

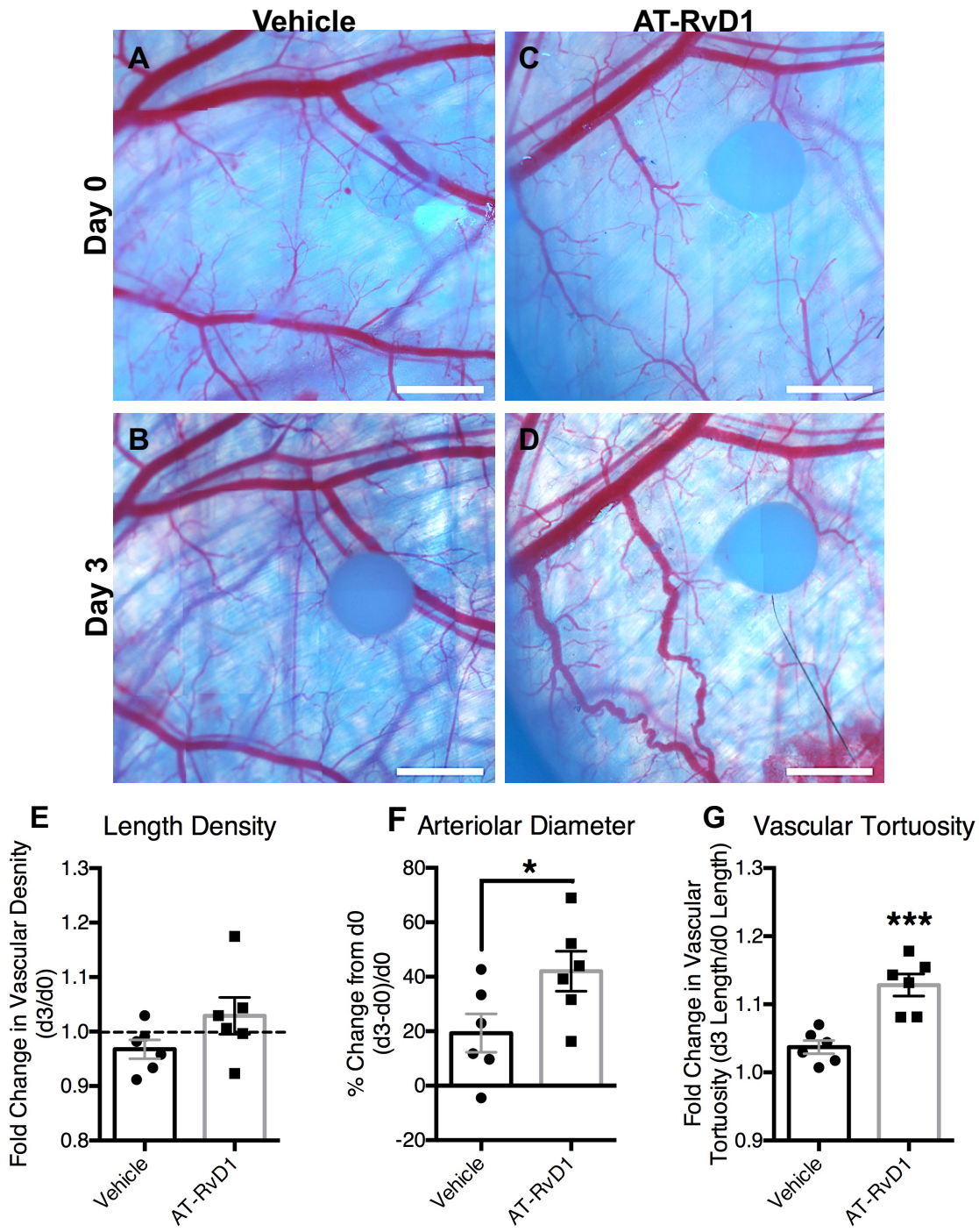

Figure 16. Delivery of AT-RvD1 promotes vascular remodeling. Brightfield micrographs of dorsal tissue at (A, C) day 0 and at (B, D) day 3 following treatment with AT-RvD1 loaded PLGA films. Quantification of the vascular metrics (E) length density, (F) arteriolar diameter, and (G) tortuosity. Data presented as mean ± S.E.M. Statistical analyses were performed using two-tailed t-tests *$p<0.05$, ***$p<0.001$ n=6 animals per group. Scale bars, 1mm

While we were unable to discern differences in vascular length density using brightfield imaging, we have previously demonstrated that whole mount CD31 immunostaining can reveal changes to capillary-level microcirculation that is undetectable by brightfield microscopy[71]. Whole mount confocal images of both background tissue away from the biomaterial implant and peri-implant CD31+ immunostained vessels revealed small vessels that were not observable with brightfield microscopy (Figure 17A-D). Analysis of CD31 length per unit area at one day after surgery revealed no differences in length density between background and peri-implant area in animals receiving AT-RvD1-loaded or empty PLGA implants (Figure 17E). However, at day 3, AT-RvD1 delivery from PLGA films significantly increased the density of CD31+ vessels near the implant compared to background and also compared to PLGA-only implant in the window chamber (Figure 17F).

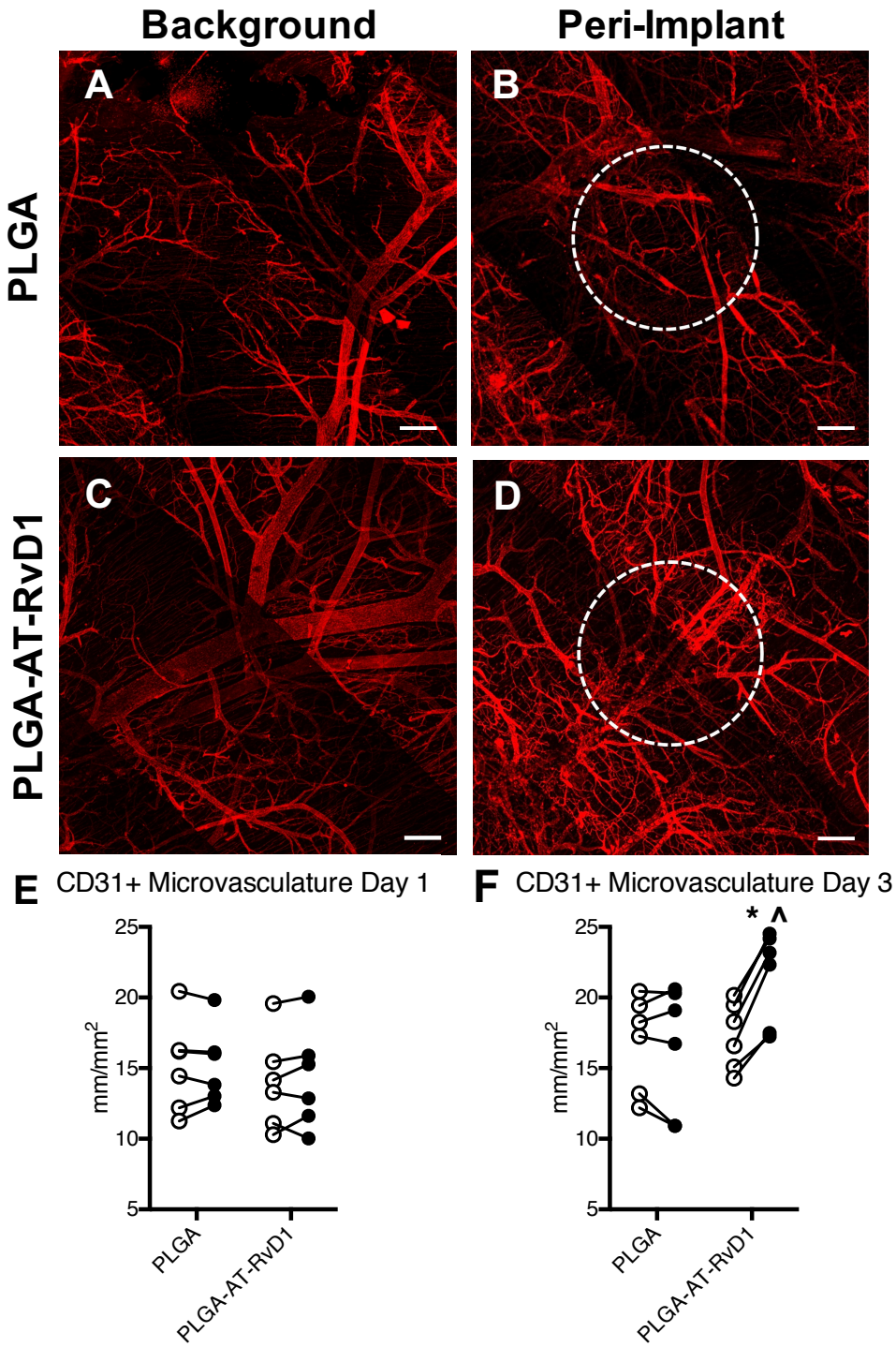

Figure 17. AT-RvD1 delivery enhances growth of CD31+ microvasculature. Whole mount confocal images of dorsal tissue at day 3 following treatment with AT-RvD1-loaded PLGA films. (A, C) Background microvasculature and peri-implant vasculature treated with (B) PLGA films and (D) AT-RvD1-loaded films. Quantification of microvascular length density at (E) day 1 and (F) day 3 after film implantation. ○= background

vasculature, ●= peri-implant vasculature. Statistical analysis was performed using Repeated Measures two-way ANOVA with Sidak's post-hoc test for multiple comparisons *$p<0.05$ compared to background, ^$p<0.05$ compared to PLGA implant, n=6, lines connect paired analysis of background and peri-implant vasculature in each animal.

3.4 Discussion

Acute inflammation is a protective response mounted by the host after injury and/or infection[91]. During acute inflammation, polymorphonuclear neutrophils are recruited to the site of inflammation through the expression of pathogen- or damage-associated molecular patterns [53]-[55]. These neutrophils, along with activated tissue resident macrophages, trigger the sequential release of proinflammatory mediators such as eicosanoids, cytokines, chemokines, and proteases, and these mediators drive leukocyte recruitment and activation[22, 53, 144]. In the case of a minor injury or infection, the acute inflammatory response will subside and return to homeostasis via the active process of inflammation resolution, signified by diminished number and activity of neutrophils and macrophage phenotype switching, phagocytosis, and egress[145, 146]. However, in large wounds or in diseases such as arthritis or atherosclerosis, acute inflammation may continue unabated and progress to chronic inflammation, where persistent accumulation and activation of neutrophils and mononuclear cells results in fibrosis and tissue damage[147-150]. In the field of biomaterials and tissue engineering, inflammation that is allowed to continue unabated can impair host-implant integration and tissue regeneration, leading to implant failure[151-154]. Therefore, balancing processes of inflammation and resolution are vital to ensuring the success of biomaterial and tissue engineered scaffolds. Here, we utilized a locally-delivered dual-acting lipid mediator to regulate active inflammatory

processes and drive resolution by inhibiting neutrophil infiltration and increasing the presence of anti-inflammatory monocytes and macrophages.

Resolvins are in a class of molecules that have been deemed specialized pro-resolving mediators that are produced during the acute inflammatory response. Their actions drive the restoration of tissue homeostasis and prevention of fibrosis after the acute inflammatory response through a dual anti-inflammatory pro-resolution mechanism by which the activities of pro-inflammatory cells are dampened and those of anti-inflammatory cells are enhanced[113]. Currently, there are many studies investigating resolvins for various therapeutic applications that seek to leverage their pro-resolving function. For example, intravenous AT-RvD1 can suppress inflammatory responses and protects against kidney injury in a murine model of acute kidney injury[155]. Additionally, RvD1 can modulate human and murine T cell differentiation, while enhancing the generation of T-regulatory cells[101]. While these studies have shown promising therapeutic uses for AT-RvD1, little exploration has been done into the utilization of biomaterials to locally deliver AT-RvD1 to areas of inflammation after injury. We have shown here for the first time that sustained delivery of AT-RvD1 from PLGA scaffolds over several days results in differences in myeloid cell accumulation to skin after injury compared to a one-time dose of dissolved AT-RvD1. The dosage of AT-RvD1 delivered via topical saline was 100ng, while 10.2ng AT-RvD1 on average were loaded into each biomaterial film. We found that both biomaterial-delivered AT-RvD1 and AT-RvD1 solution were able to significantly reduce neutrophil infiltration after one day, but only AT-RvD1-loaded scaffolds were able to increase Ly6Clo AMs, while decreasing Ly6Chi IMs after three days, indicating that sustained release at a lower dose is better able to modulate the cellular response after injury.

These findings motivated us to investigate further how local delivery of AT-RvD1 via a biomaterial is able to modulate inflammation and promote tissue regeneration.

In the process of wound healing without infection, it was previously believed that neutrophils had little to no bearing on the outcome of tissue repair[156]. However, recent studies exploring the role of neutrophils in wound healing have shown that excessive neutrophil infiltration into tissue can impair repair through the release of neutrophil extracellular traps (NETs), reactive oxygen species (ROS) and proteolytic enzymes, specifically in the context of diabetes and post-myocardial infarction cardiac remodeling [82, 128, 130, 156-158]. Excessive neutrophil recruitment and persistent activation is associated with chronic inflammation, fibrosis, and poor healing [33, 159, 160] . Additionally, targeted depletion of neutrophils in mice has been found to accelerate wound closure[161]. High neutrophil counts in relation to lymphocytes and macrophages have also been clinically associated with poor outcomes in a number of diseases, including colon cancer and atherosclerosis[162, 163]. For instance, patients with an elevated neutrophil to lymphocyte ratio are more likely to experience cardiac death and mortality after acute myocardial infarction [158, 164], and mice with pancreatic cancer that have an elevated neutrophil-to-macrophage ratio are more likely to develop severe ascites or bowel obstruction[142]. In the present study, we demonstrate reduced neutrophils present at one day after injury in mice treated with AT-RvD1-loaded films via flow cytometry and quantification of whole mount IHC. Resolvins have been shown to block neutrophil transendothelial migration through inhibition of neutrophil chemotaxis towards cytokine gradients created during the inflammatory process[165]. Neutrophil levels were elevated in the blood but reduced in tissue, and neutrophils that did migrate into the tissue were

unable to infiltrate further through the tissue. These data suggest that the local delivery of AT-RvD1 can not only block transendothelial migration of neutrophils as has been demonstrated previously via systemic treatment with resolvins, but can also prevent further tissue damage by inhibiting neutrophil migration through the interstitial tissue. Animals treated with AT-RvD1 also had a lower neutrophil-to-monocyte/macrophage ratio at 3 days after surgery, and we propose that this metric can be used to indicate a positive correlation to inflammation resolution and the prevention of chronic inflammation.

During tissue regeneration, the remodeling and expansion of wound-associated vasculature is critical to ensure tissue oxygenation, nutrient delivery, and cell recruitment [71]. Recently, a newly discovered subset of neutrophils has been described that stimulate angiogenesis in response to VEGF[44]. We have found that CD49d+ neutrophils accumulate in injured dorsal tissue three days after treatment with AT-RvD1-loaded films, and these neutrophils can actively participate in vascular remodeling and network expansion. We have previously shown that the recruitment of Ly6Clo AMs using SDF-1α-loaded hydrogels or FTY720-releasing films is associated with increased angiogenesis and arteriogenesis during inflammation[18, 71, 166]. Here we have shown that the local delivery of AT-RvD1 is able to enhance accumulation of AMs in the dorsal tissue as early as three days after surgery. In addition to increasing the ratio of AMs to IMs, M2 alternatively activated macrophages were also increased in the tissue of AT-RvD1-loaded film-treated animals. These specific subsets of monocytes and macrophages are able to directly influence vascular remodeling [59, 167, 168], and increased AM/IM and M2/M1 ratios are associated with enhanced tissue regeneration and healing[70, 71]. The mechanisms of these observed increases in anti-inflammatory subsets of monocytes and

macrophages could be a result of increased monocyte recruitment from circulation. Alternatively, AT-RvD1 may alter in situ monocyte/macrophage polarization towards AM/M2 due to direct action by AT-RvD1 on macrophages or through external factors, such as phagocytosis of apoptotic neutrophils[169]. Local AT-RvD1 delivery was also able to modulate the peri-implant cytokine profile towards a pro-angiogenic/arteriogenic environment, with significant elevation in VEGF, SDF-1α, and IL-4, cytokines that contribute to vascular remodeling and the recruitment of cells that participate in vascular remodeling[170-173]. Indeed, the enhanced arteriolar diameter and vascular tortuosity we observed with brightfield microscopy and expansion of microvasculature observed with confocal imaging 3 days after implantation are early hallmarks of sustained arteriogenesis and vascular remodeling.

Taken together, localized delivery of AT-RvD1 allows for dual targeting of both pro-inflammatory and pro-regenerative cells involved in inflammation and wound healing. Modulation of initial neutrophil infiltration allows for reduced overall tissue damage and primes the tissue for regeneration and healing. Enhanced accumulation of anti-inflammatory monocyte and macrophage cell subsets further reduce inflammation and promote early tissue regeneration and vasculogenesis. These results establish localized delivery of AT-RvD1 as a promising approach to modulate the innate immune response to reduce tissue damage associated with excessive inflammation and promote therapeutic outcomes such as vascular remodeling.

3.5 Materials and Methods

3.5.1 Fabrication of loaded and unloaded polymeric thin films

Films loaded with AT-RvD1 or unloaded were made as previously described[18]. Briefly, PLGA (50:50 DLG 5E – Evonik Industries) was solubilized in dichloromethane using a sonicator at 37°C until dissolved. Ten µg (100µL) AT-RvD1 (Cayman Chemical) were added to make AT-RvD1-loaded films. Solutions were cast in Teflon molds, and stored at -20°C until full organic solvent evaporation was observed. Films were then lyophilized for 24 hours. A 1mm biopsy punch was used to produce films used in studies. The morphology of the films were examined by scanning electron microscopy (SEM). Films were coated with Au for 45 seconds by a Quorum Q-150T ES sputter coater and imaged with a Hitachi SU8010 field emission scanning electron microscope.

3.5.2 Quantification of AT-RvD1 release from PLGA films via High Performance Liquid Chromatography (HPLC) measurements

The in vitro release of AT-RvD1 from PLGA films was quantified with HPLC. In the release study, 1mm diameter films were placed into 200µL phosphate-buffered saline (PBS) and incubated at 37°C. At predetermined timepoints, the PBS was removed for analysis and replaced with new PBS. Samples were analyzed with a Shimadzu UFLC High Performance Liquid Chromatograph (Columbia, MD, USA) equipped with a Shimadzu Premier C18, 5µm (250x4.6mm) column. AT-RvD1 elution was measured at 8.6 minutes using a wavelength of 301nm. Known quantities of AT-RvD1 were used to generate a standard curve relating AT-RvD1 mass to total peak area. Using serial dilutions, we determined that the limit of detection was below 0.5pg/µL. The total amount of AT-RvD1 in each release sample was calculated using the standard curve.

3.5.3 In vitro macrophage phagocytosis assay

AT-RvD1-loaded PLGA films and empty PLGA films were placed into 1mL Dulbecco's modified Eagle medium (Gibco) containing 1mM sodium pyruvate (Gibco) and 2mM L-glutamine (Gibco) supplemented with 10% Fetal Bovine Serum (FBS, Gibco) overnight. Conditioned media was added to 1x105 RAW264.7 cells (ATCC) cultured in 24-well plates. After one hour of treatment, Fluoresbrite® Polychromatic Red latex beads (0.5μm, Polysciences) that were opsonized in 10% FBS for 60 minutes were added at a ratio of 5:1 beads per cell and were allowed to incubate at 37°C for 4 hours. After incubation, the media was removed and cells were fixed with ice cold methanol for 10 minutes. Fixed cells were then imaged via brightfield and epifluorescence microscopy to detect both cells and phagocytized latex beads. These images were merged in ImageJ, and the total number of beads internalized by cells were counted.

3.5.4 Myeloperoxidase activity of neutrophils

MPRO neutrophil progenitor cells (ATCC) were cultured using Iscove's modified Dulbecco's medium (Gibco) containing 10 ng/ml murine granulocyte macrophage colony stimulating factor, 80% and heat-inactivated horse serum, 20%. Terminal granulocytic differentiation of MPRO cells was initiated by replating cells in fresh medium containing $1 \times 10{-}5$ M all-trans Retinoic Acid and culturing for one week to ensure full differentiation. AT-RvD1-loaded PLGA films and empty PLGA films were placed into 1mL MPRO differentiation medium overnight. Release media was added to 1x106 differentiated neutrophils and cells were treated for four hours. Myeloperoxidase (MPO) activity was then measured using a Colorimetric Activity Assay Kit (MAK068, Sigma) according to kit instructions at a sample size of 1x105 cells per well.

3.5.5 Dorsal skin fold window chamber surgery

Animal experiments were performed using sterile techniques in accordance with an approved protocol form the Georgia Institute of Technology Institutional Animal Care and Use Committee. Male C57BL/6 mice (Jackson) aged 6-12 weeks were anesthetized by inhaled isofluorane and surgically fitted with sterile dorsal skinfold window chambers (APJ Trading Co.) as previously described[18] . Briefly, the dorsal skin was shaved, depiliated, and sterilized via three washes with 70% ethanol and chlorhexidine. The dorsal skin was drawn away from the back of the mouse and one side of the titanium frame was attached to the underside of the skin. Sterile surgical micro scissors were then used to expose the microvasculature through the removal of the epidermis and dermis in a 12mm diameter circle. Mice were implanted with two of the same films (either empty PLGA vehicle film or AT-RvD1-loaded PLGA film) placed on opposite sides of the window chamber. Before implantation, the films were washed in 70% ethanol for 30 seconds, followed by washing with sterile Ringer's solution for 30 seconds. Exposed tissue was then sealed with a sterile glass coverslip. Mice were administered sustained-released buprenorphine i.p. (0.1-0.2 mg/kg) and allowed to recover in heated cages. All mice received standard laboratory diet and water ad libitum throughout the course of the experiment.

3.5.6 Vascular metrics

Mice were anesthetized with isofluorane, the glass window was removed, and dorsal tissue was superfused with adenosine in Ringer's solution (1mM) to prevent desiccation and to maximally dilate exposed vessels. The mouse was mounted on a microscope stage and imaged non-invasively at 5x magnification on a Zeiss Imager.D2

microscope with AxioCam MRC 5 color digital camera (Zeiss). Images were acquired on day 0 immediately following film implantation and again on day 3. Microvascular length density measurements were made within a 4000x4000 pixel square region of interest (ROI) around the film. Vessels within these ROIs were traced and total vessel length per unit area was quantified via ImageJ. Arteriolar diameter measurements were made within the ROIs by identifying arteriolar-venular pairs at day 0. Internal diameter changes were measured via ImageJ and day 3 diameters were normalized to day 0. Vascular tortuosity measurements were made within the ROIs by measuring the distance metric – the path length of a meandering curve divided by the linear distance between endpoints in ImageJ.

3.5.7 Tissue harvest and flow cytometry

To collect samples for flow cytometry analysis, mice were euthanized via CO2 asphyxiation. Peripheral blood was collected via cardiac puncture. Erythrocytes within blood were lysed with ammonium chloride (StemCell Technologies) and the remaining leukocytes were isolated for flow cytometry analysis. Bone marrow was collected via centrifugation (1000g for 5 mins) of isolated tibiae. The dorsal tissue was excised and digested with collagenase type 1-A (1mg/ml, Sigma) at 37°C for 30 minutes and further separated with a cell strainer to create a single cell suspension. Single cell suspensions of tissues, blood, and bone marrow were stained for flow cytometry analysis using standard methods and analyzed on a FACS-AriaIIIu flow cytometer (BD Biosciences). The antibodies used for identifying cell populations of interest were: PerCP-Cy5.5 conjugated anti-CD45 (BioLegend), APC-Cy7 conjugated anti-CD11b (BioLegend), BV421 conjugated anti-CD11b (BioLegend), APC conjugated anti-Ly6C (BioLegend), BV510 conjugated anti-Ly6C (BioLegend), APC-Cy7 conjugated anti-Ly-6G (BioLegend), PE-

Cy7 conjugated anti-GR-1 (BioLegend), APC conjugated anti-F4/80 (BioLegend), PE-Cy7 conjugated anti-CD206 (BioLegend), AlexaFluor488 conjugated anti-CD86 (BioLegend), PE conjugated anti-CD49d (BioLegend), PerCP-Cy5.5 conjugated anti-CXCR4 (Biolegend), APC conjugated anti-VEGFR1 (Biolegend), and PE-Cy7 conjugated anti-VEGFR2 (Biolegend). Staining using BV dyes was performed in the presence of Brilliant Stain Buffer (BD Biosciences). Positivity was determined by gating on fluorescence minus one controls.

3.5.8 High dimensional analysis of flow cytometry data

t-SNE is a nonlinear dimensionality reduction algorithm developed by van der Maaten and Hinton21. T-SNE is able to embed high-dimensional data into a space of two or three dimensions, which is then be visualized in the form of a scatter plot, where similar cells are represented by nearby points and dissimilar cells are represented by distant points. Prior to tSNE dimensional reduction, each flow cytometry sample was pre-gated to select live, single cells, CD11b+ Ly6G+ neutrophils and then downsampled to up to 1500 events in FlowJo Version 10.2. After downsampling, each sample was electronically barcoded so that all samples could be concatenated to into a single file for tSNE analysis. A composite tSNE map that utilized data points from all samples (8 total samples: 4 vehicle and 4 AT-RvD1, repeated for day 1 and day 3). tSNE analysis was executed in FlowJo software using the following surface markers: CD11b, Ly6G, CD49d, CXCR4, VEGFR1, and VEGFR2. The following tSNE parameters were used: 1000 iterations, 30 perplexity, 200 Eta (learning rate), and 0.5 theta.

SPADE1,2 is a visualization tool that was initially designed to organize heterogeneous populations of single-cell data onto a 2D tree representation on the basis of similarities across user-selected markers. The nodes of the tree represent clusters of cells that are similar in marker expression. SPADE uses the size and color of each node to denote the number of cells and median marker expression. SPADE was performed through MATLAB. MATLAB-based SPADE automatically generates the tree by performing density-dependent down-sampling, agglomerative clustering, linking clusters with a minimum spanning-tree algorithm and up-sampling based on user input. The SPADE tree was generated by exporting uncompensated pre-gated live, single cells, CD11b+ Ly6G+ neutrophils. The markers used to build the SPADE tree were SSC, FSC, CD11b, Ly6G, CD49d, CXCR4, VEGFR1, and VEGFR2. The following SPADE parameters were used: Apply compenstation matrix in FCS header, Arcsinh transformation with cofactor 150, neighborhood size 5, local density approximation factor 1.5, max allowable cells in pooled downsampled data 50000, target density 20000 cells remaining, and number of desired clusters 100. The resultant SPADE tree was auto-annotated by MATLAB based on differences in marker expression.

3.5.9 Tissue whole mount immunohistochemistry and confocal imaging

Following euthanasia, mouse vasculature was perfused with warm saline and then with 4% paraformaldehyde until tissues were fixed. The dorsal tissue was excised and permeabilized overnight at 4°C with 0.2% saponin. The tissues were blocked overnight in 10% mouse serum at 4°C. Tissues were incubated at 4˚C overnight in staining solution containing 0.1% saponin, 5% mouse serum, 0.5% fatty-acid free bovine serum albumin, and the following fluorescently conjugated antibodies: Alexa Fluor 594 anti-CD31

antibody (1:100 dilution, BioLegend) for blood vessel visualization, Alexa Fluor 488 anti-Ly-6G (1:200 dilution, BioLegend) for visualization of neutrophils, Alexa Fluor 647 anti-CD68 (1:200 dilution, ABD Serotec) for visualization of monocytes/macrophages, and Alexa Fluor 647 anti-CD49d (1:200 dilution, BioLegend) for visualization of pro-angiogenic neutrophils[174]. Tissues were washed four times for 30 minutes with 0.2% saponin and once with PBS and then mounted in 50/50 glycerol/phosphate buffered saline. Mounted samples were imaged on a Zeiss LSM 710 NLO confocal. Tiled z-stacks at 10x magnification were taken for analysis of CD31+ vasculature. Crops of 1000x1000 pixels of background vasculature or peri-implant vasculature were used for measurement of CD31+ length density. For vessel density measurements, vessels were traced and total vessel length per unit area was quantified via ImageJ. Crops of 332x332μm at 20x magnification in the peri-implant area were taken for image analysis in Imaris™ (Bitplane). Images were then blinded and rendered in Imaris by a third party. Cells expressing Ly-6G or CD68 were identified in Imaris using the surface tool. Pro-angiogenic neutrophils co-expressing CD49d and Ly-6G were also identified using the surface tool. Ly-6G+, CD68+, or Ly-6G+CD49d+ surfaces were identified by smoothing with a 1μm grain size and automatic thresholding on absolute intensity. Touching objects were split using a seed points diameter of 10μm. CD31+ vasculature was identified in Imaris using the same surface method as described above, also applying a 1μm grain size, but instead manually selecting the threshold value optimized for each image, and manually applying the volume filter to remove small debris. Distance to vasculature calculations between neutrophils and CD31+ vasculature were made by applying a distance transformation to the CD31+ surface and recording the median position of each neutrophill relative to CD31+ vessels.

3.5.10 Cytokine measurements

For cytokine measurements, 4mm biopsy punches of tissue centered around each biomaterial implant were harvested after euthanasia. Tissue biopsy punches were combined for each animal, digested for 30 min at 37°C in 1mg/mL collagenase-type 1A, and disaggregated through a cell strainer. Protein was isolated from the single cell suspension in RIPA buffer containing Halt™ Protease and Phosphatase Inhibitor Cocktail (diluted to 1X, ThermoFisher Scientific) for 45 minutes on ice. Following cell lysis, total protein was obtained by centrifugation for 15 minutes at 14,000xg and 4°C. To determine the total protein concentration in each sample, a bicinchoninic acid assay (BCA assay) was carried out using a Pierce™ BCA Protein Assay Kit (ThermoFisher Scientific) according to kit instructions. Cytokine measurements were made using the Mouse Magnetic Luminex Screening Assay (catalog number LXSAMSM, R&D Systems) according to kit instructions. Kit analytes included CCL2/MCP-1/JE, CXCL12/SDF-1α, FGF-β, G-CSF, GM-CSF, IFN-γ, IGF-1, IL-10, IL-12p70, IL-4, IL-6, MMP-9, TNF-α, and VEGF. Cytokine results were normalized to sample total protein.

3.5.11 Statistical analysis

All statistical analyses were performed using Graphpad Prism version 6.0 (La Jolla, CA). Results are presented as mean ± standard error of the mean (SEM). For pairwise comparisons, unpaired two-tailed t-tests with Welch's correction, if variance was significantly different, were used. For grouped analyses, one-way ANOVA with Tukey's post-test was used for multiple comparisons. For grouped analyses comparing data over time, two-way ANOVA with Tukey's post-hoc test was used. Unless otherwise noted,

$p<0.05$ was considered statistically significant. For analysis of cellular distance to vasculature, data reflect cells counted from three ROIs acquired across 3-4 animals per group, and statistical comparisons were made using a two-tailed Mann-Whitney test.

CHAPTER 4. DUAL-LOADED IMMUNOMODULATORY HYDROGELS RECRUIT PRO-REGENERATIVE INNATE AND ADAPTIVE IMMUNE CELLS TO AREAS OF INJURY

4.1 Introduction

The immune response to injury is a complex process that involves the orchestration of functions of many different cell populations that work in coordination to restore tissue homeostasis. In healthy individuals or in the case of small wounds, tissue regeneration and the return to normal function proceed without any necessary outside intervention. However, in the case of large wounds or in disease states such as diabetes or after organ transplant, the process of the immune response to wound healing is dysregulated and may prevent normal tissue regeneration, leading to wound closure failure or a chronic inflammatory state. In order to mitigate the immune dysregulation present during these states, there is a rapidly expanding body of research dedicated to the targeting and manipulation of the immune response to injury and inflammation. Extensive research has been carried out describing the roles of single immune populations during the process of tissue regulation. For example, depletion of neutrophils has been shown to delay wound closure in aged mice, and clinical observations note that neutropenic individuals often have difficulty healing wounds [25, 39]. Additionally, ablation of monocyte and macrophage pools in zebrafish and salamanders have resulted in failure of limb or tail regeneration, indicating their indispensability to the regenerative process [26, 27]. These studies demonstrate the extensive crosstalk and interplay between cell types during wound healing – that no one cell is the master orchestrator of tissue regeneration.

Although it is clear that there is no one cell responsible for the coordination of the regenerative process, there are specific cell subsets within the larger umbrella of immune cells that have been positively identified as “pro-regenerative”. Within the monocyte and macrophage families, subsets have been identified in both mice and humans that have disparate functions and roles during inflammation. Monocytes may exist as classical monocytes (CD11b+Ly6Chi in mice and CD14+CD16- in humans) that exhibit largely pro-inflammatory characteristics – or as patrolling non-classical monocytes (CD11b+Ly6Clow in mice and CD14lowCD16+ in humans) [47]. These non-classical monocytes patrol the resting endothelium during homeostasis, but after injury they infiltrate into tissue and secrete VEGF, TGF-ß, and IL-10 and are able to promote angiogenesis and matrix deposition [49, 175-177]. We have shown that targeted recruitment of these specific monocytes enhances microvascular network expansion after sterile injury, and that they are able to preferentially expand the population of “anti-inflammatory” macrophages [61, 94, 166, 178]. By extension, macrophages exist *in vivo* on a spectrum from M1 “pro-inflammatory” to M2 “anti-inflammatory” [179]. M2 anti-inflammatory macrophages are identified by their expression of the mannose receptor CD206 along with canonical macrophage markers MerTK and CD64 [168]. These M2 macrophages can be further divided into M2a-c subsets, and the M2a and M2c subsets have, in particular, been shown to exhibit pro-regenerative, anti-inflammatory characteristics, such as the ability to release IL-10, support angiogenesis, and ameliorate fibrosis and tissue damage in the context of kidney injury, lung injury, and myocardial infarction [18, 23, 70-72]. In addition to the mononuclear phagocyte system, we now know

that other cells in the innate and adaptive immune systems can also positively influence regeneration.

Dendritic cells (DCs) are antigen presenting cells that release cytokines and are responsible for influencing both innate and adaptive immune responses after microbial infection or tissue injury. Traditionally, their function is to detect and capture foreign antigen and present those antigens to T lymphocytes to induce their activation, differentiation, and subsequent action [180]. Additionally, DCs are also involved in promoting tolerance to self-antigens and can induce regulatory T cell (Treg) expansion under the correct conditions[181]. Previously, their roles in wound healing were unexplored, but new studies have shown that DCs are active mediators of healing after injury, and depletion of DCs adversely affects burn wound healing and ventricular function after myocardial infarction [182-184]. These studies indicate an under-studied cell population that has the ability to tune the wound healing response. On the adaptive immune side, the role of Tregs in wound healing is gaining increased recognition. Tregs are CD3+CD4+CD25+ lymphocytes that have the ability to suppress T effector cell responses and induce anergy. Tregs are most commonly recognized for their roles in inhibiting autoimmunity through the release of immune inhibitory cytokines such as TGF-ß and IL-10 and blocking T lymphocyte costimulation via CTLA-4 [86, 109, 185, 186]. Recently, Tregs have also been shown to be critical for repair and regeneration in numerous tissues after injury, including skin, lungs, skeletal muscle, and cardiac muscle [74-78]. It is clear that there are a multitude of immune cell subsets that can aid in the promotion of tissue repair after injury and enriching the wound microenvironment with as many of these pro-

regenerative cells as possible is one strategy in the quest to increase the body's ability to respond to injuries.

One strategy for modulating the local immune cell population after injury is through local delivery of biomolecules via implanted biomaterials. Because we are seeking to recruit immune cells able to stimulate repair from many branches of the immune, it is unlikely that delivery of one biomolecule will be able to sufficiently affect the recruitment of all cell subsets of interest. Therefore, we have identified two bioactive factors capable of eliciting this response: aspirin-triggered resolvin d1 (AT-RvD1) and IL-10. AT-RvD1 is part of a class of "specialized proresolving mediators" (SPMs) capable of redirecting the immune response towards resolution [187]. SPMs have broad effects over a variety of myeloid cells, including the limitation of neutrophil transendothelial migration, the modulation of cytokine release from monocytes and macrophages, and the prevention of dendritic cell maturation[113, 155, 188]. AT-RvD1 has been shown to mitigate tissue injury after asthma-induced lung injury, acute kidney injury, and in a model of the autoimmune disease Sjögren's syndrome [121, 155, 189].

Interleukin 10 (IL-10) is a cytokine which plays a critical role in the control of immune responses. It is expressed by both innate and adaptive immune cells including monocytes, macrophages, dendritic cells, and T cell subsets [105]. IL-10 treatment of dendritic cells prevents maturation, resulting in decreased MHC-II surface receptor expression and subsequent increased release of IL-10 [107]. These IL-10-producing DCs have the ability to induce functional Tregs, and IL-10 signaling on Tregs is required for Treg suppression of the TH17 responses [106, 190]. Additionally, IL-10 can act on other T helper subsets to prevent their costimulation and proliferation [105]. Aside from its

actions on antigen presenting cells and adaptive immune cells, IL-10 has been shown to play an essential role in the regulation of scar formation during wound healing and can reduce fibrotic deposition and scar formation after injury [106, 191]. These qualities of IL-10 make it an attractive agent for the promotion of wound healing due to its ability to direct anti-inflammatory effector functions of lymphoid cell subsets.

Previously, we have shown that local delivery of AT-RvD1 via biomaterial is able to increase the recruitment and accumulation of anti-inflammatory, pro-regenerative myeloid immune cells. Here, we seek to draw upon and extend our previous findings through the development of a dual-delivery hydrogel system capable of enriching the injury niche with not only known anti-inflammatory myeloid populations, but anti-inflammatory lymphocyte populations as well. We chose to co-deliver the lipid small molecule AT-RvD1 along with the protein IL-10 with the goal of attaining dual delivery kinetics of these two factors. We characterize the release kinetics and bioactivity of a hydrogel loaded with modified human IL-10 and AT-RvD1 and show that thiolation of IL-10 can allow for tethering to the PEG-MAL hydrogel backbone without affecting the bioactivity of IL-10. Using the murine dorsal skinfold window chamber as a test bed to measure the response to immunomodulatory hydrogels, we demonstrate that not only is the recruitment of anti-inflammatory myeloid cells enhanced by AT-RvD1 delivery, but combination IL-10+ATRvD1 treatment is able to concurrently increase populations of dendritic cells and T cells involved in wound healing. These results indicate that dual delivery of IL-10 and AT-RvD1 has broad effects on the recruitment of pro-regenerative, anti-inflammatory innate and adaptive immune cells and can result in the modulation of the immune response after injury to promote tissue regeneration and healing.

4.2 Results

4.2.1 Thiolation of IL-10 modulates the release profile but maintains bioactivity

We engineered degradable poly(ethylene glycol) (PEG) hydrogels using 10 kDa 4-arm PEG macromers containing terminal maleimide groups (PEG-MAL) that can react with free cysteines on peptides or full-length proteins. PEG-MAL macromers were crosslinked with the cysteine-flanked peptide GCRDVPMSMRGGDRCG (VPM) that contains a protease cleavage site (Figure 18A). Combination of functionalized PEG-MAL with VPM spontaneously forms a hydrogel in less than 1 minute (Figure 18B). Human IL-10 does not possess a free cysteine in its structure and cannot interact with PEG-MAL macromers during hydrogel formation. We loaded 250ng fluorescently tagged unmodified human IL-10 into a hydrogel and measured its release. The hydrogels released the unmodified IL-10 very quickly, with 58.24 ± 0.67ng released within the first 30 minutes (Figure 18C), 175 ±1.34ng after 2 hours and 209.62 ± 1.73ng after 6 hours. At 24 hours, the gels had released 227.40 ± 1.71ng of the loaded IL-10, over 90% of the initial dose. By day 5, 235 ± 1.73ng total IL-10 was released from the gel, and only 22.39 ± 4.85ng was recovered from the digested gel. We then attempted to functionalize the IL-10 with free cysteines in order to allow for interaction with the PEG-MAL macromer, which could then result in a more gradual release. We chose to thiolate the iL-10 using Traut's reagent (2-iminothiolane), a thioimidate compound that reacts with primary amines to form sulfhydryl groups. Using a molar excess of 30 for Traut's reagent, the concentration of thiol groups found on the IL-10 was determined to be 0.893 ± 0.98 uM. This corresponds to roughly 3

free cysteine groups per IL-10 molecule. When the release of thiolated IL-10 from PEG-MAL hydrogels is measured, we found that the thiolation greatly affects the kinetics. In contrast to the unmodified IL-10, thiolated IL-10 releases 7.67 ± 2.76 ng after 30 minutes, 26.91 ± 2.91 ng at 2 hours, 32.39 ± 2.67ng at 6 hours, and 42.03 ± 2.45ng by 24 hours (Figure 18C). The thiolated IL-10 released gradually with a measured release of 73.28 ± 3.55ng at 5 days, with 176.72 ± 5.42 ng remaining IL-10 that recovered from the gel after digestion (Figure 18D). We also measured the release of AT-RvD1 from the PEG-MAL hydrogels. AT-RvD1 was released from the gels in a manner similar to that of the unmodified IL-10, with 87.66 ± 1.29ng of the total loaded 100ng dose released by 24 hours. By day 5, only four more nanograms were released, and the total release was measured to be 91.24 ± 1.11ng (Figure 18E). When the release was measured from dual-loaded gels, no effect of dual loading was observed on either release profile (not shown).

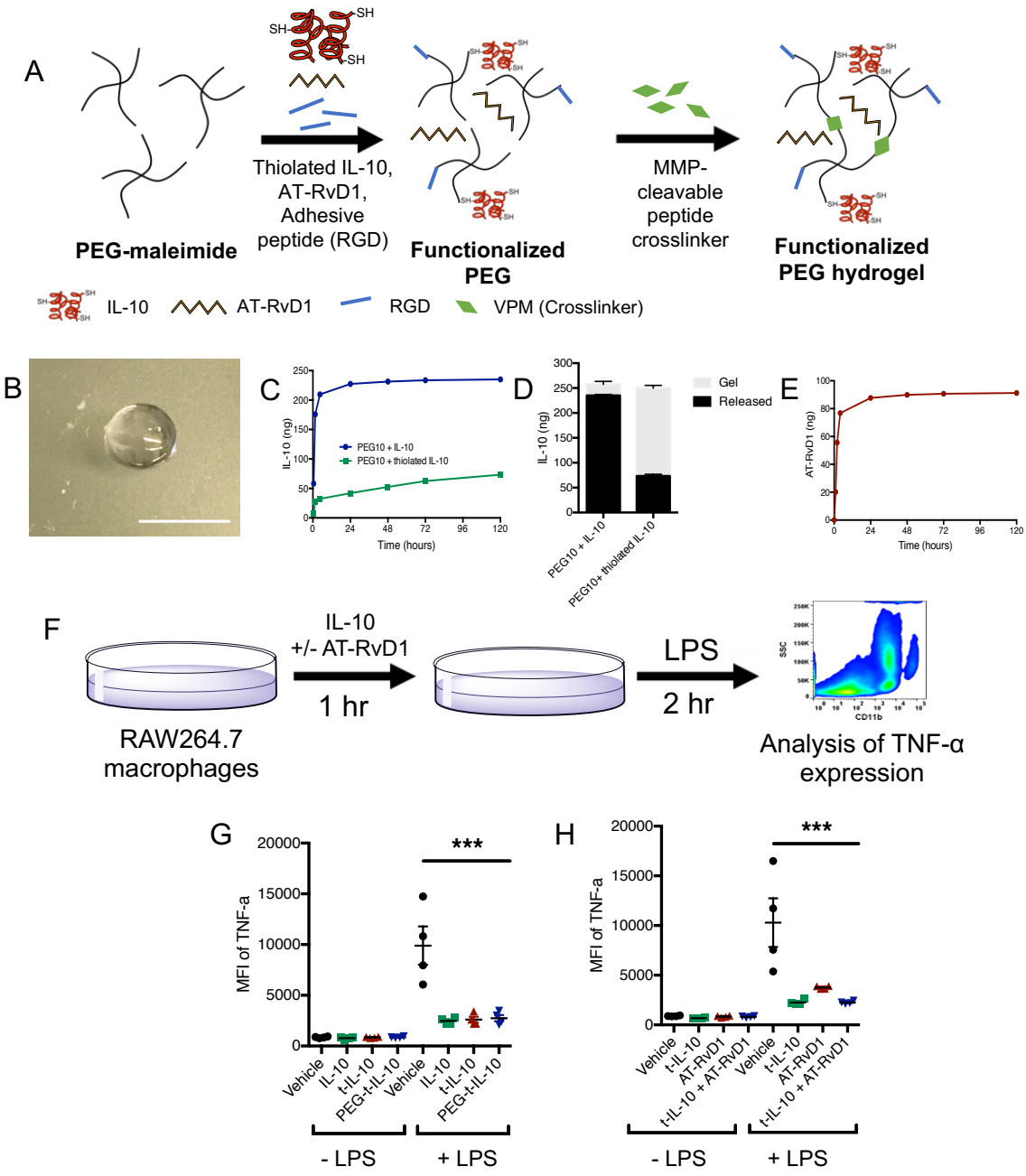

Figure 18. Hydrogel schematics, release profiles, and bioactivity. (A)Hydrogel fabrication method (B) Resultant macroscopic image of preformed hydrogels (C) Release of unthiolated and thiolated IL-10 from 10kDA PEG-MAL hydrogels over the course of 5 days (D) Amount of IL-10 or thiolated IL-10 remaining in the gels at the end of the release study. (E) HPLC measurements of AT-RvD1 release from PEG-MAL hydrogels. (F) Bioactivity assay schematic (G) Bioactivity of IL-10 following thiolation and PEG conjugation (H) Bioactivity of AT-RvD1 and IL-10 combinations. Statistical analysis was performed using one-way ANOVA with Tukey's post-hoc test, ***p>0.001, n=4.

We then wanted to ensure that the thiolation of IL-10 or subsequent conjugation with PEG-MAL did not have an effect on its bioactivity. IL-10 has previously been shown to suppress TNF- α release by RAW264.7 macrophages after treatment with LPS [192]. We adapted the assay reported previously and utilized intracellular cytokine staining and flow cytometric analysis to assess TNF- α levels in RAW264.7 macrophages (Figure 18F). First, we compared unmodified IL-10, thiolated IL-10 (t-IL-10), and thiolated IL-10 conjugated with PEG-MAL (PEG-t-IL-10) and found that all three were able to significantly reduce TNF- α expression after treatment with LPS compared to vehicle control (Figure 18G). We then compared thiolated IL-10 to AT-RvD1 and co-treatment of AT-RvD1 and IL-10. Again, we observed a significant reduction in TNF- α expression across all groups after LPS treatment compared to control (Figure 18H). Altogether, this characterization data indicates that thiolation with Traut's reagent is able to modify the release of IL-10 while maintaining its bioactivity, and that dual loaded hydrogels containing thiolated IL-10 and AT-RvD1 have temporally independent release profiles. All subsequent experiments utilized thiolated IL-10, and IL-10 in text and figures will refer to thiolated IL-10.

4.2.2 Immunomodulatory PEG-MAL hydrogels alter myeloid recruitment dynamics

We utilized the murine dorsal skinfold window chamber model to characterize the immune response to immunomodulatory PEG-MAL hydrogels after tissue injury. This model allows for quantification of host responses to injury and biomaterials through methods including flow cytometry and cytokine measurements, as well as longitudinal intravital imaging to track real-time inflammation-mediated remodeling of microvascular networks [18, 61, 71]. To examine the recruitment of circulating myeloid cells to the

injured dorsal tissue we utilized flow cytometry at days one, three, and seven after injury and implantation of the hydrogels. Animals received one unloaded hydrogel injected on one side of the window chamber and a hydrogel loaded with AT-RvD1, thiolated IL-10, or both AT-RvD1 and thiolated IL-10 combination treatment (Figure 19A).

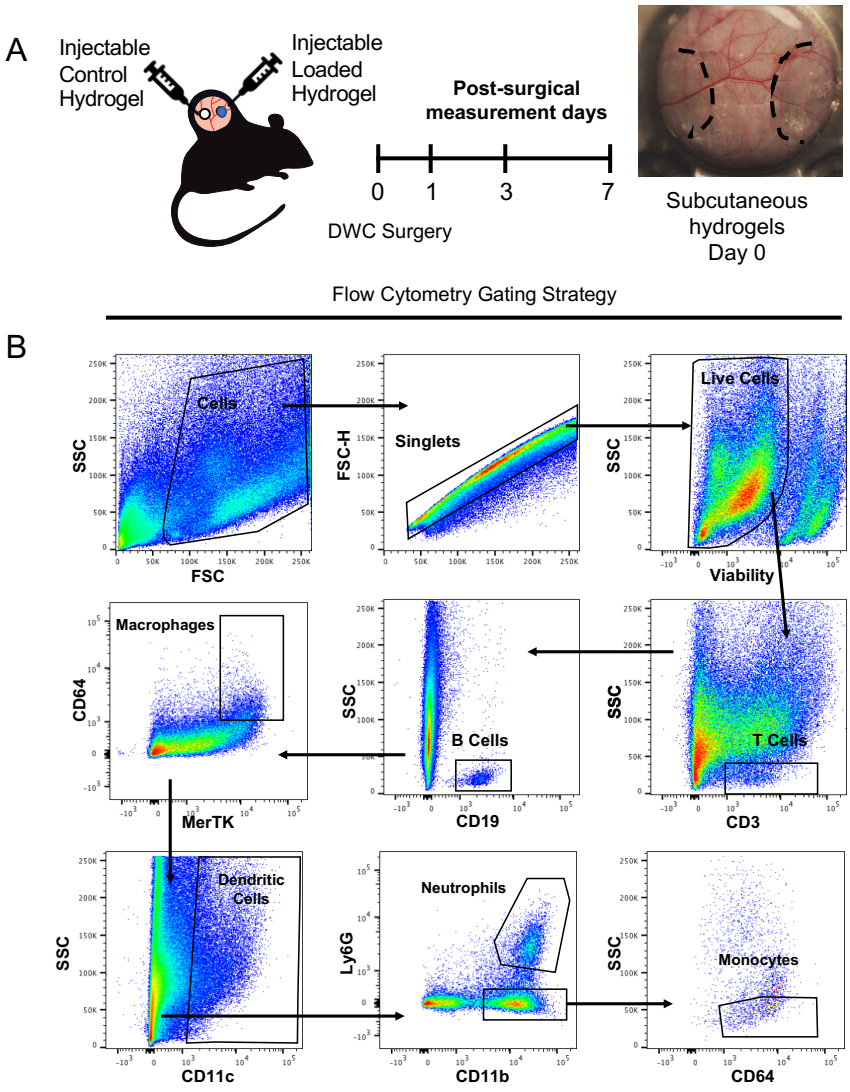

Figure 19. *In vivo* experimental overview and flow gating strategy (A) Experimental overview of dorsal skinfold window chamber experiments and hydrogel placement. (B) Flow cytometry gating strategy showing major cell types investigated with our panels .

The hydrogels contained 100ng AT-RvD1 and 250ng IL-10, and these doses were chosen based on prior studies utilizing these treatments [193, 194]. Neutrophils and monocytes were gated out of T cells, B cells, macrophages, and dendritic cells (Figure 19B). Neutrophils were immunophenotyped as CD11b+Ly6G+, and monocytes were gated on CD11b+CD64+SSClo with differential Ly6C expression to discriminate between Ly6Chi and Ly6CLow populations. Neutrophils dominated the CD11b+ cell population at day 1, comprising nearly 80% of Cd11b+ cells across all groups at day 1 (Figure 20A), with a decrease in abundance at days 3 and 7. However, AT-RvD1 and combination IL-10+AT-RvD1 hydrogels had significantly decreased percentages of neutrophils in the tissue compared to internal unloaded hydrogel control across all surveyed timepoints consistent with previous findings, although there were no significant differences in neutrophil accumulation over time between treatment groups (Figure 20A).

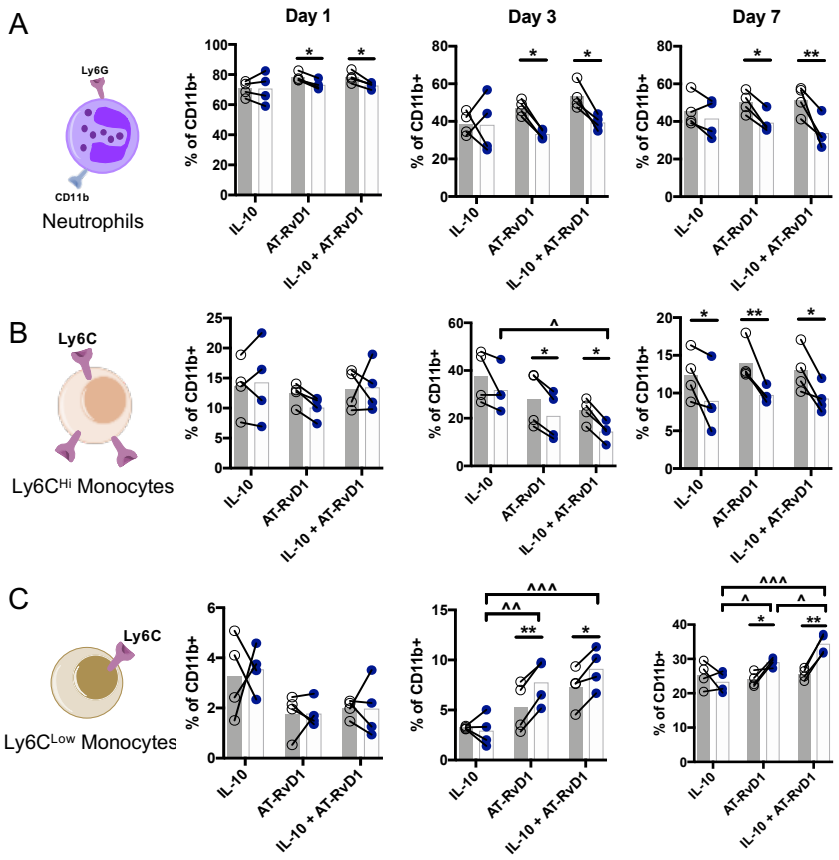

Figure 20. Neutrophil and Monocyte recruitment kinetics in the dorsal tissue. Flow cytometric analysis of (A) neutrophil, (B) Ly6Chi monocyte, and (C) Ly6CLow monocyte recruitment into the dorsal skinfold window chamber following treatment with immunomodulatory PEG-MAL Hydrogels. Open circles correspond to unloaded internal control, closed circles are treated tissue. Statistical analysis was performed using two-way repeated measures ANOVA with Tukey's or Bonferroni post-hoc test. Data presented as internal control and treatment with connecting lines. *p>0.05, **p>0.01 compared to internal control, ^p>0.05, ^^p>0.01, ^^^p>0.001 compared to other treatment group, n=4.

Monocyte recruitment and dynamics are also affected by immunomodulatory PEG-MAL hydrogels. We previously have shown that biomaterial films loaded with AT-RvD1 are able to decrease Ly6CHI monocyte infiltration in tissue while increasing the population of Ly6CLow monocytes. Using the PEG-MAL delivery system, we again observe significant decreases in Ly6CHI monocytes compared to internal control at days 3 and 7 after treatment with AT-RvD1-loaded hydrogels (Figure 20B) alone and in combination

with IL-10, with dual loaded hydrogels significantly decreasing the proportion of Ly6Chi monocytes when compared to IL-10 treatment. Ly6Chi monocyte recruitment to injured tissue peaks at around 3 days and gradually decreases after[47, 61]. In gels loaded only with IL-10, there is no change in the recruitment of Ly6Chi monocytes to injured tissue compared to internal control at day 3, but at day 7, however, the population of Ly6Chi monocytes around IL-10-loaded gels is decreased significantly (Figure 20B). This delay in treatment effect may be due to the slower release profile of IL-10 compared to AT-RvD1. Ly6CLo monocyte recruitment was unaffected at day 1 across all groups but increased significantly compared to control at days 3 and 7 with AT-RvD1 or combination therapy. The release of IL-10 alone had no effect on the recruitment dynamics of Ly6CLow monocytes (Figure 20C). At days 3 and 7, Ly6CLow monocytes in AT-RvD1 or IL-10+AT-RvD1 groups were significantly higher than in IL-10 treatment. Additionally, at day 7, the Ly6CLow population after dual-loaded hydrogel implant was significantly higher than AT-RvD1-only hydrogels, indicating a possible synergistic effect of AT-RvD1 and IL-10 on Ly6CLow recruitment and accumulation.

4.2.3 Anti-inflammatory macrophages accumulate after AT-RvD1 local delivery

After profiling the recruitment of circulating immune cell subsets in response to immunomodulatory hydrogels, we extended our analysis to macrophages and specific macrophage subpopulations. We examined dynamic changes in macrophages at days 1, 3, and 7 after tissue injury and implantation of PEG-MAL hydrogels. Macrophages are identifiable with flow cytometry by their surface receptor expression of MerTK and CD64 (Figure 19B). Initially, macrophages comprised a small percentage of the total cells found in the injured tissue but increased to nearly 10 percent of the live cell population in all

treatment groups by day 7, significantly higher than internal control (Figure 21A). Expansion of macrophage populations is a hallmark of the resolution of inflammation and is necessary for tissue regeneration and wound healing [195]. We then used flow cytometry and whole mount immunohistochemical staining to identify specific macrophage subpopulations present in the tissues over time.

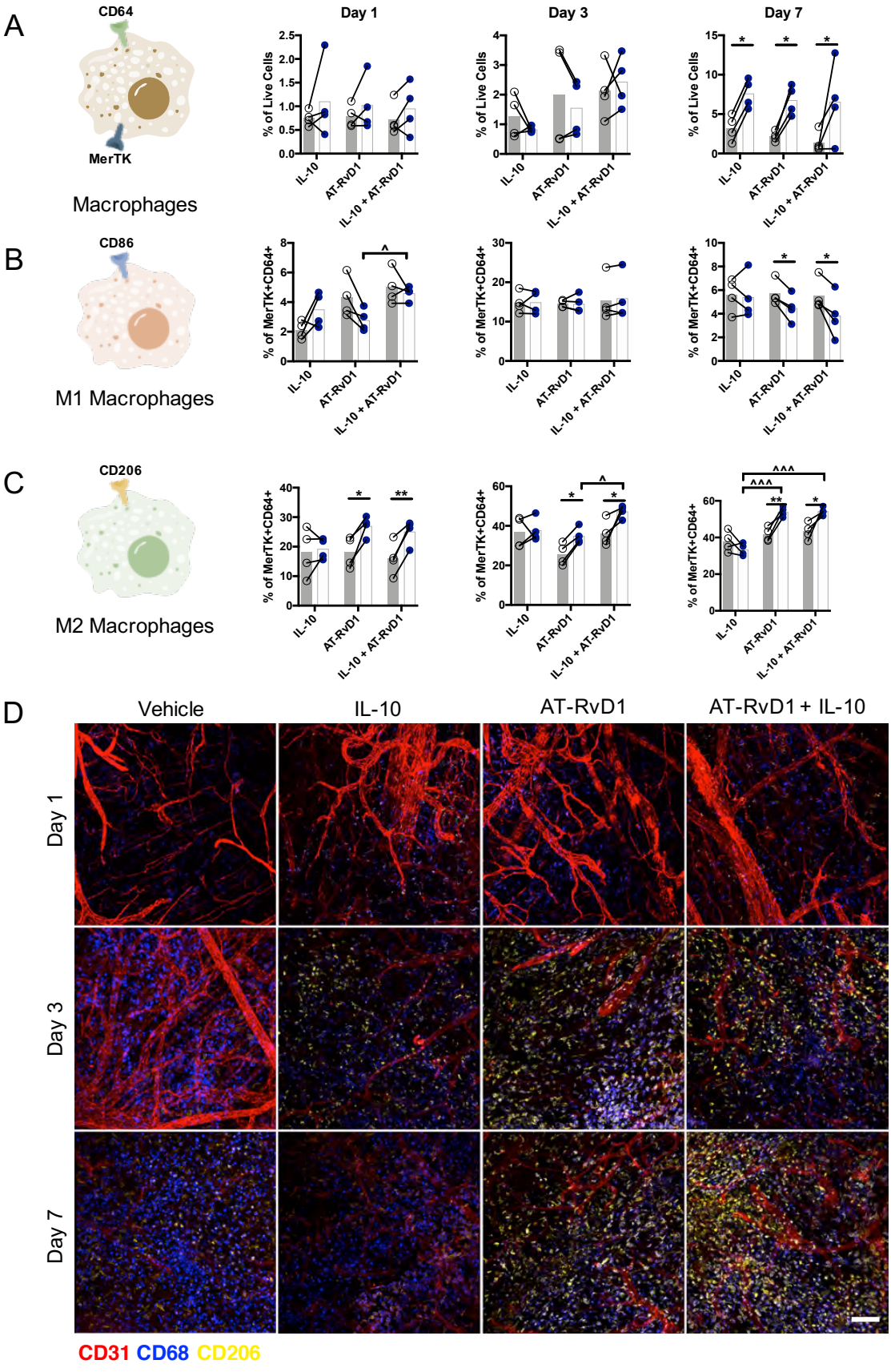
A
CD64
MerTK
Macrophages
Day 1
Day 3
Day 7
% of Live Cells
IL-10
AT-RvD1
IL-10 + AT-RvD1
B
CD86
M1 Macrophages
% of MerTK+CD64+
C
CD206
M2 Macrophages
D
Vehicle
IL-10
AT-RvD1
AT-RvD1 + IL-10
Day 1
Day 3
Day 7
CD31 CD68 CD206

Figure 21. Macrophage recruitment and polarization in dorsal tissue. Flow cytometric analysis of (A) macrophage, (B) CD86+ M1 Macrophage, and (C) CD206+ M2 macrophage popluations in the dorsal skinfold window chamber following treatment with immunomodulatory PEG-MAL Hydrogels. (D) Whole mount confocal microscopy showing M2 macrophage and total macrophage accumulation in the tissue following immunomodulatory hydrogel treatment. Open circles correspond to unloaded internal control, closed circles are treated tissue. Statistical analysis was performed using two-way repeated measures ANOVA with Tukey's or Bonferroni post-hoc test. Data presented as internal control and treatment with connecting lines. *p>0.05, **p>0.01 compared to internal control, ^p>0.05, ^^p>0.01, ^^^p>0.001 compared to other treatment group, n=4, scale bar 100μm.

Macrophages were subclassified into M1 and M2 phenotypes as previously described [196]. M1 classically activated macrophages were characterized by their expression of the costimulatory molecule CD86 and did not express the mannose receptor CD206. At day 1, CD86+ macrophages made up a small fraction of the total macrophage population. There were no differences between treatment and corresponding internal controls at day 1, however, the proportion of CD86+ M1 macrophages was significantly higher in animals treated with the combination IL-10+AT-RvD1 hydrogels compared to animals treated with AT-RvD1-only hydrogels (Figure 21B). This increase was transient, as there were no differences between any groups by day 3 after injury and gel implant. Temporally, we observed an increase in the M1 population at day 3 when M1 macrophages comprised on average 15% of the total macrophage population. The M1 population decreased by day 7 and was significantly decreased after AT-RvD1 or combination IL-10+AT-RvD1 treatment compared to control. Conversely, M2 alternatively activated macrophages were characterized as CD86-CD206+. At day 1, these macrophages made up a higher proportion of the total macrophage population, possibly due to pre-existing populations of tissue resident macrophages that express CD206[197]. We observed significant increases in the M2 macrophage population at 24 hours in the AT-RvD1-treated and IL-10+AT-RvD1

treated animals compared to internal control. At days 3 and 7 the average proportion of M2 macrophages had increased compared to the previous timepoint but did not change between IL-10 treated tissue and internal control. Similar to day one, we saw significant increases in the M2 population after AT-RvD1 and dual delivery of IL-10 and AT-RvD1 compared to control at days 3 and 7 (Figure 21C). This accumulation of M2 macrophages occurred at a faster rate with dual delivery hydrogels, as the population of M2 macrophages was significantly increased in IL-10+AT-RvD1 treated animals compared to AT-RvD1-only delivery (Figure 21C) at day 3, indicating a modulation in recruitment or differentiation kinetics driven by co-delivery of these two factors.

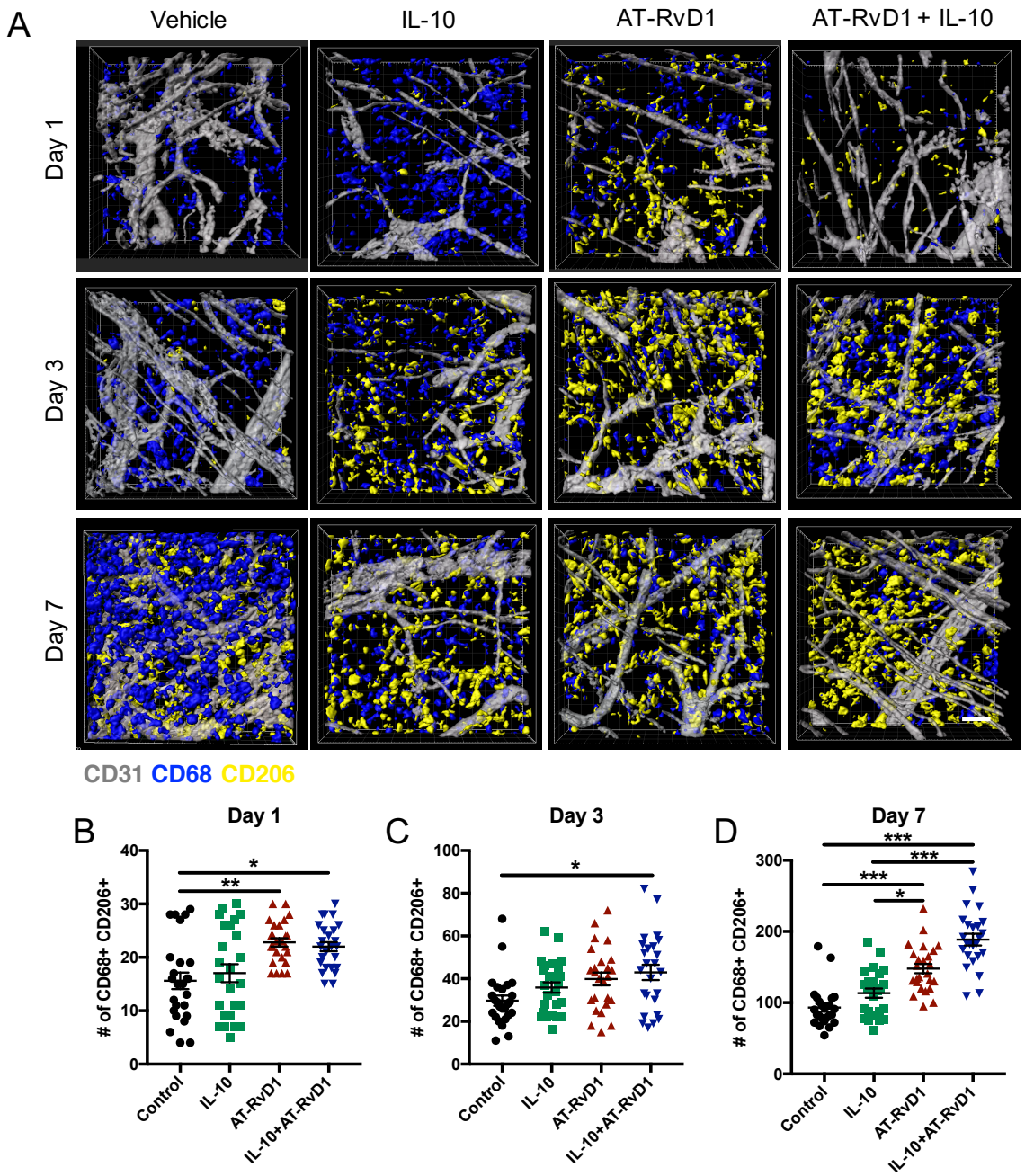

Figure 22. 3D analysis of M2 macrophage populations in dorsal tissue (A) Imaris renderings of CD68+ macrophage and CD206+ M2 macrophage accumulation over time. (B-D) Quantification of total CD68+ CD206+ double positive cells found in Imaris renderings after each timepoint. Scale bars, 30µm. Data presented as mean ± S.E.M. Statistical analyses were performed using Mann-Whitney Test *p<0.05, **p>0.01 ***p<0.001, n>100 cells, across 3-4 animals per group.

Additionally, we stained whole mount dorsal tissue for the pan-monocyte/macrophage marker CD68 and M2 marker CD206 and used Imaris to render and quantify the accumulation of M2 macrophages compared to the total monocyte and macrophage population over time. Representative 20x confocal images are seen in figure 4d, demonstrating the increase in the total CD68+ population over time. Qualitatively, these images show increased CD68+CD206+ cellular expression in the AT-RvD1 and IL-10+AT-RvD1 groups (Figure 21D). We found that quantification of 3D renderings confirms the qualitative findings and shows a steady increase over time from day one to day seven in the accumulation of CD68+ CD206+ macrophages following AT-RvD1-only or combination IL-10+AT-RvD1 treatment (Figure 22A-D) Single treatment with IL-10 only did not significantly increase the population of CD206+ macrophages over time.

4.2.4 Characterization of Dendritic Cell and Lymphocyte Recruitment Dynamics

Given the increasing knowledge of the roles immune system and plays in promoting wound healing and tissue regeneration, we quantified the temporal response of dendritic cells and lymphocytes to immunomodulatory PEG-MAL hydrogels. Dendritic cells have been shown to play previously unknown roles in the wound healing cascade, and specifically the CD11c+ IL-10+ tolerogenic or regulatory subset has been shown to enhance left ventricle function and remodeling following acute myocardial infarction and is able to stimulate the proliferation of Tregs[184, 198] .Here, we show that dual delivery of AT-RvD1 and IL-10 is able to reduce the overall frequency of CD11c+ dendritic cells at day 3 compared to AT-RvD1 loaded PEG-MAL hydrogels (Figure 23A).

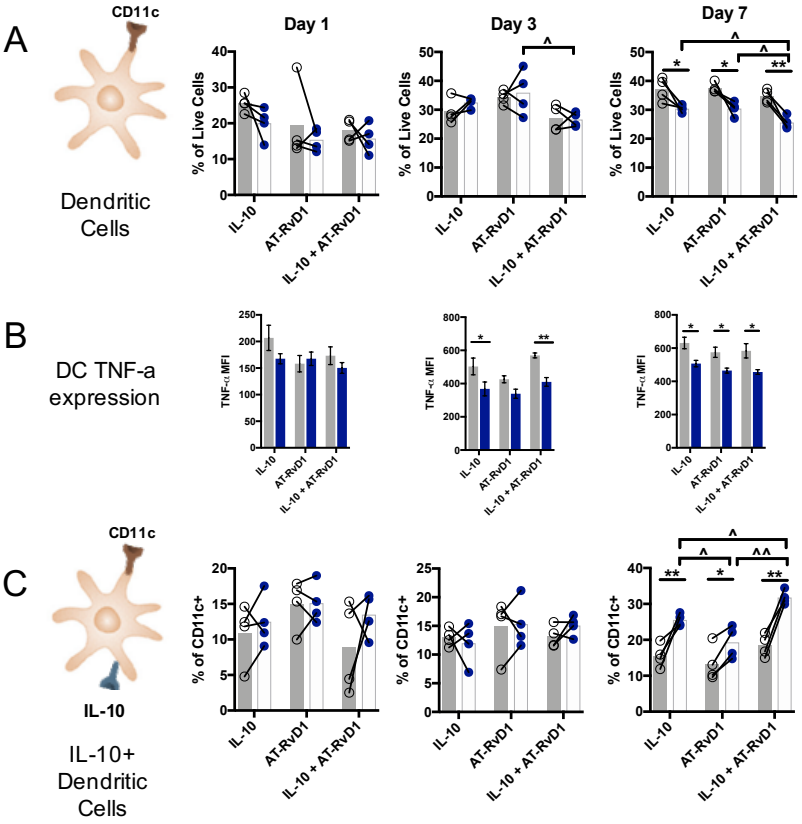
A
CD11c
Dendritic Cells
Day 1
Day 3
Day 7
% of Live Cells
IL-10
AT-RvD1
IL-10 + AT-RvD1
B
DC TNF-a expression
TNF-α MFI
C
CD11c
IL-10
IL-10+ Dendritic Cells
% of CD11c+

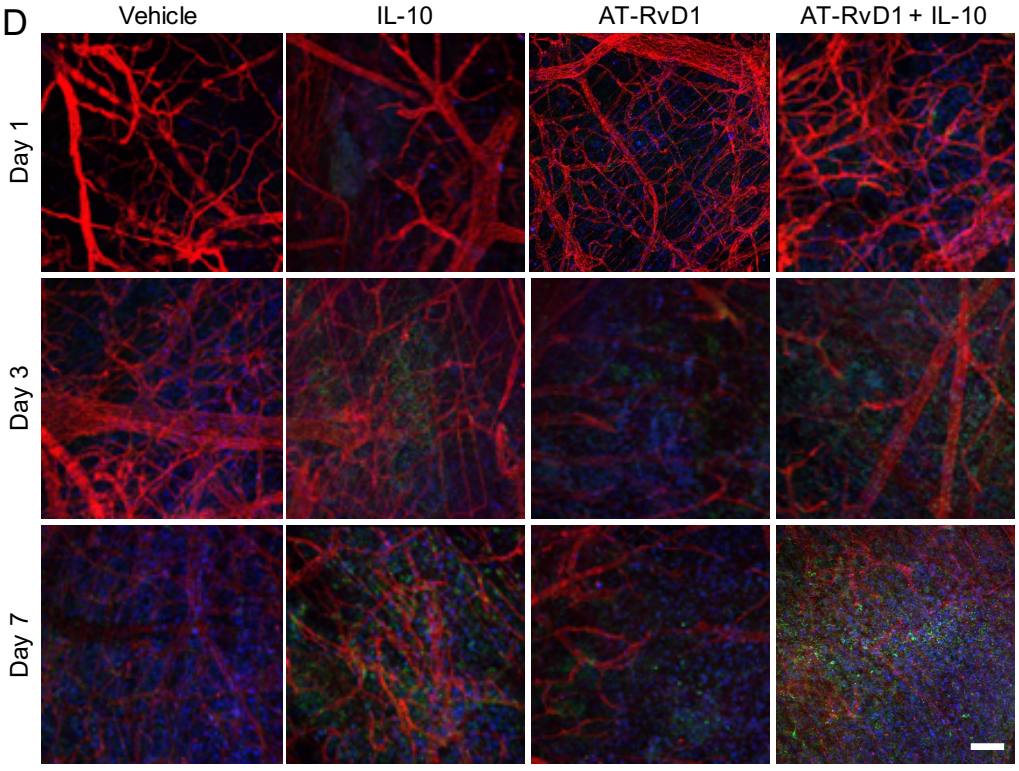
D
Vehicle
IL-10
AT-RvD1
AT-RvD1 + IL-10
Day 1
Day 3
Day 7
CD31 CD11c IL-10

Figure 23. Dendritic cell populations in the dorsal tissue Flow cytometric analysis of (A) total CD11c+ dendritic cell, (B) DC TNF-α intracellular cytokine staining, and (C) IL-10+ DC populations in the dorsal skinfold window chamber following treatment with immunomodulatory PEG-MAL Hydrogels. (D) Whole mount confocal microscopy showing dendritic cells and IL-10 staining in the tissue following immunomodulatory hydrogel treatment. Open circles correspond to unloaded internal control, closed circles are treated tissue. Statistical analysis was performed using two-way repeated measures ANOVA with Tukey's or Bonferroni post-hoc test. Data presented as internal control and treatment with connecting lines. *p>0.05, **p>0.01 compared to internal control, ^p>0.05, ^^p>0.01 compared to other treatment group, n=4, scale bar 100μm.

At day 7, the frequency of total dendritic cells was reduced across all groups compared to internal control, and the combination treatment was able to significantly reduce dendritic cell proportion in injured tissue compared to gels loaded with only AT-RvD1 or IL-10 (Figure 23A). Like monocytes and macrophages, dendritic cells are able to carry out pro- and anti-inflammatory effector functions, and pathologic dendritic cell activation leading to increased inflammatory cytokine production and stimulation of the adaptive immune system has been associated with chronic inflammatory disorders such as systemic lupus erythematosus and rheumatoid arthritis [199]. Consistent with our hypothesis that IL-10 and AT-RvD1 delivery are able to reduce the activation of pro-inflammatory pathways, we observe decreased intracellular TNF- α expression in CD11c+ dendritic cells at day 3 in the IL-10 and IL-10+AT-RvD1 hydrogel treatment groups, and reduced TNF- α expression across all groups at day 7 (Figure 23B). We also observe significant increases in IL-10+ dendritic cells after one week across all groups and found that IL-10+DCs were significantly increased in combination IL-10+AT-RvD1 treatment compared to IL-10 only and AT-RvD1 only treatments (Figure 23C).

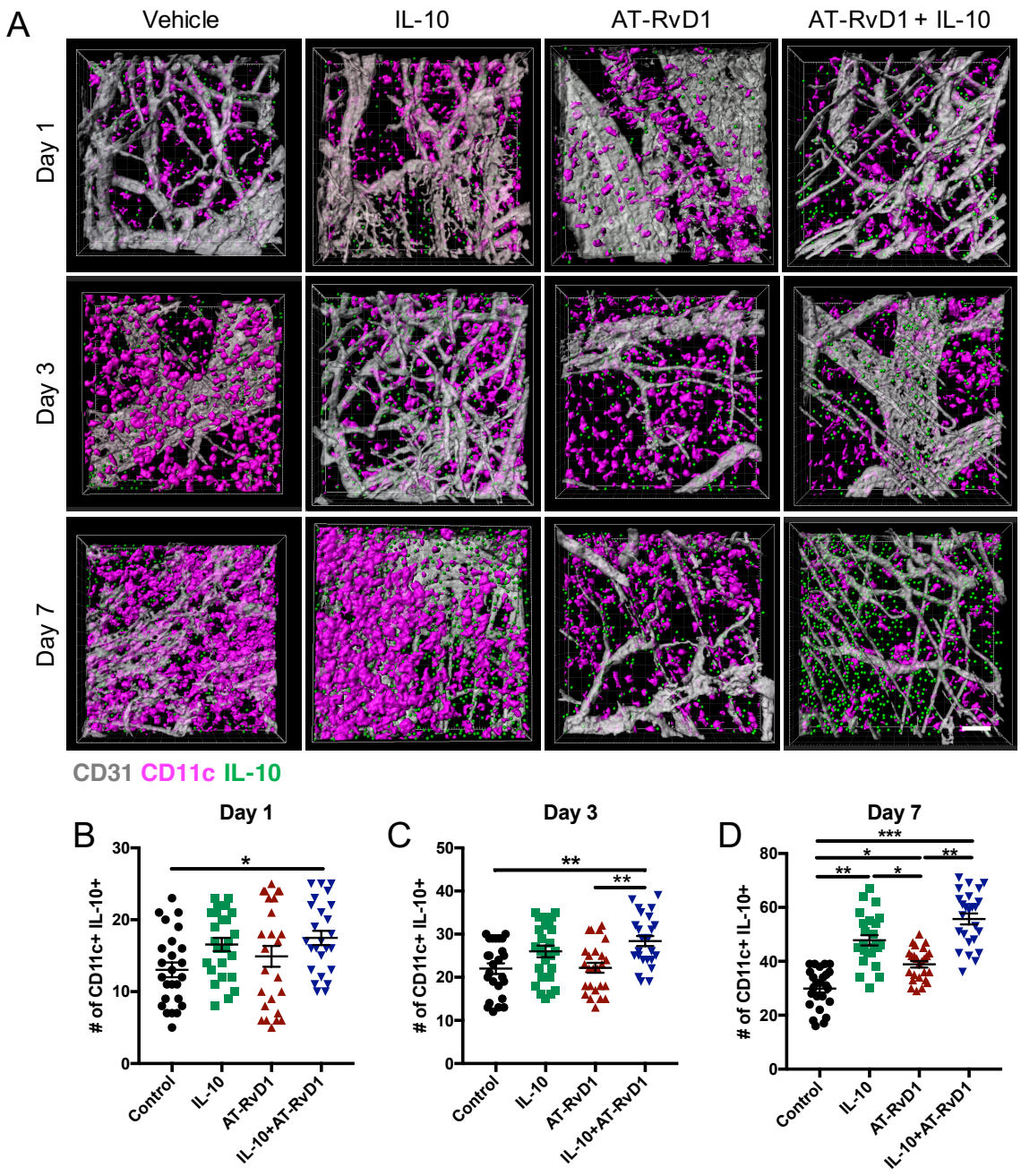

Figure 24. 3D analysis of dendritic cell and IL-10 colocalization. (A) Imaris renderings of CD11c+ dendritic cell and IL-10 staining over time. (B-D) Quantification of total CD11c+ surface and IL-10+ spot colocalization found in Imaris renderings after each timepoint. Scale bars, 30µm. Data presented as mean ± S.E.M. Statistical analyses were performed using Mann-Whitney Test *p<0.05, **p>0.01 ***p<0.001, n>100 cells, across 3-4 animals per group.

These findings were further confirmed through quantification of immunohistochemical staining for CD11c and IL-10. Imaris renderings of dorsal tissue were used to measure CD11c and IL-10 coexpression levels (Figure 24A). The number of CD11c cells also coexpressing IL-10 was significantly higher after IL-10+AT-RvD1 treatment compared to control at all time points (Figure 24B-D). This constrasts with our flow cytometric findings, indicating that there may be an early localized enrichment of CD11c+IL-10+ DCs in the peri-implant area that is drowned out by the larger pool of conventional DCs in the surrounding tissue. At day 7, there were significantly more IL-10 expressing CD11c DCs following treatment with IL-10. AT-RvD1 treatment increased IL-10 DC populations compared to control, but not to the level of IL-10 or IL-10+AT-RvD1 treatments.

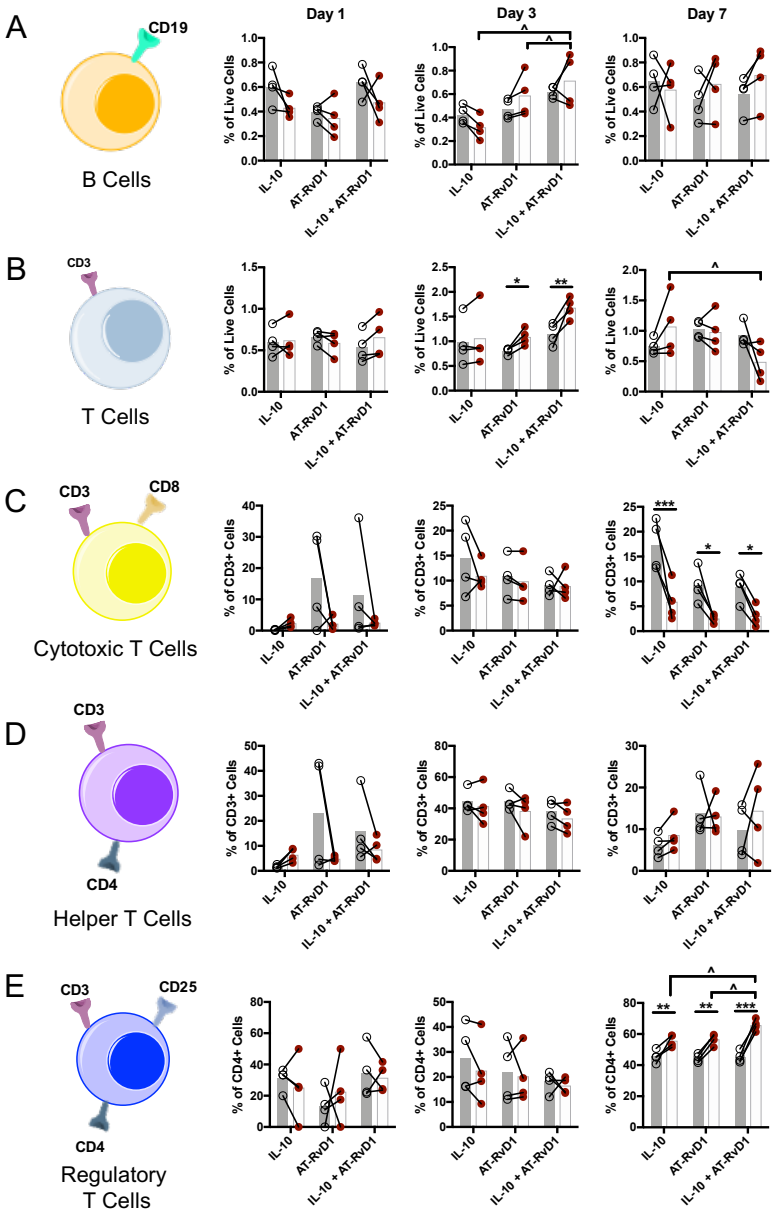

Figure 25. Lymphoid recruitment kinetics in the dorsal tissue Flow cytometric analysis of (A) B cell, (B) total T cell, (C) CD8+ T cell, (D) CD4+ T cell, and (E) CD25+ Treg recruitment into the dorsal skinfold window chamber following treatment with immunomodulatory PEG-MAL Hydrogels. Open circles correspond to unloaded internal control, closed circles are treated tissue. Statistical analysis was performed using two-way repeated measures ANOVA with Tukey's or Bonferroni post-hoc test. Data presented as internal control and treatment with connecting lines. *p>0.05, **p>0.01, ***p>0.001 compared to internal control, ^p>0.05 compared to other treatment group, n=4.

.

To complete our inquiry into the immune response to PEG-MAL immunomodulatory hydrogels, we used flow cytometry to quantify lymphocyte infiltration after dorsal skinfold window chamber surgery. We chose to quantify CD19+ B cells, total CD3+ T cells, CD8+ cytotoxic T cells, CD4+ helper T Cells, and CD4+ CD25+ regulatory T cells (Treg). The overall proportion of both B cells and T cells out of the total live cell population found in the dorsal skin remained relatively constant across all timepoints, with B cells comprising less than 1% of the total cells measured and T cells ranging from 0.5% to 2% at the highest levels (Figure 25A-B). At day 3, we found that AT-RvD1 and IL-10+AT-RvD1 treatment significantly increases the B cell population compared to IL-10 treatment (Figure 25A). However, the potential roles that B cells play in tissue regeneration and wound healing remain unknown. We observed a significant increase in the total T cell population at day 3 in animals treated with AT-RvD1 or combination IL-10+AT-RvD1 compared to internal control. At day 7, there was a subsequent decrease in total T cells, and this level was significantly decreased after IL-10+AT-RvD1 treatment compared to IL-10-only hydrogels (Figure 25B). CD8+ cytotoxic T cells and CD4+ helper T cells made up small fractions of the T cell population one day after injury (Figure 25C-D). The majority of CD3+ T cells at one day were CD4-CD8- double negative cells, which are a population of T cells currently being investigated for having context-dependent disparate functions[200]. At later timepoints, we see expansion of the CD4+ and CD8+ populations until day 7, where there is a significant reduction in CD8+ t cells in all treatment groups compared to internal controls (Figure 25C-D). We then tracked the kinetics of CD25+ Treg accumulation over time and found that, while there were no differences after one and three days, by day 7, Tregs comprised over 50% of the total CD4+ T cell population in all groups,

a proportion significantly higher than corresponding internal controls (Figure 25E). Additionally, we found that the dual-loaded IL-10+AT-RvD1 hydrogels significantly increase the population of Tregs in tissue compared to both IL-10-only and AT-RvD1-only hydrogels.

4.2.5 Vascular remodeling as a model outcome measure following immunomodulatory hydrogel implantation

Finally, we examined vascular bed remodeling in the window chamber as a measure of tissue regeneration, given the major role that vascular expansion and remodeling plays during wound healing. We used longitudinal brightfield intravital microscopy to track changes in the dorsal skin vascular networks after implantation of immunomodulatory hydrogels. We took brightfield images on day 0 immediately following surgery and gel injection and used those images as baseline measurements. We took images again on postoperative days 3 and 7. After 7 days, there are marked increases in vascular tortuosity and overall vascularity of the dorsal skin compared to day 0 and also compared to the internal control, especially noticeable in the AT-RvD1 and IL-10+AT-RvD1-treated skin (Figure 26A).

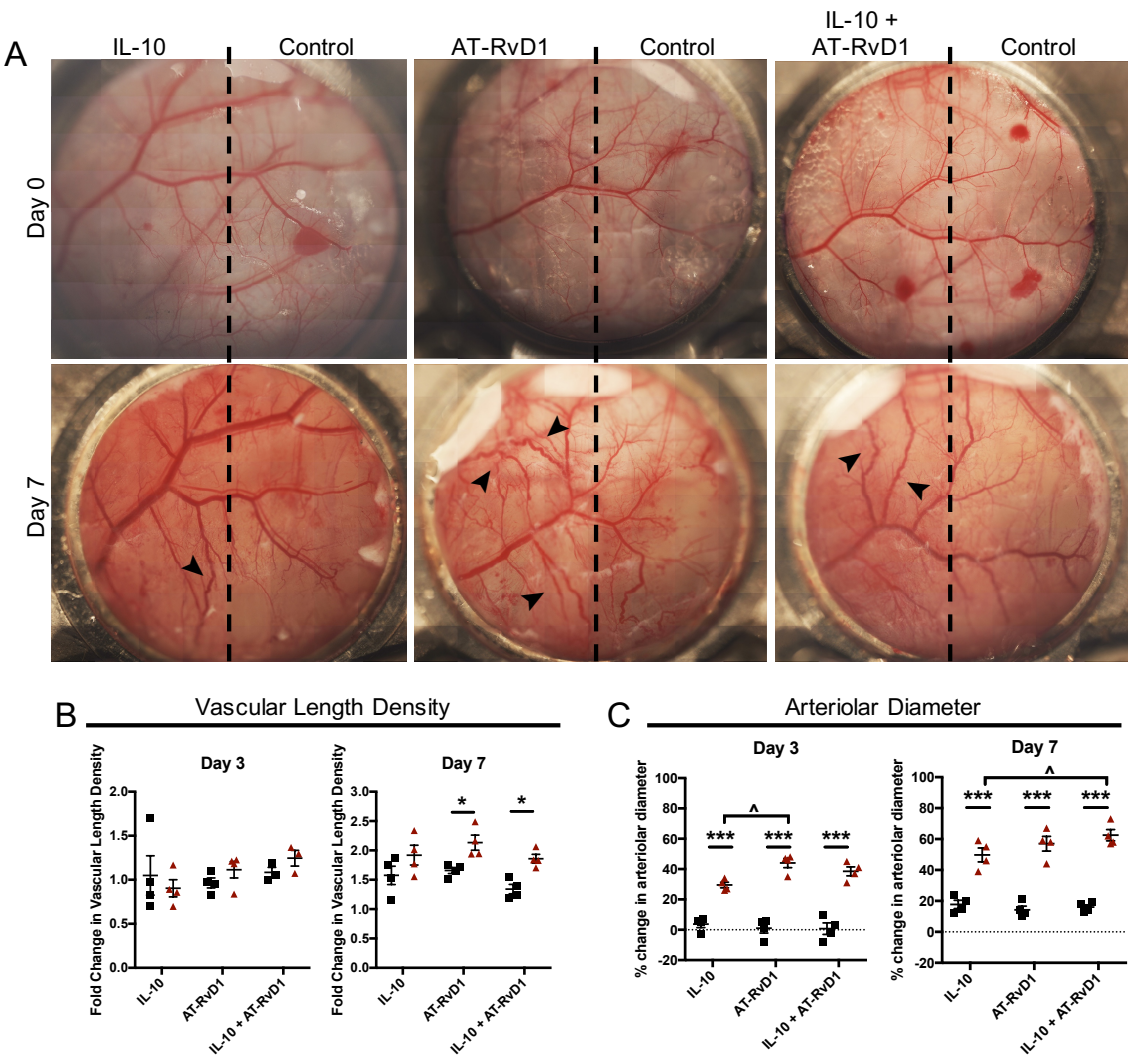

Figure 26. Vascular remodeling following immunomodulatory hydrogel injection (A)Brightfield micrographs of dorsal tissue at day 0 and at day 7 following treatment with immunomodulatory PEG-MAL hydrogels. Quantification of the vascular metrics (B) length density and (C) arteriolar diameter. Data presented as mean ± S.E.M. Statistical analyses were performed two-way repeated measures ANOVA with Tukey's and Bonferroni post hoc tests. *p<0.05, **p>0.01, ***p<0.001 compared to internal control, ^p>0.05 compared to treatment group. n=4 animals per group. Scale bars, 1mm.

We quantified the changes in vasculature through two established metrics of angiogenesis – vascular length density, and arteriolar diameter. We did not see significant changes in the overall length density of the vasculature after treatment with IL-10 only hydrogels compared to control at days 3 or 7 (Figure 26B). We do, however, observe

significant increases in vascular length density in animals treated with AT-RvD1 alone or in combination with IL-10 (Figure 26B). When measuring arteriolar diameter, immunomodulatory PEG-MAL hydrogels significantly increase arteriolar diameter compared to internal control at days 3 and 7 (Figure 26C). There is also a significant increase in AT-RvD1 arteriolar diameter compared to IL-10 at day 3, but this increase is only transient. By day 7, IL-10+AT-RvD1 had significantly increased the arteriolar diameter compared to IL-10 and not AT-RvD1 alone (Figure 26C). In summary, this data shows that immunomodulatory hydrogels are able to modulate vascular remodeling and expansion after implantation, and that dual-delivery of IL-10+AT-RvD1 is able to enhance these remodeling processes above other groups.

4.3 Discussion

The use of biomaterial implants to deliver cells or bioactive molecules capable of directing the host immune response after injury can modulate processes critical to the restoration of tissue homeostasis, such as cellular cytokine release, vascular remodeling, or deposition of extracellular matrix. It is becoming increasingly apparent that these processes are regulated not only by cells of the innate immune system, such as monocytes and macrophages, but that cells of the adaptive immune system play active and important roles. It is our goal to develop a material that can enrich the wound microenvironment with pro-regenerative cells of both the innate and adaptive immune system to enhance the regenerative response. Due to the wide variety of cell types involved, it is unlikely that single delivery is sufficient to recruit and activate all of these cells, and that delivery of multiple factors is necessary to generate the desired immune response. We have previously shown that local delivery of AT-RVD1 from polymer thin films is able to improve vascular

remodeling and enhance the accumulation of Ly6Clow non-classical monocytes and CD206+ M2 macrophages [178]. To attain a higher level of control over both innate and adaptive immune cell recruitment, we have developed a hydrogel-based system capable of the dual delivery of two factors crucial for the recruitment and activation of pro-regenerative cells of both the myeloid and lymphoid lineages. PEG-MAL hydrogels were engineered to achieve simultaneous *in vivo* release of both AT-RvD1 and IL-10. We found that both AT-RvD1 and IL-10 alone are able to modulate the recruitment of various inflammatory and anti-inflammatory immune cells, but dual delivery of these factors enhances the recruitment and accumulation of Ly6Clow monocytes, CD206+ M2 macrophages, IL-10+ dendritic cells, and Tregs, suggesting a synergistic interplay between AT-RvD1 and IL-10 that allows for increased control of the recruitment of cells from the innate and adaptive immune system compared to either treatment on its own.

We have previously developed a dual-delivery protein-small molecule hydrogel system using PEG-diacrylate as the polymer backbone [166]. Here, we engineered a PEG-maleimide-based hydrogel system that allows for the dual release of AT-RvD1 and IL-10. This PEG-MAL system allows for the incorporation of adhesive peptides into the hydrogel backbone, as well as control over gelling and degradation kinetics through the modification of component pH and chosen peptide crosslinker [201]. This control over gelation time allows for these hydrogels to be used as preformed implants or as an injectible *in situ* gelling system, depending on the context and desired material properties, allowing a greater application flexibility than other hydrogel systems which may require ultraviolet light or harsh chemicals for crosslinking and must be formed *ex vivo*. Because human IL-10 does not have a free cysteine group available for interaction with the maleimide groups, we

utilized the thiolation reagent 2-iminothiolane to add these groups to the IL-10. Without the addition of thiol groups, approximately 90% of the loaded unmodified IL-10 was released *in vitro* after 24 hours. After thiolation, the release of IL-10 was much slower, with nearly 70% of the loaded IL-10 remaining in the gel at day 5. The thiolated IL-10 was also able to modulate the expression of TNF- α in RAW264.7 macrophages following LPS treatment, indicating that thiolation does not affect the ability of IL-10 to modulate pro-inflammatory responses after inflammatory stimulus. The AT-RvD1, which was not tethered to the PEG-MAL backbone, was delivered from the hydrogel primarily in a burst release over the first 24 hours, consistent with our previous release kinetics from AT-RvD1-loaded PLGA thin films. This dual-release profile will allow for fast release of AT-RvD1 after *in situ* hydrogel gelation to target the myeloid first responders followed by a more gradual release over time of thiolated IL-10 to influence the activity of cells involved in the later stages of the inflammatory response, mimicking the natural progression of the immune response.

The accumulation of immune cells in injured tissue is important in the process of restoring tissue homeostasis after injury, but perhaps more important is the cellular phenotype and effector functions [63]. For example, macrophages and exist on a spectrum of activation ranging from pro- to anti-inflammatory, with the M1 CD86+CD206- phenotype considered to be more pro-inflammatory, and the M2 CD86-CD206+ phenotype considered to be more anti-inflammatory [202]. Persistent accumulation and activation of M1 macrophages has been associated with disease states such as type 2 diabetes and atherosclerosis [137], but complete blockage of M1 pathways has been associated with impaired tissue repair and wound healing [64]. When designing immunomodulatory

materials with the overall goal of ameliorating inflammation and promoting tissue repair, it is important to consider the necessary balance between allowing pro-inflammatory signaling to occur and amplifying anti-inflammatory signals, as both are needed in the regenerative process [67]. Indeed, allowing an unabated "M2-like" anti-inflammatory response can result in excessive tissue remodeling and fibrosis [179]. We subcutaneously injected immunomodulatory hydrogels containing IL-10, AT-RVD1, or a combination of these factors into excisional skin wounds and chronicled the immune response to these hydrogels over time. We observed significant decreases in the recruitment of circulating pro-inflammatory immune cells following delivery of immunomodulatory hydrogels – namely, hydrogels containing AT-RvD1 dampened local neutrophil infiltration, while IL-10 and AT-RvD1 treatment modulated Ly6Chi infiltration. However, these treatments were not able to completely block the recruitment of these pro-inflammatory cells. Additionally, with our combination treatment we saw a transient increase in M1 macrophages after one day followed by a significant decrease in this population by day 7 in animals treated with AT-RvD1 or the combination hydrogels. Taken together, these findings indicate that while these immunomodulatory hydrogels are indeed capable of modulating the immune system, they still allow for the necessary actions of "pro-inflammatory" cell subsets. On the other hand, the recruitment of Ly6CLow monocytes and M2 macrophages was significantly increased at days 3 and 7 following AT-RvD1 treatment. Interestingly, IL-10 only treatment was not able to modulate the recruitment of these immune cell subsets, but dual delivery of IL-10 and AT-RvD1 significantly increased these populations compared to AT-RvD1-only hydrogels, indicating the existence of a synergistic feed-forward mechanism between AT-RvD1 and IL-10 that is able to amplify

the recruitment of differentiation of these anti-inflammatory cells. Our finding of increased CD206+ M2 macrophages via flow cytometric analysis was further supported using analysis of whole mount immunohistochemistry, where we observed significantly more CD68+CD206+ cells in the peri-implant dorsal tissue. This synergy may be explained by recent expanded understanding of the M2 subset of macrophages. This population exists in at least three polarization states, deemed M2A, M2b, and M2c [203]. M2a and M2c have similar effector functions, but M2c is polarized by IL-10, whereas M2a is polarized in the presence of IL-4 [69]. Dual delivery of AT-RvD1 and IL-10 could increase the M2c pool, thereby expanding the overall CD206+ population. However, more in-depth studies examining the gene expression of the CD206+ macrophages treated with AT-RvD1 only or combination therapy is needed to definitively differentiate between M2a and M2c macrophage subsets.

It was then our goal to expand our inquiry into cell subsets involved in wound healing that we not explored previously, dendritic cells and lymphocytes. We are particularly interested in the populations of dendritic cells polarized by IL-10. These DC subsets have been sometimes called “tolerogenic DCs” or DC-10s, and have the ability to signal to Treg populations and promote their activity. Additionally, these tolerogenic DCs have been shown to improve cardiac function and survival after myocardial infarction through the induction of Tregs and promotion of neovascularization and amelioration of pathologic left ventricle wall remodeling [204]. Due to these actions, IL-10+ DCs may serve as a cellular bridge between the pro-regenerative arms of the innate and adaptive immune systems. We found that combination IL-10+AT-RvD1 treatment reduces the overall CD11c+ DC population at day 3 and 7 following injury compared to AT-RvD1-

only treatment. We observed significant decreases in overall expression of TNF- α within the DC population among all groups compared to control, indicating the ability of all treatments to diminish the pro-inflammatory activity of immune cells. By day 7, flow cytometric and whole mount immunohistochemistry analysis showed that IL-10+AT-RvD1 combination treatment significantly expanded the population of IL-10+ DCs. When we measured IL-10 staining via IHC, we saw additional IL-10 that was not colocalized with CD11c. This IL-10 staining could be extracellular IL-10 that has been released from cells and is in the interstitial tissue. The IL-10 could also be intracellular IL-10 present within Tregs. Future analyses could modify our IHC staining panels to include a T cell marker to visualize the contributions of these cells. Owing to the ability of IL-10+ DCs to signal to lymphocytes, we also examined the kinetics of B and T lymphocytes to the injured dorsal tissue. It remains unclear as to what role B lymphocytes may play in the wound healing process, and the implications of the observed transient increase in B cells with IL-10+AT-RvD1 combination treatment must be explored further. Within the T lymphocyte pool, different subsets and their roles in wound healing have previously been studied. CD8+ cytotoxic T cells have been shown to secrete IFN-y and TNF- α and can delay bone fracture healing and osteogenesis [205]. Subsets of CD4+ T helper (Th) cells have been shown to have differing roles on the inflammatory process, and the Th2 response is associated with an increased pro-regenerative response [72]. We did not observe changes in the overall CD4+ Th pool after immunomodulatory biomaterial implantation, but more thorough discrimination of the Th pool may show differences in the type of Th response elicited by hydrogel implantation. Although we did not see any differences in the total Th population, we found that IL-10 and AT-RvD1 are able to significantly increase the

proportion of CD4+ CD25+ Tregs by one week. Similar to the synergy observed in the monocyte and macrophage populations, combination IL-10+AT-RvD1 therapy significantly increases the Treg population over internal control, as well as over the IL-10 or AT-RvD1 single therapy. Tregs can modulate neutrophil behavior and can direct monocyte and macrophage polarization through the secretion of IL-10, IL-4, and IL-13 [206, 207]. Tregs also contribute to wound healing via the attenuation of conventional CD8+ and CD4+ T cell activity, although Treg activity seems to be largely tissue dependent [77]. In skin, Tregs can inhibit M1 inflammatory activity and promote wound closure via the Jag1-Notch signaling pathway[74]. Overall, recruitment of IL-10+ DCs and Tregs is associated with positive wound healing outcomes.

Post-injury vascular remodeling is a crucial step in the tissue repair process that is necessary to ensure the delivery of nutrients and recruited cells to the regenerating tissue. The vascular network is expanded via formation of new vessels and by remodeling of existing vasculature. This vascular network expansion is carried out by recruited leukocytes of many varieties, including monocytes, macrophages and T lymphocytes [135, 202, 208]. Leukocytes are able to drive this process through the secretion of growth factors and matrix-remodeling enzymes [43, 170, 174, 208-211]. We have previously shown that local delivery of FTY720, SDF-1a, and AT-RvD1 are able to promote vascular remodeling processes. In this study, we show that immunomodulatory bioamterials loaded with IL-10, AT-RvD1, or combination are able to affect vascular remodeling over time. IL-10 single therapy is able to enhance arteriolar enlargement but is not able to promote expansion of the vascular network. On the other hand, AT-RvD1 and combination treatments significantly increased both arteriolar caliber and vascular network length density,

indicating a remodeling of existing vasculature as well as expansion of new vessels. While we cannot definitively prescribe a mechanism underlying these findings, increased vascular network expansion may be associated with non-classical monocyte and M2 macrophage accumulation observed after AT-RvD1 therapy that was not seen following IL-10-only therapy. Overall, the dual delivery of IL-10 and AT-RvD1 via PEG-MAL hydrogel is able to enhance the recruitment of pro-regenerative immune cells of both myeloid and lymphoid lineages and modulate innate wound healing processes, such as vascular remodeling after injury. This dual-delivery system has the potential to improve therapeutic wound healing outcomes following trauma or tissue transplantation via synergy of cellular recruitment and polarization processes to promote anti-inflammatory cell recruitment and activity.

4.4 Methods

4.4.1 Thiolation of IL-10

Carrier-free recombinant human IL-10 was purchased from BioLegend. IL-10 was thiolated using 30 molar excess of Traut's reagent (Sigma) for one hour in PBS containing 0.1uL EDTA per uL buffer to chelate free metals. The thiolation reaction was shaken at RT for one hour. Thiolated IL-10 was separated from unreacted Traut's reagent using a Zeba desalting column according to manufacturer's instructions. Thiolation was detected using a Measure-IT™ Thiol Assay Kit (Invitrogen) according to kit instructions. Number of thiol groups per IL-10 was calculated using the concentration of detected thiols and the known concentration of IL-10 in each measured sample.

4.4.2 Hydrogel Fabrication

Four-arm poly(ethylene glycol) (PEG, 10 kDA molecular weight) end-functionalized with maleimide (>95% purity, Laysan Bio) at 4.5% weight/volume was used for all hydrogel formulations. PEG macromers were functionalized with RGD peptide (GRGDSPC), crosslinked with the cysteine-flanked peptide VPM (GCRDVPMSMRGGDRCG) (AAPPTec) in 0.5M MES buffer, pH 5.5. The final concentration of RGD was 1.0mM. Gels were also loaded with 50ug/mL IL-10, and 4ug/mL AT-RvD1 (Cayman Chemical). The crosslinker concentration was based on the concentration of non-reacted maleimide groups remaining on PEG macromers. For hydrogels used in animal studies, all components were filtered through a spin column after pH measurements and kept under sterile conditions until injection into the animals. To generate pre-formed hydrogels for release studies, the hydrogel was formed on a sterilized petri dish. After crossslinking, hydrogels were incubated at 37˚C for 15 minutes and then swelled in PBS for at least 30 minutes. Release of thiolated and unthiolated IL-10 was measured over time in 1% BSA solution using IL-10 tagged Alexa Fluor 405 NHS Ester (Life Technologies) according to the manufacturer's recommendation and quantified using a standard curve of known fluorescent IL-10 concentrations. Release of AT-RvD1 was measured with a Shimadzu UFLC High Performance Liquid Chromatograph (Columbia, MD, USA) equipped with a Shimadzu Premier C18, 5µm (250x4.6mm) column. AT-RvD1 elution was measured at 8.6 minutes using a wavelength of 301nm. Known quantities of AT-RvD1 were used to generate a standard curve relating AT-RvD1 mass to total peak area. Using serial dilutions, we determined that the limit of detection was below 0.5pg/µL. The total amount of AT-RvD1 in each release sample was calculated using the standard curve.

4.4.3 Macrophage TNF- α Expression Assay

Expression of TNF- α by RAW264.7 macrophages after treatment with Lipopolysaccharide was used as a metric for measuring bioactivity of IL-10 and AT-RvD1. One million RAW264.7 cells were cultured in 6 well plates with Dulbecco's modified Eagle medium (Gibco) containing 1mM sodium pyruvate (Gibco) and 2mM L-glutamine (Gibco) supplemented with 10% Fetal Bovine Serum (FBS, Gibco). Cells were pretreated with IL-10, thiolated IL-10, PEGylated thiolated IL-10, AT-RvD1, AT-RvD1 and thiolated IL-10 combination, or control PBS for one hour. Pretreatment dosages were equal to dosages loaded into hydrogels. Pretreatment was removed and cells were washed once with PBS. Cells were then stimulated with 50ng/mL LPS for two hours in 2mL media supplemented with 100uL Brefeldin-A (manufacturer) per mL cell culture media. Cells were removed from wells and fixed with 4% paraformaldehyde for 30 minutes at RT. Cells were permeabilized through two washes of PBS containing 1% FBS and 0.1% Saponin. Cells were stained for TNF- α (eBioscience) and TNF- α staining was detected using a FACS-AriaIIIu flow cytometer (BD Biosciences).

4.4.4 Dorsal Skinfold Window Chamber Surgery

Animal experiments were performed using sterile techniques in accordance with an approved protocol form the Georgia Institute of Technology Institutional Animal Care and Use Committee. Male C57BL/6 mice (Jackson) aged 6-12 weeks were anesthetized by inhaled isofluorane and surgically fitted with sterile dorsal skinfold window chambers (APJ Trading Co.) as previously described [178]. Briefly, the dorsal skin was shaved, depiliated, and sterilized via three washes with 70% ethanol and chlorhexidine. The dorsal skin was

drawn away from the back of the mouse and one side of the titanium frame was attached to the underside of the skin. Sterile surgical micro scissors were then used to expose the microvasculature through the removal of the epidermis and dermis in a 12mm diameter circle. 25ul sterile hydrogels were then mixed, drawn into a syringe, and injected underneath the exposed vascular bed. For internally controlled experiments, the unloaded control hydrogel was injected on the caudal side of the window chamber, and the loaded hydrogel was injected rostrally. Exposed tissue was then sealed with a sterile glass coverslip. Mice were administered sustained-released buprenorphine i.p. (0.1-0.2 mg/kg) and allowed to recover in heated cages. All mice received standard laboratory diet and water ad libitum throughout the course of the experiment.

4.4.5 Vascular Metrics

Mice were anesthetized with isofluorane, the glass window was removed, and dorsal tissue was superfused with adenosine in Ringer's solution (1mM) to prevent desiccation and to maximally dilate exposed vessels. The mouse was mounted on a microscope stage and imaged non-invasively at 5x magnification on a Zeiss Imager.D2 microscope with AxioCam MRC 5 color digital camera (Zeiss). Images were acquired on day 0 immediately following film implantation and again on days 3 and 7. Microvascular length density measurements were made within a 4000x4000 pixel square region of interest (ROI) around the film. Vessels within these ROIs were traced and total vessel length per unit area was quantified via ImageJ. Arteriolar diameter measurements were made within the ROIs by identifying arteriolar-venular pairs at day 0. Internal diameter changes were measured via ImageJ and days 3 and 7 diameters were normalized to day 0.

4.4.6 Tissue Harvest and Flow Cytometry

To collect samples for flow cytometry analysis, mice were euthanized via CO2 asphyxiation. The dorsal tissue was excised and digested with collagenase type 1-A (1mg/ml, Sigma) at 37°C for 30 minutes and further separated with a cell strainer to create a single cell suspension. Single cell suspensions of dorsal tissue were stained for flow cytometry analysis using standard methods and analyzed on a FACS-AriaIIIu flow cytometer (BD Biosciences). Dead cells were excluded through staining using Zombie Red fixable viability stain (BioLegend). The antibodies used for identifying cell populations of interest were: PE conjugated MerTK (Biolegend), PE-Cy7 conjugated MHC-II (BioLegend), BV605 conjugated CD206 (BioLegend), BV510 conjugated Ly6C (BioLegend), APC-Cy7 conjugated Ly6G (BioLegend), BV711 conjugated CD64 (BioLegend), BV785 conjugated CD19 (BioLegend), APC conjugated Cd11b (BioLegend), BV421 conjugated CD11c (Biolegend, FITC conjugated CD86 (BioLegend), PerCP-Cy5.5 conjugated CD3 (Biolegend), BV785 conjugated CD8 (BioLegend), BV605 conjugated CD4 (BioLegend), and BV711 conjugated CD25 (BioLegend). Staining using BV dyes was performed in the presence of Brilliant Stain Buffer (BD Biosciences). Cells were stained for intracellular cytokines using PE conjugated IL-10 (BioLegend) and PE-Cy7 conjugated TNF- α (eBiosciences). Positivity was determined by gating on fluorescence minus one controls. Absolute quantification of cell numbers was performed by adding 25μL of AccuCheck counting beads to flow cytometry samples (Thermo Fisher Scientific).

4.4.7 Tissue Whole Mount Immunohistochemistry and Confocal Imaging

Following euthanasia, mouse vasculature was perfused with warm saline and then with 4% paraformaldehyde until tissues were fixed. The dorsal tissue was excised and permeabilized overnight at 4°C with 0.2% saponin. The tissues were blocked overnight in 10% mouse serum at 4°C. Tissues were incubated at 4˚C overnight in staining solution containing 0.1% saponin, 5% mouse serum, 0.5% fatty-acid free bovine serum albumin, and the following fluorescently conjugated mouse antibodies: Alexa Fluor 594 anti-CD31 antibody (1:100 dilution, BioLegend) for blood vessel visualization, Brilliant Violet 421 anti-CD68 (1:200 dilution, BioLegend) for visualization of macrophages, and Alexa Fluor 647 anti-CD206 (1:200 dilution, Biolegend) for visualization of M2 macrophages. The following unconjugated antibodies were also used: Biotin anti-CD11c (1:200 dilution, BioLegend) for visualization of dendritic cells, and Rabbit polyclonal anti-IL-10 (1:200 dilution). Tissues were washed four times for 30 minutes with 0.2% saponin and stained with Streptavidin-conjugated Alexafluor 430 (1:200 dilution, Invitrogen) and Goat anti-rabbit Alexa Fluor 488 (1:200 dilution, Abcam) secondary antibodies for 4 hours at room temperature. Tissues were washed twice for 30 minutes with 0.2% saponin and again overnight at 4˚C. Specimens were then washed once in PBS for 30 minutes and mounted in 50/50 glycerol/phosphate buffered saline. Mounted samples were imaged on a Zeiss LSM 710 NLO confocal.

4.4.8 Statistical Analysis

All statistical analyses were performed using Graphpad Prism version 6.0 (La Jolla, CA). Results are presented as mean ± standard error of the mean (SEM). For grouped analyses, one-way ANOVA with Tukey's post-test was used for multiple comparisons. For internally controlled experiments, two-way ANOVA was used. Tukey's post-hoc test was

utilized when comparing paired samples, and Bonferroni's post hoc test was employed when comparing between treatment groups. Unless otherwise noted, $p<0.05$ was considered statistically significant.

CHAPTER 5. IMMUNOMODULATORY HYDROGELS LOCALLY MODULATE THE IMMUNE RESPONSE TO ALLOGRAFT TISSUE

5.1 Introduction

Solid organ transplantation procedures have been on the rise in the past decade in the United States and currently, organ transplant is the most effective treatment option in the context of end-stage organ failure [2, 8]. The most common procedures are kidney, liver, heart, and lung transplantations, but our ability to perform other transplant procedures including vascularized composite allograft of face or upper limb is increasing and soon these procedures may become more commonplace [2]. Currently, the use of post-transplantation immunosuppressive regimens (IS) has resulted in significant increases in survival after solid organ allograft, with rates nearing 90% after one year[9]. Donated tissue rejection is prevented through the use of systemic immunosuppression (IS) regimens that alter the immune response and block the recognition of and response to donor antigens [212]. Despite decreases in acute rejection of transplants with IS, significant complications stemming directly from systemic IS are still prevalent, in both the acute and chronic time frame after transplant. Chronic use of systemic IS is associated with an increased risk of opportunistic infection, particularly fungal infection, lymphoproliferative disorders, and wound toxicity including cardiovascular disease or renal failure[2, 3]. Acutely, surgical wound complications following transplantation are still extremely common [3]. Therefore, there exists an opportunity to try to prevent acute post-surgical wound healing complications through the development of alternative therapies outside of systemic IS that

are able to exploit endogenous mechanisms of wound healing and tissue acceptance to prevent acute wound closure complications and promote early tissue integration.

Impaired wound healing after transplant surgery is one of the most common complications arising from high doses of systemic immunosuppression. Wound dehiscence and other complications have been reported in the context of nearly every transplant procedure, including heart, kidney, and liver [3, 10]. For example rates of surgical wound complications including superficial or deep wound infection, lymphocele, and wound dehiscence have been reported in 8-15% and sometimes up to 40% of heart transplant recipients compared with 0.5-10% of patients after similar general cardiac surgery procedures that do not involve transplantation [3]. These complications can be exacerbated by a multitude of patient risk factors, including age, obesity, and diabetes [11]. Given the aging population and rising obesity rates, wound healing complications following transplant are at risk of becoming more and more common. At the root of many of these wound healing complications are drugs used for IS that also impair key processes in the wound healing cascade. The mammalian target of rapamycin (mTOR) inhibitors sirolimus and everolimus, corticosteroids, and other common immunosuppressive drugs such as cyclosporine A, tacrolimus, and mycophenolate motefil have all been reported to impair wound healing processes resulting in decreases in tensile wound strength or anastomotic breaking strength in animal models [12-17]. These studies indicate that the common combinatorial approach of immunosuppression taken to prevent the rejection of transplanted organs may be compounding the impairment of processes necessary to ensure proper healing of surgical sites and prevent wound healing complications.

In lieu of systemic IS, local modulation of the immune response to transplant can potentially allow for early integration of transplanted tissue and surgical wound closure while concurrently delaying allograft rejection. In fact, many of the immune cells responsible for directing wound healing processes can also play roles in preventing the rejection of transplanted tissue. For example, we have previously shown that Ly6CLow non-classical monocytes are skewed toward long-term anti-inflammatory cell fate, and that these monocytes are active mediators of vascular remodeling and restoration of tissue homeostasis [61, 178]. Non-classical monocytes are biased progenitors of M2a/c macrophages, and these macrophages can release cytokines that reduce inflammatory dendritic cell (DC) activity [92, 93]. These non-classical monocytes can also promote regulatory T cell (Treg) differentiation through PD-1 signaling [95]. Additionally, IL-10+ DCs have previously been shown to improve ventricular function following ischemic myocardial infarction and can also promote the differentiation and activation of immunosuppressive Treg populations[184, 204, 213]. Tregs themselves have become cells of interest during regeneration and have demonstrated context-dependent involvement in wound healing processes in skin, bone, muscle, and other tissues[73, 75, 77]. In response to transplant, Tregs can facilitate graft survival through numerous molecular signaling pathways, including induction of T and B cell cycle arrest and apoptosis, secretion of suppressive cytokines such as IL-10 and TGF-ß, prevention of T cell expansion, costimulation, and activation, and inhibition of DC maturation[186, 214, 215]. Therefore, enriching the transplant milieu with these dual-acting cells is a novel therapy aimed at early graft wound healing with the ability to prevent rejection without the need for high doses of systemic IS.

We have previously developed dual-loaded poly(ethylene glycol)-maleimide (PEG-MAL) hydrogels capable of locally delivering therapeutic doses of the specialized proresolving mediator aspirin-triggered resolvin D1 (AT-RvD1) and the immunomodulatory cytokine interleukin 10 (IL-10) to enrich the injured tissue niche with pro-regenerative immune cells with the goal of promoting wound healing. We found that these hydrogels were able to increase the populations of Ly6CLow monocytes, CD206+ M2 macrophages, IL-10+DCs, and Tregs after full thickness skin injury. Delivery of these factors to injured tissue also enhanced vascular remodeling, one of the early markers of the wound healing cascade. In the present study, we utilize these previously characterized immunomodulatory hydrogels in a murine model of skin transplant to track the modulation of the immune response over time and examine graft tissue integration and acceptance. This model was chosen because it creates a robust immune response following tissue transplant and allows for numerous outcomes to be measured. We demonstrate that immunomodulatory hydrogels can tune the immune response to both syngraft and allograft skin transplant. These hydrogels enhance the recruitment of anti-inflammatory myeloid and lymphoid cells to the transplanted tissue, resulting in enhanced wound closure in the syngraft model. In complete MHC-mismatch allografts, although we are able to induce the recruitment of cells involved in wound healing and graft acceptance, the local response was ultimately unable to overcome systemic rejection signals. Although the allografts were rejected, these results indicate that local modulation of immune populations is possible after allograft, and that these immunomodulatory hydrogels could potentially be used in conjunction with systemic IS to promote wound healing after tissue transplant.

5.2 Results

5.2.1 Skin Transplant Histopathological Assessment

We utilized the murine skin transplant model to characterize the immune response to transplanted tissue and concurrent injection of immunomodulatory PEG-MAL biomaterials (Figure 27A). This model was chosen because of the overall surgical ease and its ability to elicit a spectrum of immune responses – from no rejection to swift acute rejection of grafted tissue over the course of 8-10 days. This model also allows for the utlization of numerous techniques to record outcome measures. In this work, we characterize the response to transplanted skin through flow cytometry, multiplex cytokine array, and immunohistochemical staining.

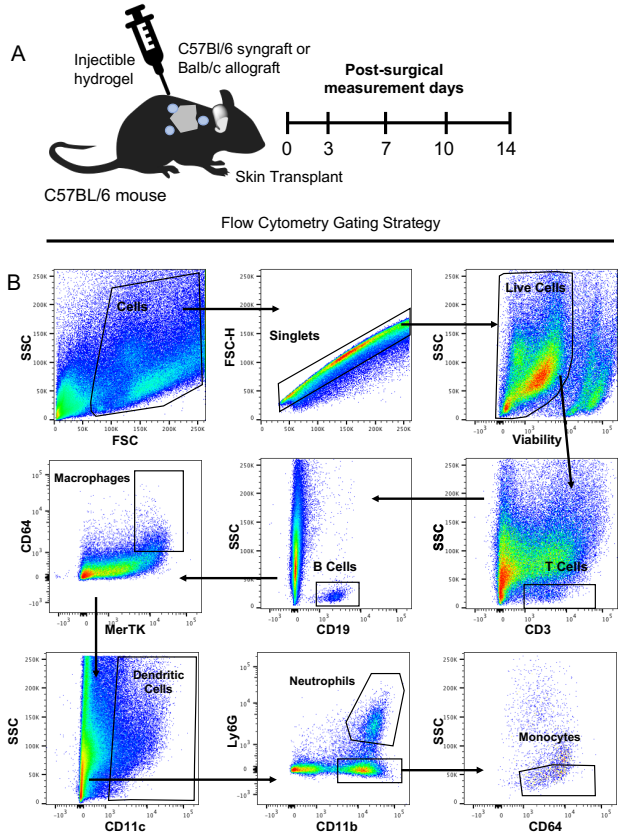

Figure 27. Skin transplant experimental schematic and flow cytometry gating strategy. (A) Experimental overview of dorsal skinfold window chamber experiments and

hydrogel placement. (B) Flow cytometry gating strategy showing major cell types investigated with our panels .

First, we examined the wound healing and integration of genetically identical donor-to-host tail skin tissue grafts and complete MHC mismatch tail skin tissue allografts . Figure 28 shows macroscopic gross images of the grafted syngraft skin over time. As expected, there was complete acceptance of all skin transplants, including control, by 14 days post-transplant, with minor wound contracture appearing after AT-RvD1-loaded hydrogel treatment. At day 10, the dual-loaded IL-10+AT-RvD1 hydrogel treatment group appeared to have complete wound closure, while control hydrogel and IL-10-only or AT-RvD1-only groups had not yet fully healed.

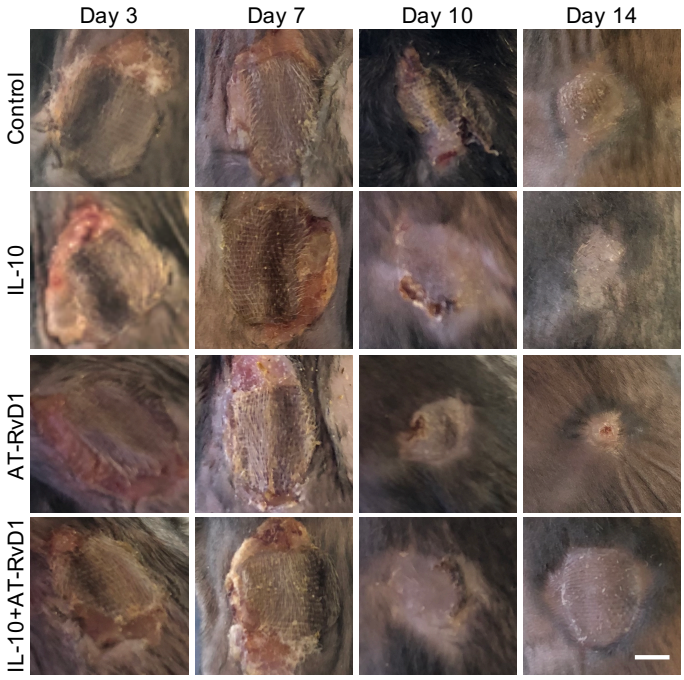

Figure 28. Macroscopic images of syngraft skin transplants. Macroscopic images showing the progression of wound healing and syngraft integration over time following injection of immunomodulatory PEG-MAL hydrogels. Scale bar 0.5mm

Figure 29 shows macroscopic images of the wound and transplanted tissue over time following allograft transplant. We observed enhanced early integration of the transplanted tissue with the host tissue following dual-loaded hydrogel treatment at day 3 compared to other groups, where the wound area remained open. At day 7, the dual-loaded hydrogel groups were still healing, while the control and IL-10-treated animals had begun to exhibit signs of transplant rejection, namely scabbing and darkening of the graft tissue. By day 10, there was marked darkening and contraction of the graft, indicating tissue rejection. By day 14, all of the allografted skin had been rejected in all groups.

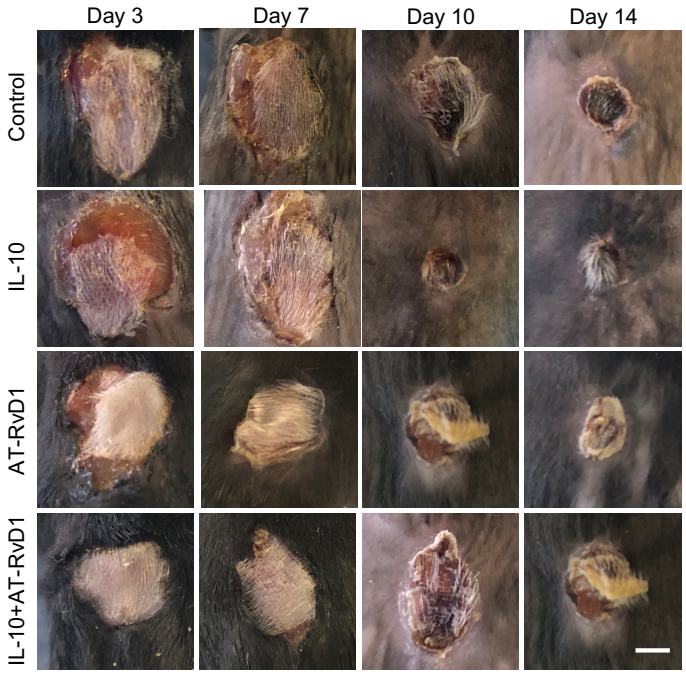

Figure 29. Macroscopic images of allograft skin transplants over time. Macroscopic images showing the progression of allograft integration and rejection over time following injection of immunomodulatory PEG-MAL hydrogels. Scale bar 0.5mm

Microscopic assessment of H&E-stained sections of the skin transplant and surrounding skin tissue revealed no observable differences in mononuclear cell infiltration or overall staining between the control or experimental groups following syngraft (Figure

30). When we examined the allograft tissue, we found that there is a marked increase in infiltration of cells into the tissue across all groups compared to syngraft. This indicates a more robust immune response following allograft compared to syngraft (Figure 30).

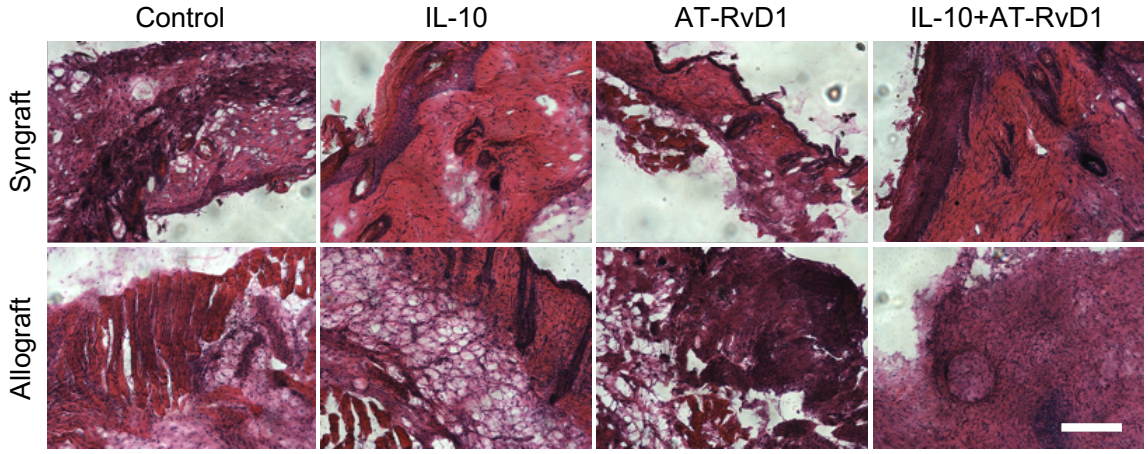

Figure 30. H&E staining of skin tissue following syngraft or allograft. 10x brighfield micrographs showing H&E staining of the skin tissue surrounding the donated skin in syngraft and allograft animals 10 days after immunomodulatory hydrogel injection. Scale bar 300μm

5.2.2 Principal Component Analysis of Flow Cytometric Measurements on Syngraft Skin Tissue

In order to quantify the kinetics of immune cell recruitment following syngraft skin transplant and immunomodulatory hydrogel injection, we harvested skin, lymph node, and blood at days 3, 7, 10, and 14 after transplant. By flow cytometry we are able to identify T cells, including T-helper, T-cytotixic, and T-regulatory subsets, B cells, macrophages and M1 and M2 subsets, dendritic and IL-10+ dendritic cell subsets, neutrophils, and

monocytes including classical and alternatively activated subsets (Figure 27B).

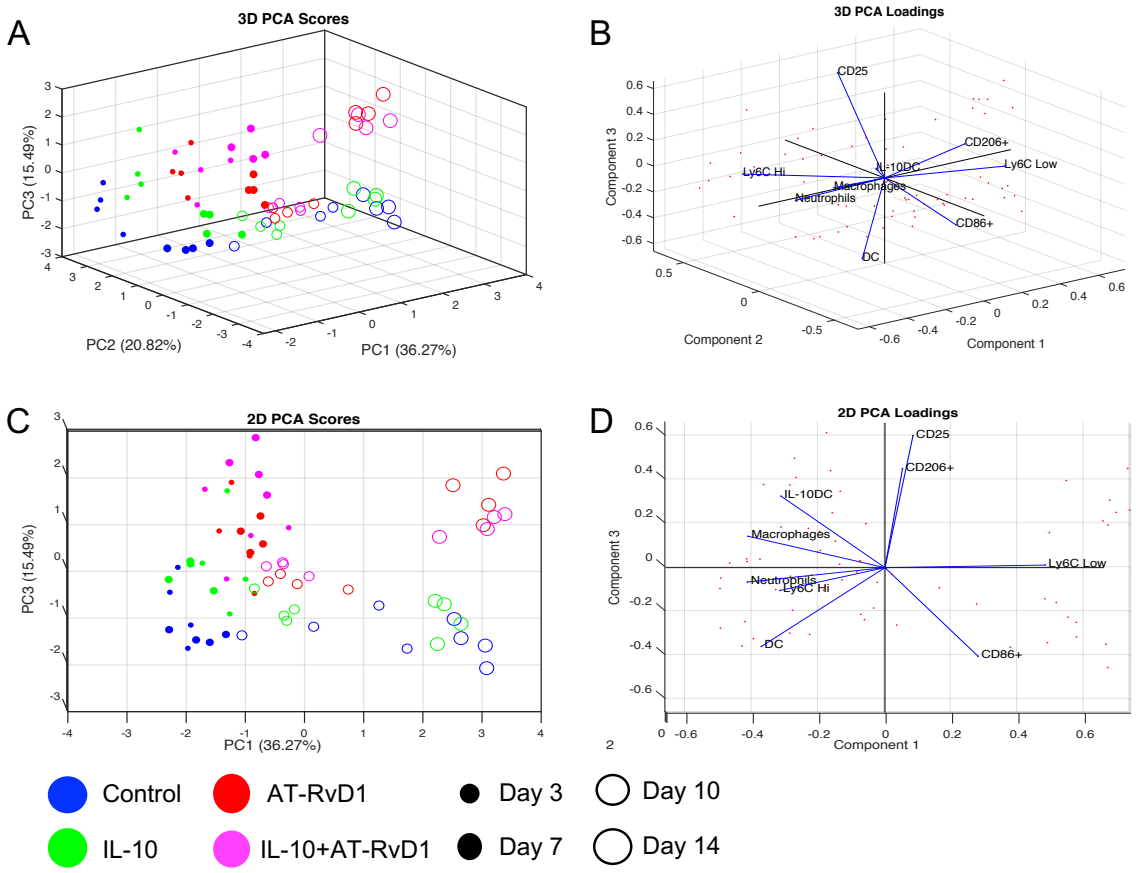

Figure 31. Unsupervised principal component analysis of flow cytometry quantification in syngraft skin transplant skin tissue(A) 3D scores plot of immunomodulatory biomaterial treatments over time. (B) 3D loadings (weight coefficients) plot of the 9 input variables in the reduced principal component space. (C-D) Scores and loadings plots reduced to two dimensions. Input variables are: Macrophages(% of cells), $CD206^{+}$ (% of Macrophages), $CD86^{+}$ (% of Macrophages), DC (% of cells), IL-10+ DCs (% of CD11c+), neutrophil (% of CD11b+), $Ly6C^{lo}$ (% of CD11b+), $Ly6C^{Hi}$ (% of CD11b+),and T_{reg} ($CD25^{+}CD4^{+}CD3^{+}$ % of $CD4^{+}CD3^{+}$). N=4 animals per treatment group at each timepoint**.**

Because this type of analysis produces large multivariate datasets, we used unsupervised principal component analysis (PCA) to describe the progression of the immune response in a reduced-dimensionality model. We wanted to see how the different hydrogel treatments modulated the immune response over time and how similar those

treatments were to the response to transplant and unloaded hydrogel. Figure 31A and B show the three-dimensional scores of each sample and the cell subsets that contribute to each sample's placement within the 3D PCA space. In the syngraft skin tissue, the first three principal components (PCs) account for 72.58% of the variability in the data. The data generally clustered by sample type and timepoint in the PC space suggesting that the different treatments produce distinct immune profiles over time. Interestingly, the combination IL-10+AT-RvD1 treatment and AT-RvD1-only treatment groups cluster together over time. This is expected due to the large number of myeloid cell subsets involved in the inflammatory response, and we have shown previously that AT-RvD1 has the largest influence on myeloid immune cells[178].

To more clearly visualize the data in the PC space, we plotted the PCA data in two dimensional pairwise plots(Figure 31C-D). When we plot PC1 vs PC3, we see that the AT-RVD1 and IL-10+AT-RVD1 treatments cluster away from the IL-10 and control groups, due to increased populations of Tregs, M2 macrophages, and IL-10+ DCs which are heavily weighted in PC3 while loading in PC1 indicates that later timepoints are distinguished by Ly6CLow monocytes, CD25 Treg, and CD86+ macrophage populations.

5.2.3 Circulating Immune Cell Recruitment After Syngraft

Given the differences observed between treatment groups observed by PCA, we then quantified the recruitment kinetics of each cell subset captured by our flow cytometric measurements over time. After syngraft and immunomodulatory hydrogel injection, we saw early modulation of circulating myeloid cell recruitment to the injured tissue. At day 3, we observe significantly fewer neutrophils in the AT-RVD1 and combination IL-

10+AT-RvD1 treatment groups compared to control or IL-10 only treatment(Figure 32A). By day 7, all treatment groups had significantly fewer neutrophils compared to control.

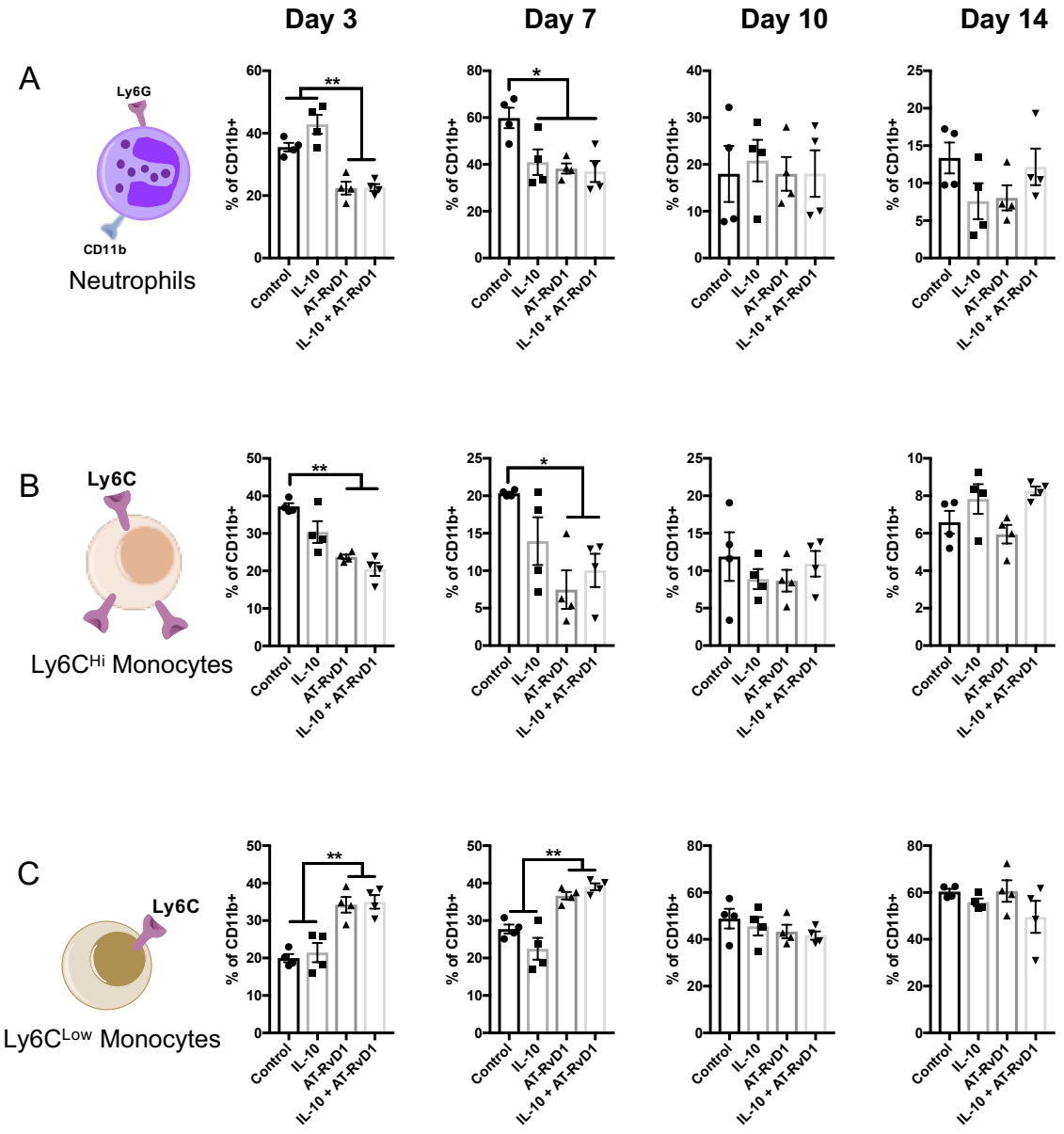

Figure 32. Neutrophil and monocyte recruitment to syngraft skin graft Flow cytometric analysis of (A) neutrophil, (B) Ly6Chi monocyte, and (C) Ly6CLow monocyte recruitment into skin following syngraft transplant and treatment with immunomodulatory PEG-MAL Hydrogels. Statistical analysis was performed using one-way ANOVA with Tukey's. post hoc test Data presented as mean ± SEM. *p>0.05, **p>0.01 , n=4.

.

When examining monocyte populations, AT-RvD1 and IL-10+AT-RvD1 hydrogels significantly reduced the classical Ly6C high population compared to control at days 3 and 7(Figure 32B). Conversely, AT-RvD1 and IL-10+AT-RvD1 significantly increased Ly6CLow alternatively activated monocytes in the tissue at days 3 and 7 compared to both control and IL-10-loaded hydrogels (Figure 32C). At all timepoints, monocyte recruitment was unaffected by IL-10 treatment, consistent with our earlier observations (Figure 32B-C). This effect is again likely due to the differences in release kinetics between AT-RvD1 and IL-10. By the time a therapeutic dose of IL-10 is released from the hydrogel, the peak recruitment period of monocytes has passed and the released IL-10 cannot modulate monocyte infiltration. When examining the temporal recruitment profile, we see similar kinetics across all groups. At day 3, the majority of circulating cells infiltrating the tissue are neutrophils and Ly6Chi monocytes(Figure 32A-B). The proportions of these cells decrease over time, as Ly6Clow cells are recruited to the tissue. Then at days 10 and 14, consistent with the progression of a normally-healing wound, no differences are seen in neutrophil or monocyte populations between all groups, and Ly6Clow monocytes comprise the majority of these cell populations (Figure 32C).

5.2.4 Anti-Inflammatory Macrophages are Increased after IL-10+AT-RvD1 Treatment in Syngraft Skin Tissue

We then analyzed the recruitment of macrophages and macrophage subsets. From days 3-10, CD64+ MerTK+ macrophages comprised 10-20% of the live cell population in the skin tissue and decreased to less than 5% by day 14 (Figure 33A). This differs from previous analysis of dorsal tissue, where monocytes made up less than 5% of infiltrating cells. This difference is likely due to the pool of tissue resident macrophages present in the

dermis that are not present after window chamber surgery. Combination IL-10+AT-RvD1 treatment significantly increased the macrophage population in the skin at day 3 compared to IL-10-only and at day 7 compared to both IL-10-only and AT-RVD1-only hydrogels (Figure 33A). At day 3, AT-RvD1 treatment also significantly increased the overall macrophage population compared to IL-10-only treatment. There were no differences in macrophages at day 10, but after 14 days, significantly more macrophages were present in the skin tissue of animals treated with AT-RVD1 hydrogels or dual-loaded hydrogels, but this increase was greater following AT-RvD1-only treatment (Figure 33A).

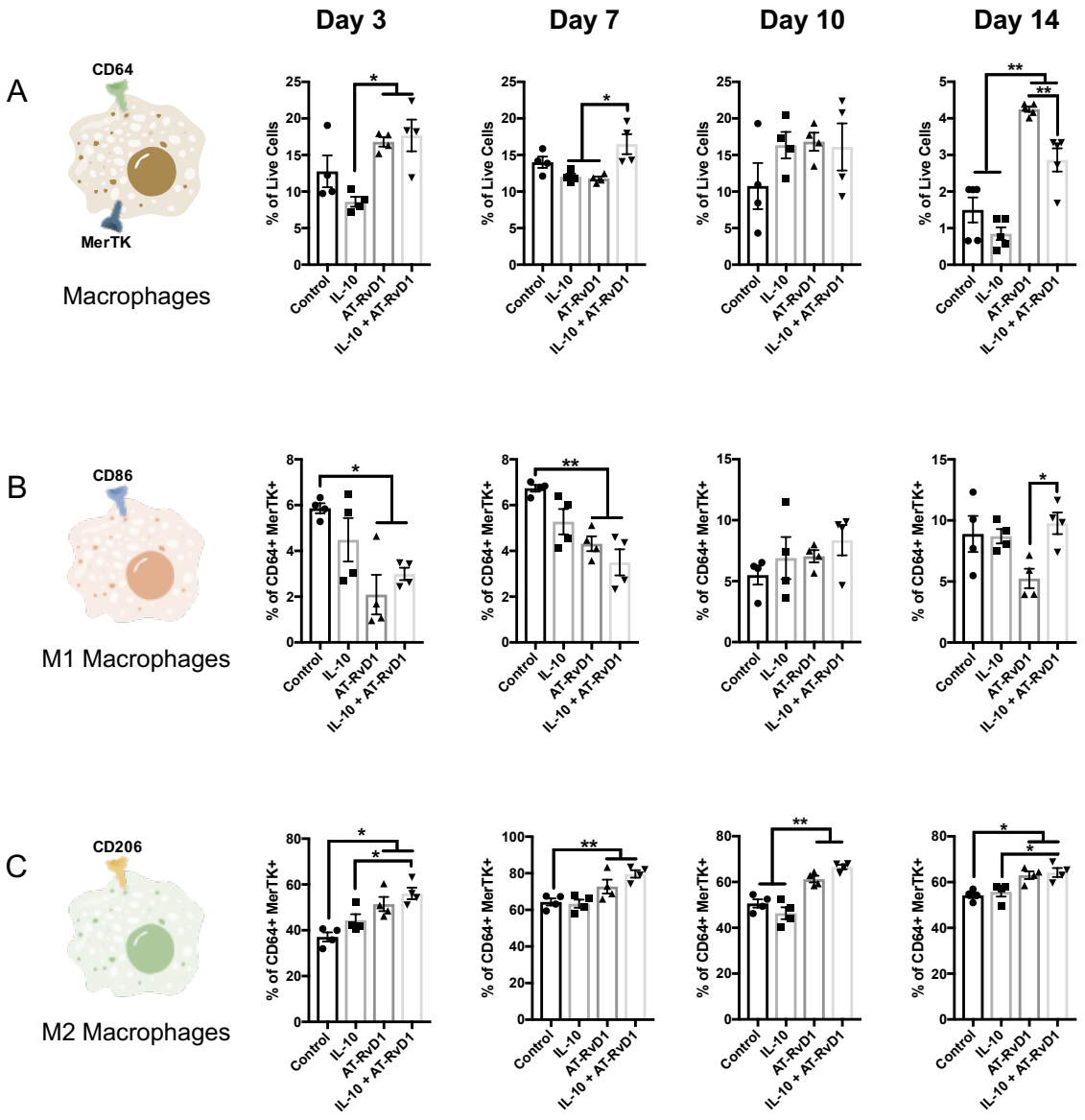

Figure 33. Macrophage recruitment to syngraft skin graft Flow cytometric analysis of (A) macrophage, (B) CD86+ Macrophage, and (C) CD206+ M2 Macrophage populations in the skin following syngraft transplant and treatment with immunomodulatory PEG-MAL Hydrogels. Statistical analysis was performed using one-way ANOVA with Tukey's. post hoc test Data presented as mean ± SEM. *p>0.05, **p>0.01 , n=4.

.

We then utilized differential surface receptor staining to analyze M1 and M2 macrophage phenotypes. M1 classical macrophages are CD86+ and CD206-. The

population of these macrophages was significantly reduced with AT-RvD1 and dual-loaded hydrogel treatment compared to control at days 3 and 7 (Figure 33B). Curiously, we observed a significant increase in M1 macrophages at day 14 in the combination treatment compared to control (Figure 33B). M2 macrophages were characterized by their expression of CD206 and do not express CD86. At all timepoints, AT-RvD1 and combination hydrogel treatment significantly increased the M2 macrophage population compared to control, and combination treatment resulted in significantly increased M2 populations compared to IL-10 only at days 3, 10, and 14 (Figure 33C). These observations indicate that the recruitment of myeloid populations is largely affected by AT-RvD1 treatment and not IL-10 delivery.

5.2.5 Dendritic Cell Recruitment to Syngraft Skin Tissue

Dendritic cells were classified based on their CD11c surface marker expression. These CD11c+ cells comprise a significant portion of the immune cell population in the skin. The predominance of these cells is likely due to the presence of resident CD11c+ Langerhans Cells, antigen presenting cells that are abundant in the dermis and epidermis [216]. At day 3, CD11c+ cells were decreased in IL-10 and AT-RvD1-only hydrogel treated groups compared to control, but not in the dual-loaded hydrogel group. We then saw a significant reduction in the DC population in IL-10+AT-RvD1-treated animals compared to all other groups. By day 14, total DCs were significantly decreased following AT-RvD1 and IL-10+AT-RvD1 combination treatments compared to control or IL-10 hydrogels (Figure 34A). We then examined the population of IL-10+ DCs, as these cells are important not only in signaling to Treg lymphocytes, but also play active roles in wound healing on their own[183]. While AT-RvD1 treatment seems to affect the overall DC

population, it does not have as much of an influence on the induction of IL-10+ DCs. Levels of IL-10DCs found in the skin after hydrogel delivery of AT-RvD1 were significantly increased compared to control at days 7 and 10, but IL-10 treatment alone or in combination with AT-RvD1 was able increase this population even further at the same timepoints (Figure 34B).

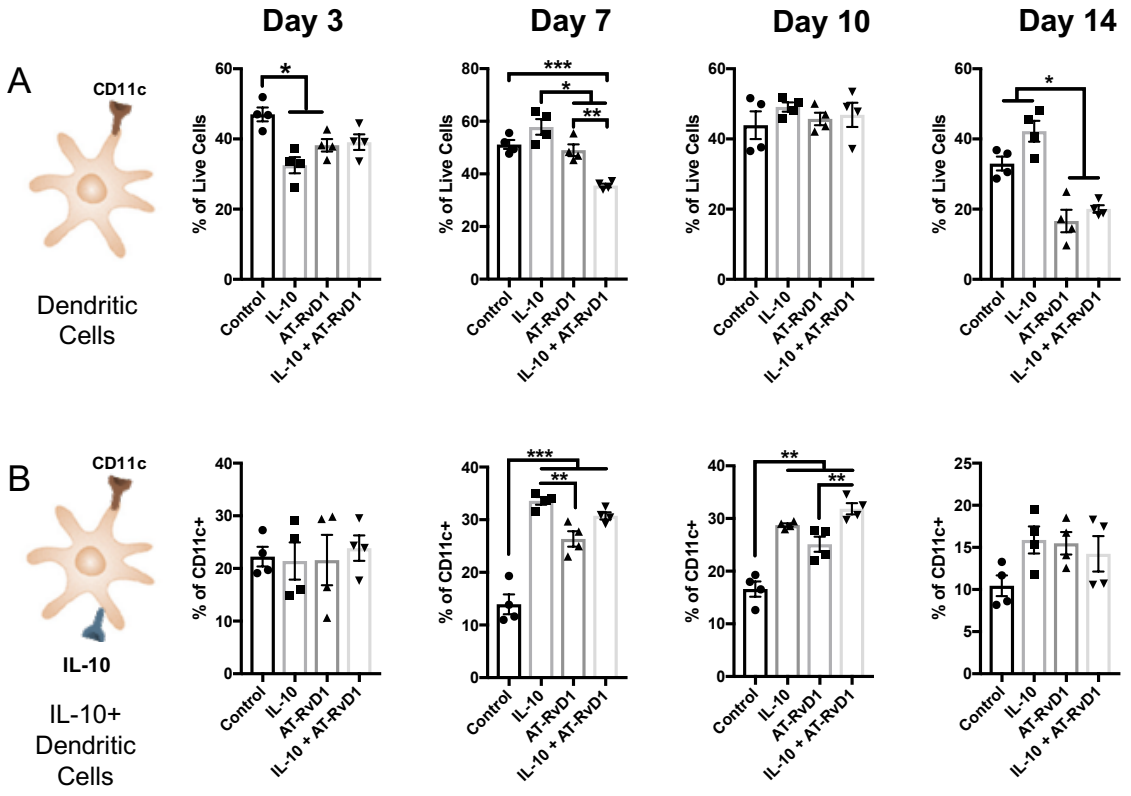

Figure 34. Dendritic cell recruitment to syngraft skin graft Flow cytometric analysis of (A) total CD11c+ dendritic cell and (B) IL-10+ DC populations in the skin following syngraft transplant and treatment with immunomodulatory PEG-MAL Hydrogels. Statistical analysis was performed using one-way ANOVA with Tukey's. post hoc test Data presented as mean ± SEM. *p>0.05, **p>0.01 , ***p>0.001 n=4.

5.2.6 Lymphoid Immune Cell Recruitment following Syngraft

We then repeated PCA on the skin after syngraft but instead this time we attempted to see if clustering of the data occurred on the basis of lymphatic cell markers. Contrasting with the earlier PCA, there is very little observable clustering both in 3D and 2D renderings (Figure 35A-D). This indicates that following syngraft, most of the differences seen in the data are due to changing dynamics of myeloid cell recruitment.

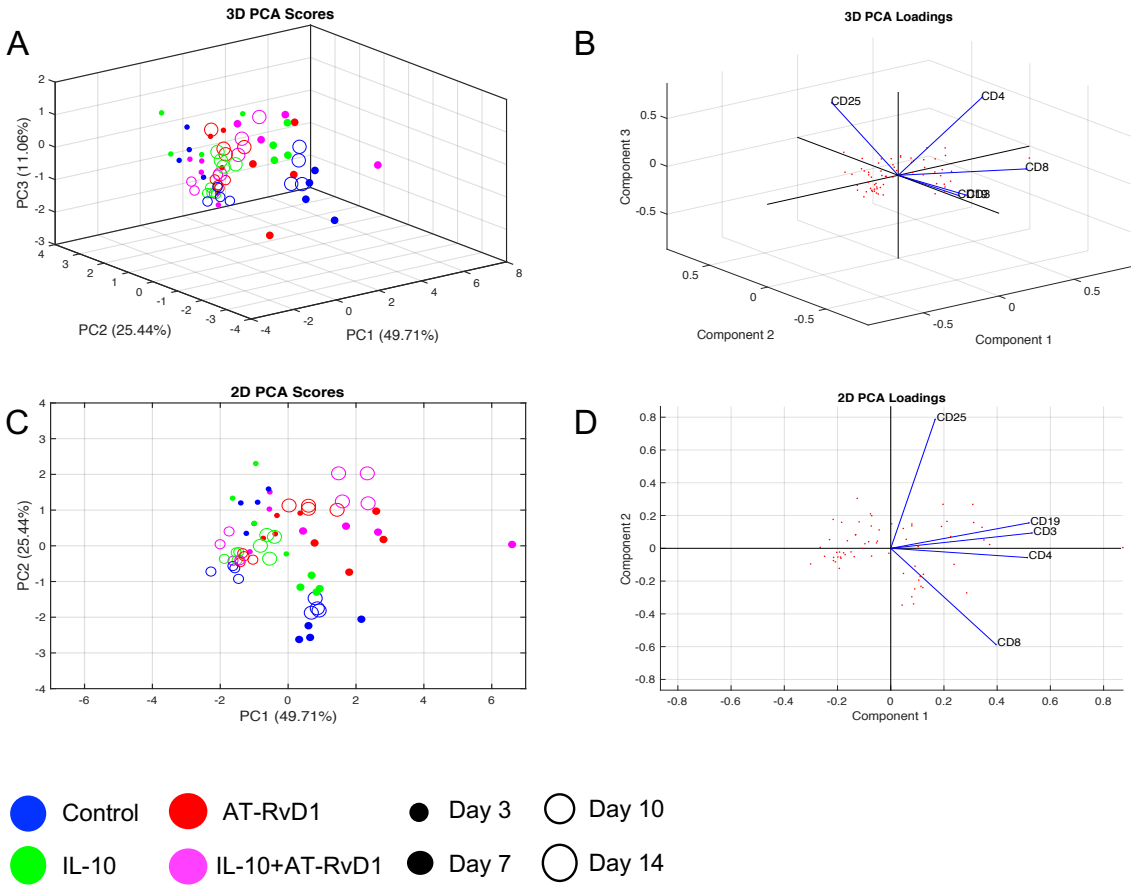

Figure 35. Unsupervised PCA of flow cytometric quantification of syngraft skin graft using lymphoid markers(A) 3D scores plot of immunomodulatory biomaterial treatments over time. (B) 3D loadings (weight coefficients) plot of the 5 input variables in the reduced principal component space. (C-D) Scores and loadings plots reduced to two dimensions. Input variables are: B cells (% of cells), T cells (% of cells), CD8+ T cells (% of CD3+), CD4+ T cells (% of CD3+), and T_{reg} ($CD25^{+}CD4^{+}CD3^{+}$ % of $CD4^{+}CD3^{+}$). N=4 animals per treatment group at each timepoint**.**

Although we do not see apparent clustering in the data due to differential lymphoid cell recruitment, there are still observed differences over time in the recruitment of these cells and subsets. Most of the differences observed between treatment groups were transient. For example, there was a significant increase in B cells in the AT-RvD1 and IL-10+AT-RvD1-treated skin compared to IL-10 at day 3, but this difference is not sustained throughout the rest of the analysis timepoints (Figure 36A). Additionally, we see significant modulation in T cells, CD8+ T cells, and CD4+ T cells at various times (Figure 36B-D). Most persistent, however, are the differences seen in the CD25+ Treg population over time. There are no changes in Tregs at 3 days, but at day 7, the proportion of CD25+ cells out of the total CD4+ T cell population was significantly increased in the skin of animals treated with IL-10+AT-RvD1-loaded hydrogels compared to all other treatment groups, with CD25+ cells comprising over 40% of the total CD4+ population in the dual-loaded hydrogel group (Figure 36E). IL-10-only treatment significantly increased Tregs over both control and AT-RvD1-only treatment. At day 10, all groups had more Tregs present compared to control, but there were no differences between groups. Then, at day 14, the differences observed at day 7 were again seen, with significant increases in Tregs following IL-10 treatment. These results demonstrate that IL-10 alone or in combination with AT-RvD1 is better able to enrich injured skin with pro-regenerative lymphocytes than AT-RvD1 treatment alone.

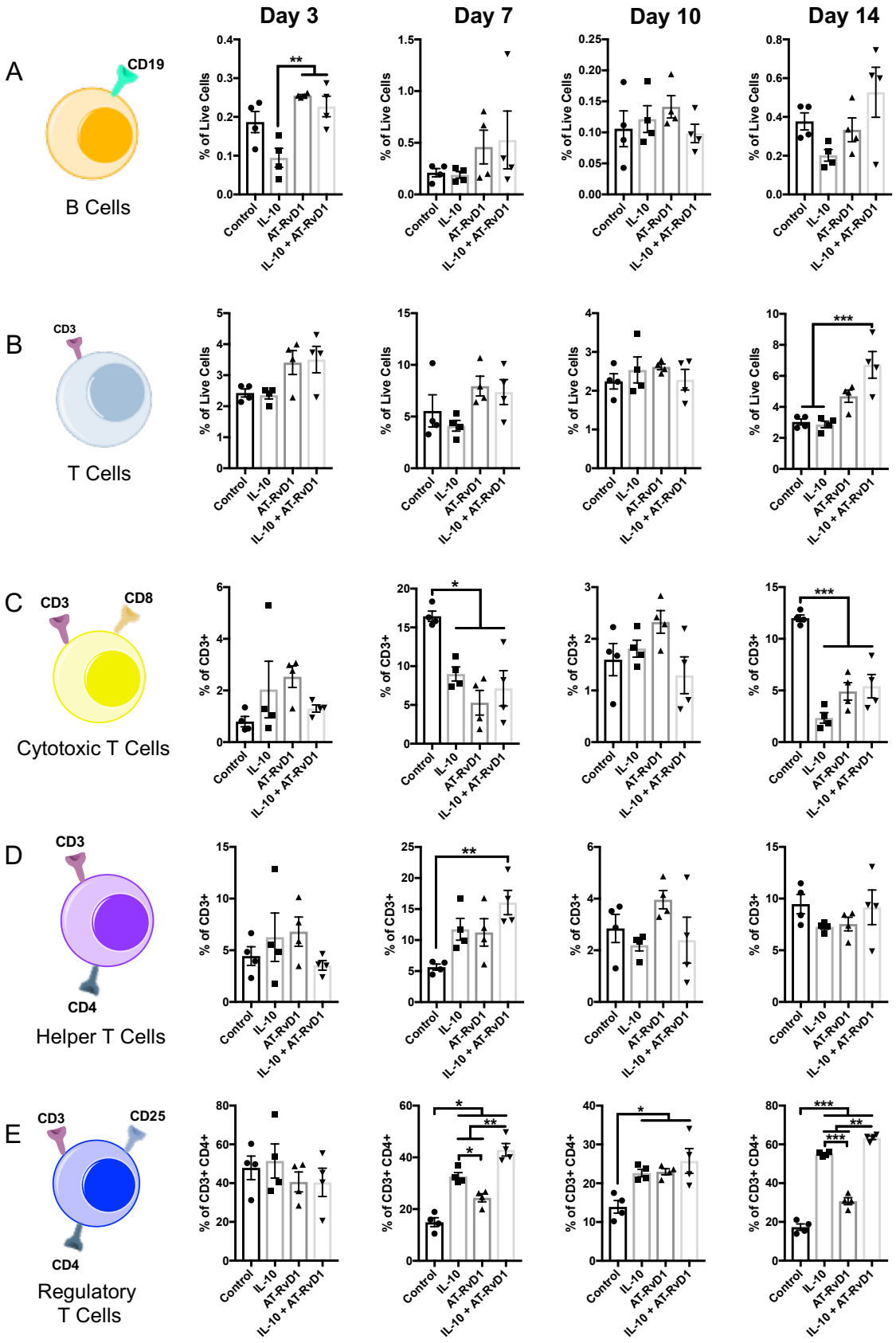
Day 3
Day 7
Day 10
Day 14
A
CD19
B Cells
B
CD3
T Cells
C
CD3
CD8
Cytotoxic T Cells
D
CD3
CD4
Helper T Cells
E
CD3
CD25
CD4
Regulatory T Cells
% of Live Cells
% of CD3+
% of CD3+ CD4+
Control
IL-10
AT-RvD1
IL-10 + AT-RvD1

Figure 36. Lymphocyte recruitment to syngraft skin graft Flow cytometric analysis of (A) B cell, (B) total T cell, (C) CD8+ T cell, (D) CD4+ T cell, and (E) CD25+ Treg recruitment in the skin following syngraft transplant and treatment with immunomodulatory PEG-MAL Hydrogels. Statistical analysis was performed using one-way ANOVA with Tukey's. post hoc test Data presented as mean ± SEM. *p>0.05, **p>0.01 , ***p>0.001 n=4.

5.2.7 Analysis of Immune Cell Profiles in Draining Lymph Nodes and Blood After Syngraft

We also performed PCA on the flow cytometry data gathered from the draining lymph nodes and blood (Figure 37 and Figure 38). PCA on these cells following syngraft and immunomodulatory hydrogel treatments are similar in that there is no definitive clustering of one treatment group from another, but the main separation that is observed in the data is from timepoint to timepoint.

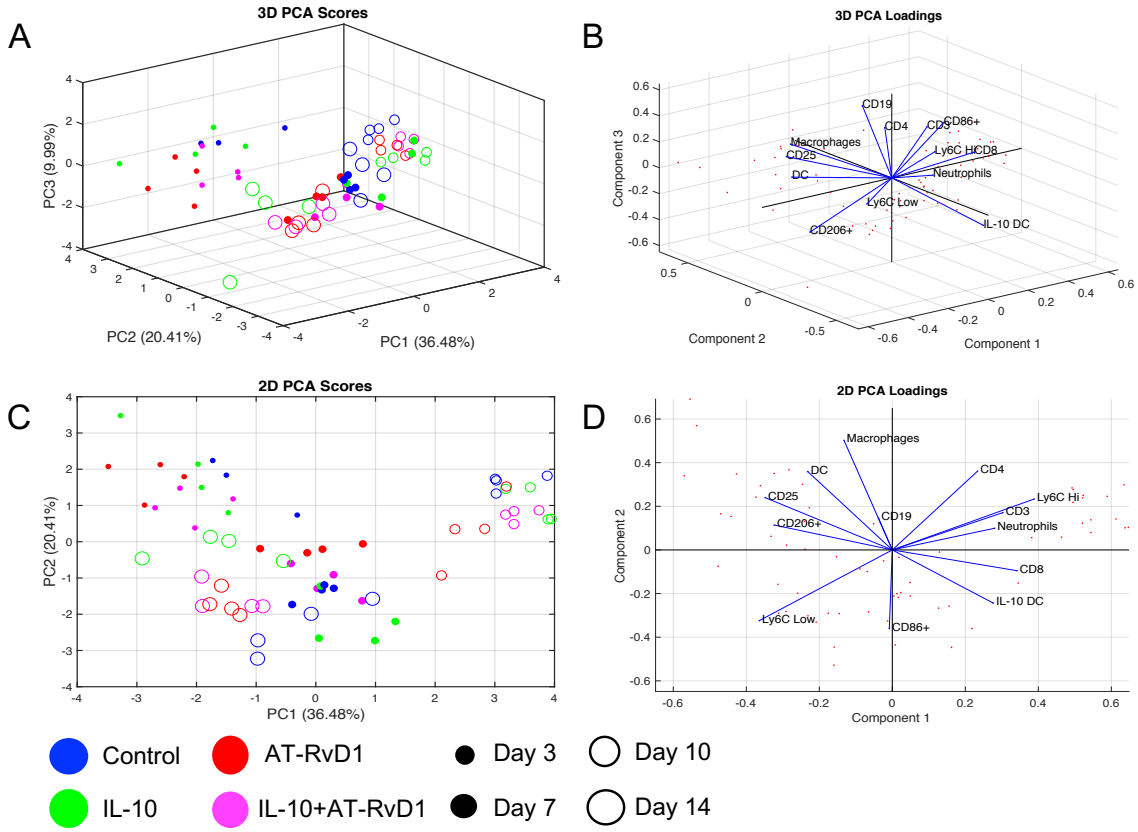

Figure 37. Unsupervised PCA of flow cytometric quantification of syngraft LN data(A) 3D scores plot of immunomodulatory biomaterial treatments over time. (B) 3D loadings (weight coefficients) plot of the 13 input variables in the reduced principal component space. (C-D) Scores and loadings plots reduced to two dimensions. Input variables are: Macrophages(% of cells), $CD206^{+}$ (% of Macrophages), $CD86^{+}$ (% of Macrophages), DC (% of cells), IL-10+ DCs (% of CD11c+), neutrophil (% of CD11b+), $Ly6C^{lo}$ (% of CD11b+), $Ly6C^{Hi}$ (% of CD11b+), B cells (% of cells), T cells (% of cells), CD8+ T cells (% of CD3+), CD4+ T cells (% of CD3+), and T_{reg} ($CD25^{+}CD4^{+}CD3^{+}$ % of $CD4^{+}CD3^{+}$). N=4 animals per treatment group at each timepoint**.**

The clustering found in the skin data is not present in the blood or LN data, indicating that the effects on the immune cell recruitment and populations are largely localized to the area of treatment itself, and there seems to be little systemic response following placement of genetically identical syngrafts.

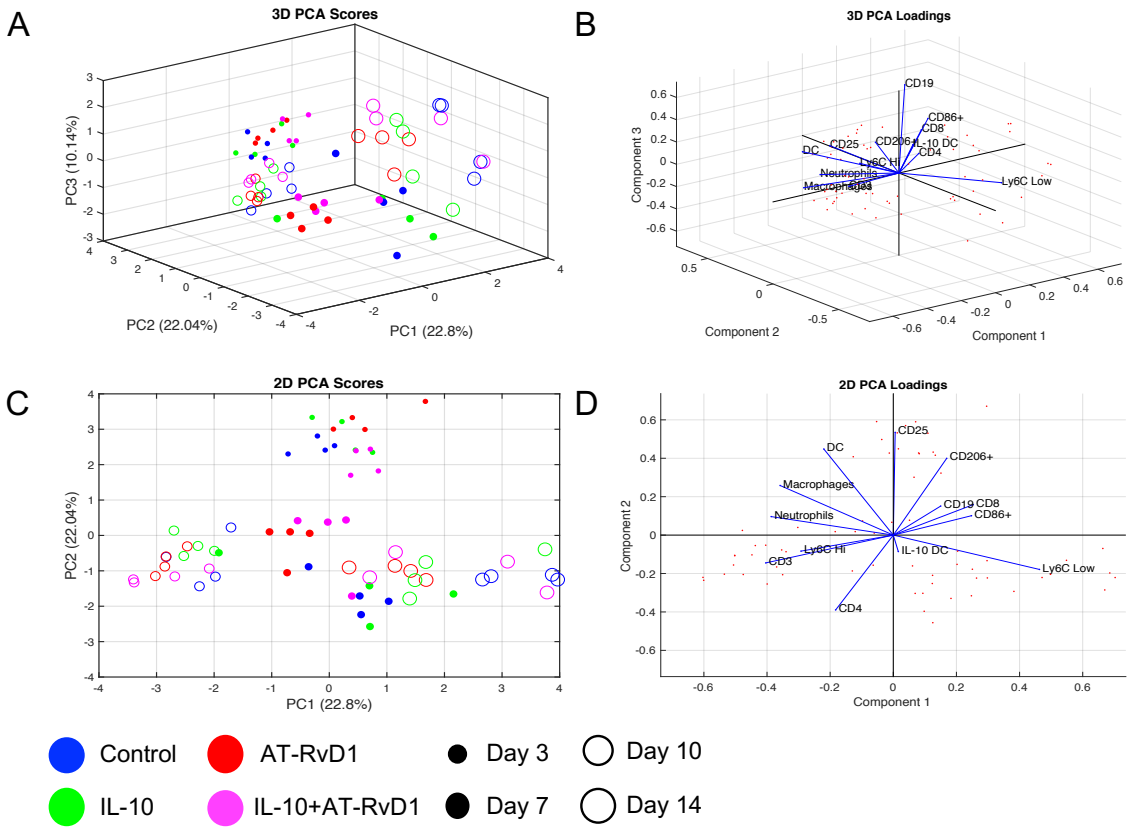

Figure 38. Unsupervised PCA of flow cytometric quantification of syngraft blood data(A) 3D scores plot of immunomodulatory biomaterial treatments over time. (B) 3D loadings (weight coefficients) plot of the 13 input variables in the reduced principal component space. (C-D) Scores and loadings plots reduced to two dimensions. Input variables are: Macrophages(% of cells), $CD206^{+}$ (% of Macrophages), $CD86^{+}$ (% of Macrophages), DC (% of cells), IL-10+ DCs (% of CD11c+), neutrophil (% of CD11b+), $Ly6C^{lo}$ (% of CD11b+), $Ly6C^{Hi}$ (% of CD11b+), B cells (% of cells), T cells (% of cells), CD8+ T cells (% of CD3+), CD4+ T cells (% of CD3+), and T_{reg} ($CD25^{+}CD4^{+}CD3^{+}$ % of $CD4^{+}CD3^{+}$). N=4 animals per treatment group at each timepoint**.**

5.2.8 Principal Component Analysis of Immune Response to Allograft

To examine the effect of immunomodulatory PEG-MAL hydrogels on the integration and acceptance of allograft transplants, we again used the murine skin transplant model where the tail skin of a Balb/C mouse was transplanted onto the back of a C57Bl/6 mouse following the generation of a full thickness defect. In the same manner

as the syngraft data, we applied PCA to the data gathered from flow cytometry on allograft skin and the surrounding tissue. Three PCs were able to account for 67% of the variability in the data, and we observed distinct clustering of the treatment groups, indicating that the immune responses generated following each treatment differed from the other treatment groups (Figure 39A-B). The observed clusters are the result of differential recruitment of subsets of myeloid and lymphoid immune cells. We then collapsed the 3D PCA scores and loadings into two dimensions so we can get a better idea of what cells are contributing to each cluster. PC1 primarily separated samples by groups, while PC3 separated the lymphoid vs myeloid cell subsets (Figure 39C-D). When we map the PCA scores onto components 1 and 3, we see separation of the AT-RvD1 and IL-10+AT-RvD1 cluster seen in the component 1 and 2 graph. In this graph, Treg and IL-10+DC populations are mapped onto quadrant one, while M2 macrophage and Ly6Clow monocytes are projected into quadrant four (Figure 39C-D). The IL-10+AT-RVD1 samples are influenced by both of these cell populations, whereas AT-RvD1-only samples have higher populations of M2 macrophages and Ly6CLow monocytes, while IL-10-only samples have higher populations of Tregs and IL-10DCs.

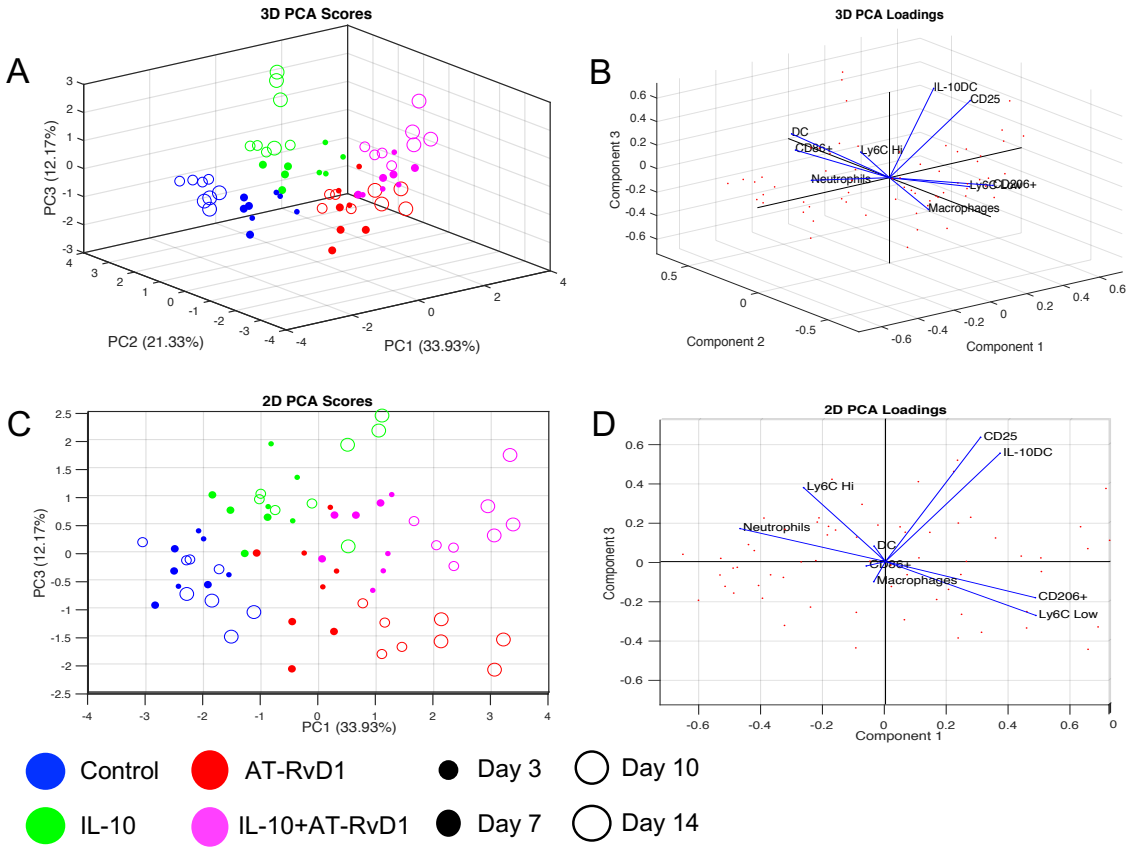

Figure 39. Unsupervised principal component analysis of flow cytometry quantification in allograft skin transplant skin tissue(A) 3D scores plot of immunomodulatory biomaterial treatments over time. (B) 3D loadings (weight coefficients) plot of the 9 input variables in the reduced principal component space. (C-D) Scores and loadings plots reduced to two dimensions. Input variables are: Macrophages(% of cells), $CD206^{+}$ (% of Macrophages), $CD86^{+}$ (% of Macrophages), DC (% of cells), IL-10+ DCs (% of CD11c+), neutrophil (% of CD11b+), $Ly6C^{lo}$ (% of CD11b+), $Ly6C^{Hi}$ (% of CD11b+),and T_{reg} ($CD25^{+}CD4^{+}CD3^{+}$ % of $CD4^{+}CD3^{+}$). N=4 animals per treatment group at each timepoint**.**

5.2.9 Circulating Myeloid Cell Recruitment into Allograft and Surrounding Tissue

As with syngraft, we next analyzed the recruitment kinetics of immune cells into the allograft and surrounding tissue over time. Neutrophil infiltration at all timepoints was attenuated by treatment with AT-RVD1 or combination IL-10+AT-RvD1 compared to

controls (Figure 40A). IL-10-only treatment had no effect on neutrophils except at day 7. Additionally, at day 14, neutrophil levels in AT-RvD1-treated tissue were significantly lower compared to IL-10-only treatment (Figure 40A).

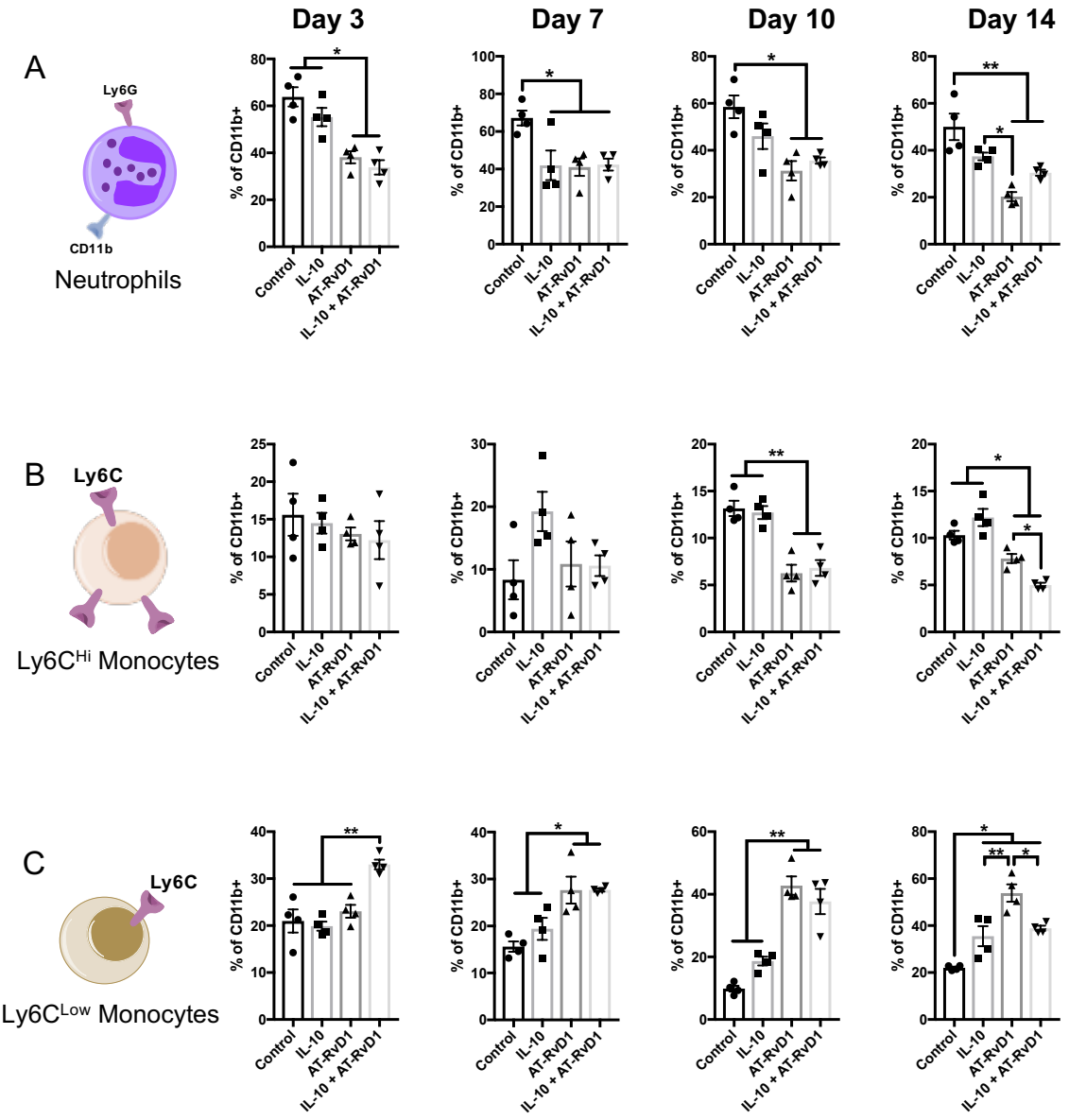

Figure 40. Neutrophil and monocyte recruitment to allograft skin transplant Flow cytometric analysis of (A) neutrophil, (B) Ly6Chi monocyte, and (C) Ly6CLow monocyte recruitment into skin following allograft transplant and treatment with immunomodulatory PEG-MAL Hydrogels. Statistical analysis was performed using one-way ANOVA with Tukey's. post hoc test Data presented as mean ± SEM. *p>0.05, **p>0.01 , n=4.

Immunomodulatory hydrogels were also able to modulate monocyte infiltration and accumulation over time. Unlike syngraft, there were no differences in Ly6Chi monocyte recruitment at days 3 or 7, but these levels were significantly reduced at days 10 and 14 in treatment groups containing AT-RvD1. (Figure 40B) We observed further reduction in Ly6Chi monocytes after dual-loaded hydrogel treatment compared to AT-RvD1-only treatment. In the Ly6CLow monocyte population, we saw significant modulation of recruitment kinetics at all timepoints (Figure 40C). At Day 3, dual-loaded hydrogels had significantly more recruitment of these cells to the skin tissue compared to all other groups. By day 7 and into day 10, the levels of Ly6CLow monocytes in AT-RvD1-treated animals were similar to that of the dual-loaded hydrogels, and both of these were significantly higher than IL-10-only treatment and control. Then at 14 days post-transplant, the high levels of Ly6CLow cells persisted in the tissue treated with AT-RvD1-only hydrogels and was significantly elevated above all other groups (Figure 40C). Ly6CLow monocytes at two weeks in the IL-10 and IL-10+AT-RvD1 treated groups were significantly higher than control, but not at the same level as AT-RvD1 only. This data indicates that even after adding allogeneic tissue to the wound area, immunomodulatory PEG-MAL hydrogels are able to modulate the recruitment and infiltration of circulating monocuclear cells and neutrophils, although the modulation observed after allograft is not the same as was seen following syngraft.

5.2.10 Macrophage Recruitment and Polarization after Allotransplant

We observed modulation of macrophage recruitment after allograft and delivery of immunomodulatory PEG-MAL hydrogels. Compared to syngraft, CD64+MerTK+ macrophages made up a smaller portion of the total live cell population, but this may be

due to increased cellular accumulation of other populations (Figure 41A). At day 3 there were no differences in macrophage accumulation between all groups. There was then a transient increase in the total macrophage population in AT-RvD1 and IL-10+AT-RvD1 combination treatments compared to control and IL-10 hydrogels. This increase was not present at day 10, and by day 14 there was an overall decrease in the population of macrophages in AT-RvD1 and IL-10+AT-RvD1 groups compared to IL-10 and control (Figure 41A).

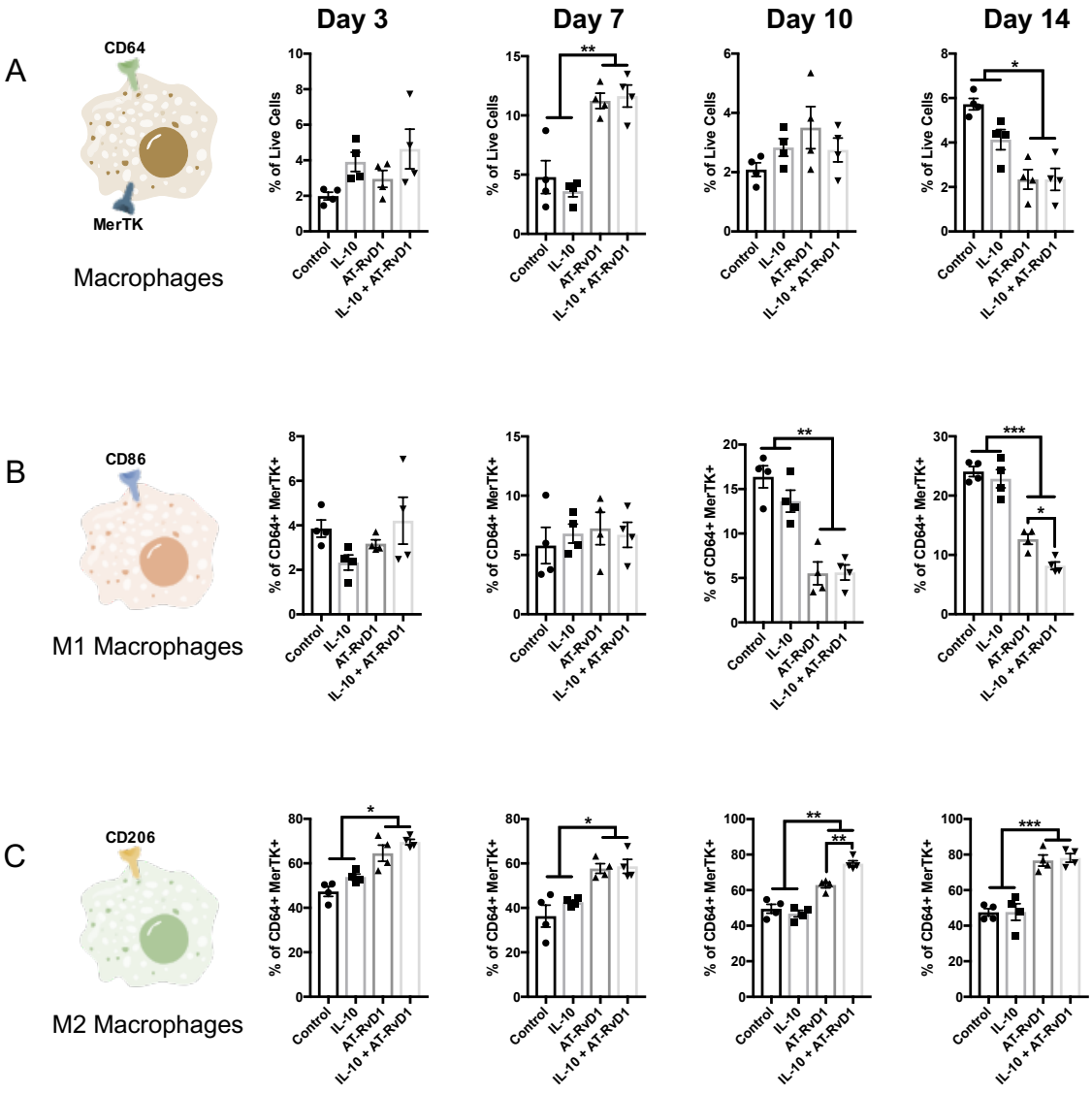

Figure 41. Macrophage recruitment to allograft skin transplant Flow cytometric analysis of (A) macrophage, (B) CD86+ Macrophage, and (C) CD206+ M2 Macrophage populations in the skin following allograft transplant and treatment with immunomodulatory PEG-MAL Hydrogels. Statistical analysis was performed using one-way ANOVA with Tukey's. post hoc test Data presented as mean ± SEM. *p>0.05, **p>0.01 , n=4.

When measuring CD86+ M1 macrophages, this population started out as a small proportion of the total macrophage pool, but then continued to grow over time, reaching over 20% of the total macrophages in control and IL-10-treated tissue, over 10% in AT-

RvD1-treated tissue, and 8% in IL-10+AT-RVD1-treated tissue (Figure 41B). The M1 population expanded more rapidly in control and IL-10-only groups and was significantly higher in these groups compared to AT-RvD1 and IL-10+AT-RvD1 at day 10 and again at day 14 (Figure 41B). When analyzing the M2 macrophage population, we see significantly higher levels of CD206+ macrophages across all timepoints in groups that received AT-RvD1 compared to groups that did not (Figure 41C). This observation is similar to what was found in the syngraft experiments, and further strengthens the conclusion that myeloid immune cell recruitment is largely influenced by AT-RvD1.

5.2.11 Total Dendritic Cell and IL-10+ Dendritic Cell Populations after Allotransplant

Dendritic cell populations were modulated after allograft and immunomodulatory hydrogel injection. CD11c+ DCs still made up a large proportion of live cells, but their levels were lower compared to syngraft, and the kinetics of their accumulation were different (Figure 42A). This is likely due to increased infiltration or expansion of other cell populations, similar to what was observed with CD64+MerTK+ macrophages. There were no differences in DCs at day 3, but they were significantly reduced at day 7 in groups receiving hydrogel formulations that contained AT-RvD1 (Figure 42A). At day 10, groups receiving hydrogels that contained IL-10 had significantly fewer CD11c+ cells compared to control or AT-RvD1-only treatment. This reduction in CD11c+ cells was transient in the IL-10-only group, as CD11c+ cells were significantly increased at day 14 compared to all other groups, whereas AT-RvD1-containing formulations significantly reduced the CD11c+ population(Figure 42A).

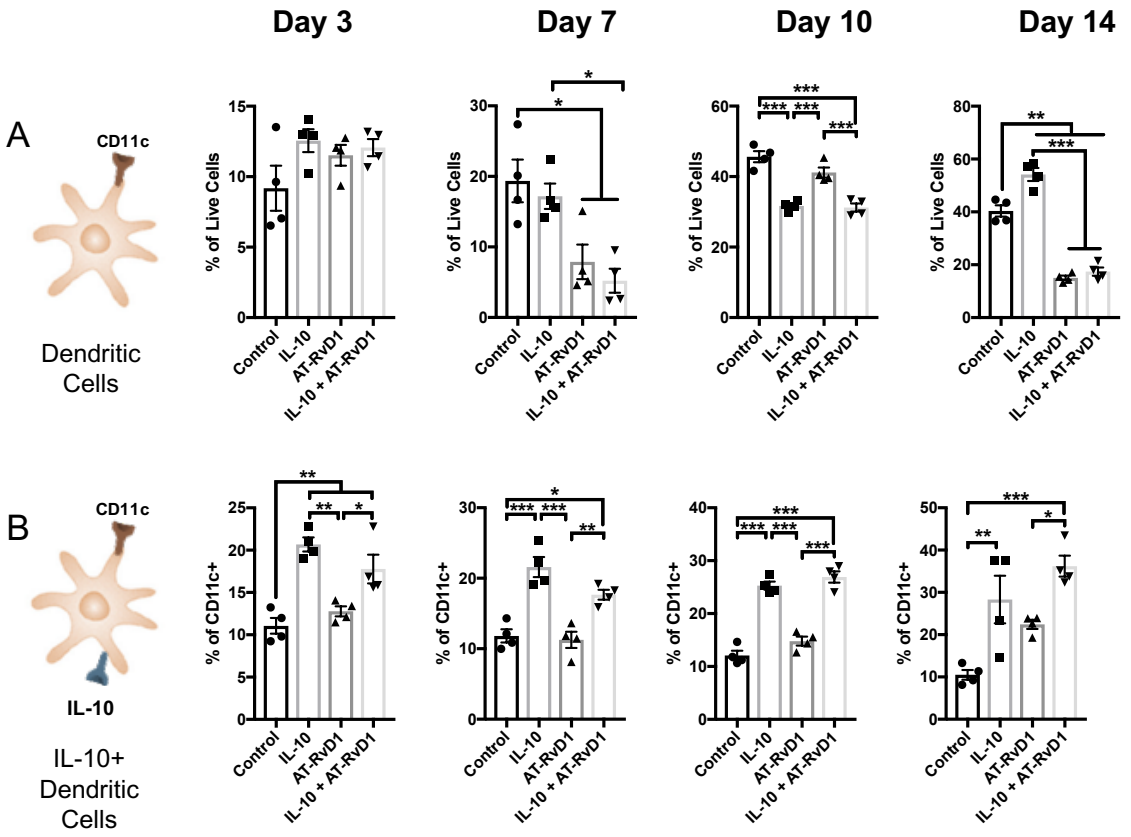

Figure 42. DC recruitment to allograft skin transplant Flow cytometric analysis of (A) total CD11c+ dendritic cell and (B) IL-10+ DC populations in the skin following allograft transplant and treatment with immunomodulatory PEG-MAL Hydrogels. Statistical analysis was performed using one-way ANOVA with Tukey's. post hoc test Data presented as mean ± SEM. *p>0.05, **p>0.01 , ***p>0.001 n=4.

Although we observed fluctuations in the total DC population, levels of IL-10DCs were largely constant between groups after allograft (Figure 42B). Starting at day 3, animals that were treated with hydrogel formulations containing IL-10 had significantly increased IL-10DC polarization than control or AT-RVD1-only tissue. We did not observe these differences in syngraft tissue at day 3, and this disparity may be due to fluctuations in the inflammatory response following allograft that result in earlier degradation of the PEG-MAL hydrogels, allowing for earlier release of IL-10 and subsequent polarization of early DCs into IL-10DCs.

5.2.12 Lymphocyte Infiltration Following Allotransplant

We again performed PCA using only lymphoid markers to see if IL-10-containing hydrogel formulations clustered together away from AT-RVD1 or control hydrogel samples. In the 3D PCA plot, there is observable clustering of these samples, likely due to the influence of CD25+ Tregs (Figure 43A-B). However, when mapping these points onto two-dimensional space, the clustering is not quite as apparent as it was in three dimensions, but samples that have been treated with IL-10 closely follow the CD25 Treg variable loading and are pulled into the quadrants where these cells are represented (Figure 43C-D).

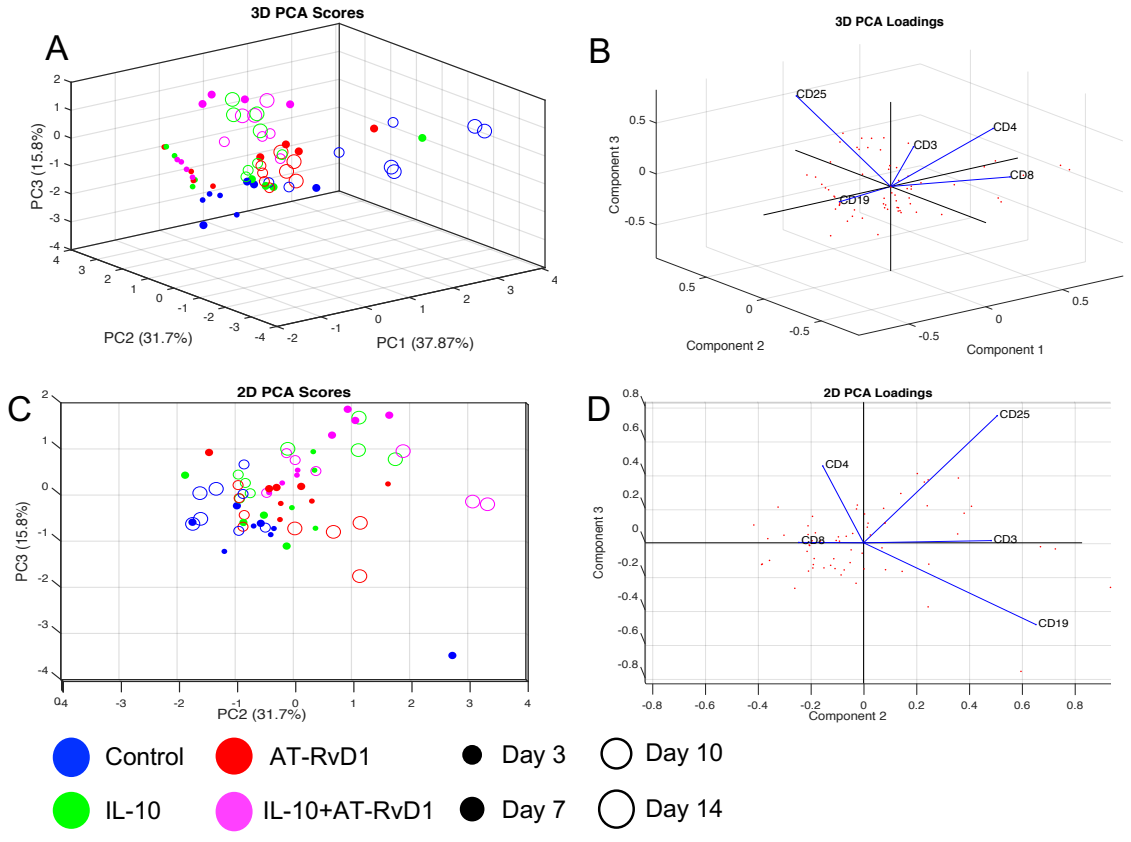

Figure 43. Unsupervised principal component analysis of flow cytometry quantification in allograft skin transplant skin tissue using lymphoid markers(A) 3D

scores plot of immunomodulatory biomaterial treatments over time. (B) 3D loadings (weight coefficients) plot of the 5 input variables in the reduced principal component space. (C-D) Scores and loadings plots reduced to two dimensions. Input variables are: B cells (% of cells), T cells (% of cells), CD8+ T cells (% of CD3+), CD4+ T cells (% of CD3+), and T_{reg} ($CD25^{+}CD4^{+}CD3^{+}$ % of $CD4^{+}CD3^{+}$). N=4 animals per treatment group at each timepoint**.**

When quantifying the overall lymphocyte recruitment to allografts, we found that the profile differs from syngraft. B cell recruitment is not different between any treatments at days 3, 7, and 10 (Figure 44A). However, there is a significant increase in cells at day 14 in the tissue that had been treated with combination IL-10+AT-RvD1 compared to all groups. B cells were significantly increased in AT-RvD1-treated tissue compared to control (Figure 44A). T cells made up a larger proportion of live cells following allograft compared to syngraft. We observed a transient increase in T cells at day 3 in AT-RvD1-treated tissue compared to control and dual-loaded hydrogels. There were no differences in T cells at day 7, but then at days 10 and 14, T cells were increased in IL-10+AT-RvD1 tissue compared to IL-10-only T cell levels (Figure 44B).

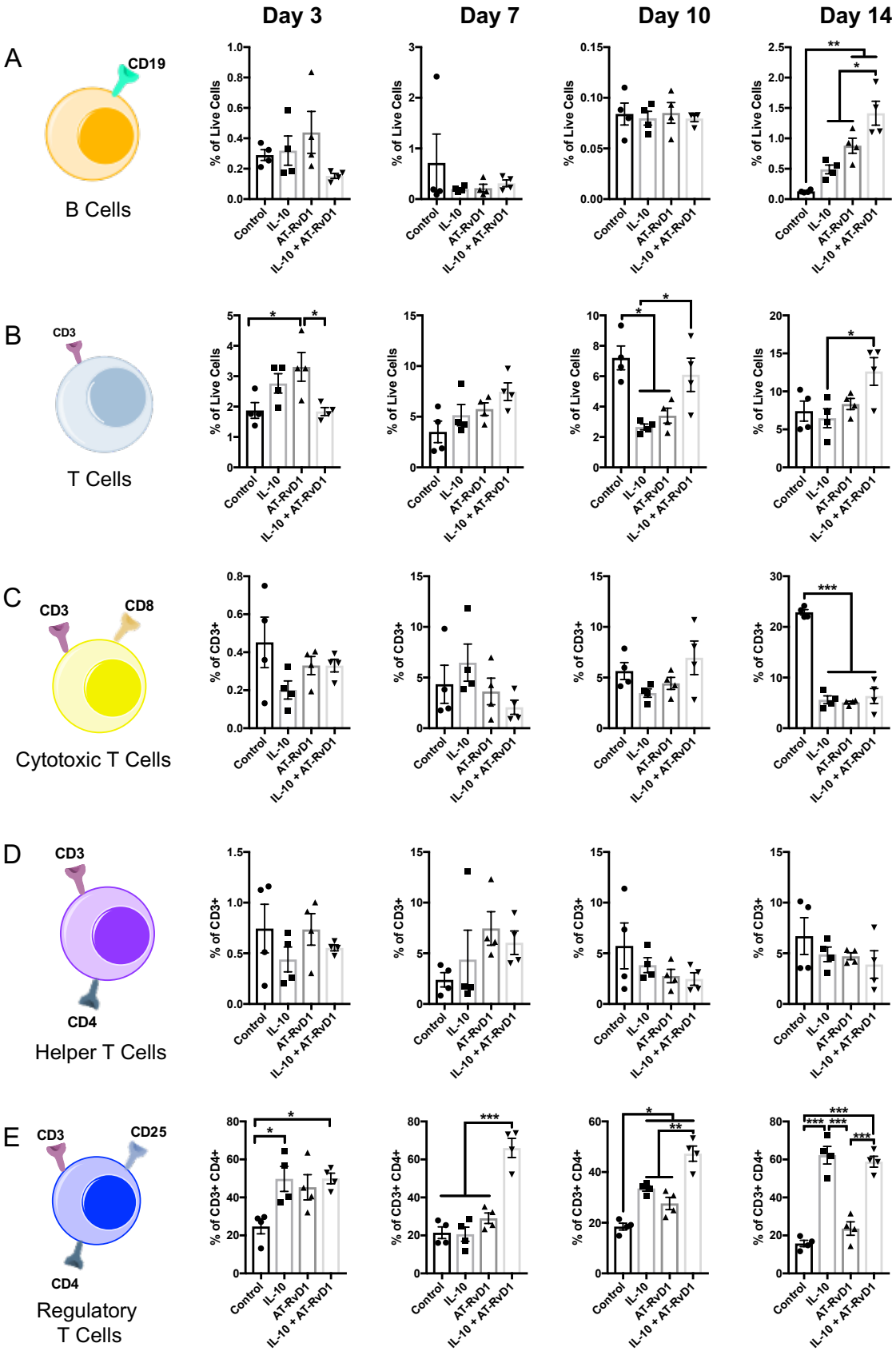
Day 3
Day 7
Day 10
Day 14
A
CD19
B Cells
B
CD3
T Cells
C
CD3
CD8
Cytotoxic T Cells
D
CD3
CD4
Helper T Cells
E
CD3
CD25
CD4
Regulatory T Cells
% of Live Cells
% of CD3+
% of CD3+ CD4+
Control
IL-10
AT-RvD1
IL-10 + AT-RvD1

Figure 44. Lymphocyte recruitment to allograft skin transplant tissueFlow cytometric analysis of (A) B cell, (B) total T cell, (C) CD8+ T cell, (D) CD4+ T cell, and (E) CD25+ Treg recruitment in the skin following allograft transplant and treatment with immunomodulatory PEG-MAL Hydrogels. Statistical analysis was performed using one-way ANOVA with Tukey's. post hoc test Data presented as mean ± SEM. *p>0.05, **p>0.01 , ***p>0.001 n=4.

Although we saw increases in T cells, we did not see modulation in the proportion of CD4+ or CD8+ cells between groups until day 14, where we observed a significant decrease in the proportion of CD8+ T cells in all treatment groups compared to controls (Figure 44C-D). However, within the CD4+ compartment, we observed differential Treg accumulation depending on the treatment type. Tregs in control allografts remained at around the level of 20% of all CD4+ T cells over the entirety of the timepoints surveyed (Figure 44E). The proportion of Tregs after IL-10 treatment increased to over 40% of CD4+ cells at day, before dipping to around 20% at one week and rising back to 40% at 10 days and reaching 60% of the total CD4+ population at two weeks. At 3 and 10 days, this was significantly higher than control, and significantly higher than control and AT-RvD1-only treatment at day 14. (Figure 44E) Treg levels following AT-RvD1 treatment did not increase as much as in tissue that was treated with IL-10m and only transiently increased compared to control at day 10. Treg recruitment to tissues receiving combination IL-10+AT-RvD1 treatment were elevated to the same levels at IL-10-only at day 3, but remained high throughout, also rising to 60% of the total CD4+ cell population.

5.2.13 Analysis of Immune Cell Profiles in Draining Lymph Nodes and Blood Following Allograft

We again performed PCA on the flow cytometry data gathered from the draining lymph nodes and blood after allograft (Figure 45 and Figure 46). PCA on these cells

following skin allograft and immunomodulatory hydrogel treatments are similar in that there is no definitive clustering of one treatment group from another. In the allograft LN PCA, there seems to be separation of the early day 3 timepoint from the rest of the data, but then the subsequent timepoints cluster together into quadrants 2 and 3. This is likely due to the strong influence of lymphocyte populations that predominate the lymph node environment (Figure 45).

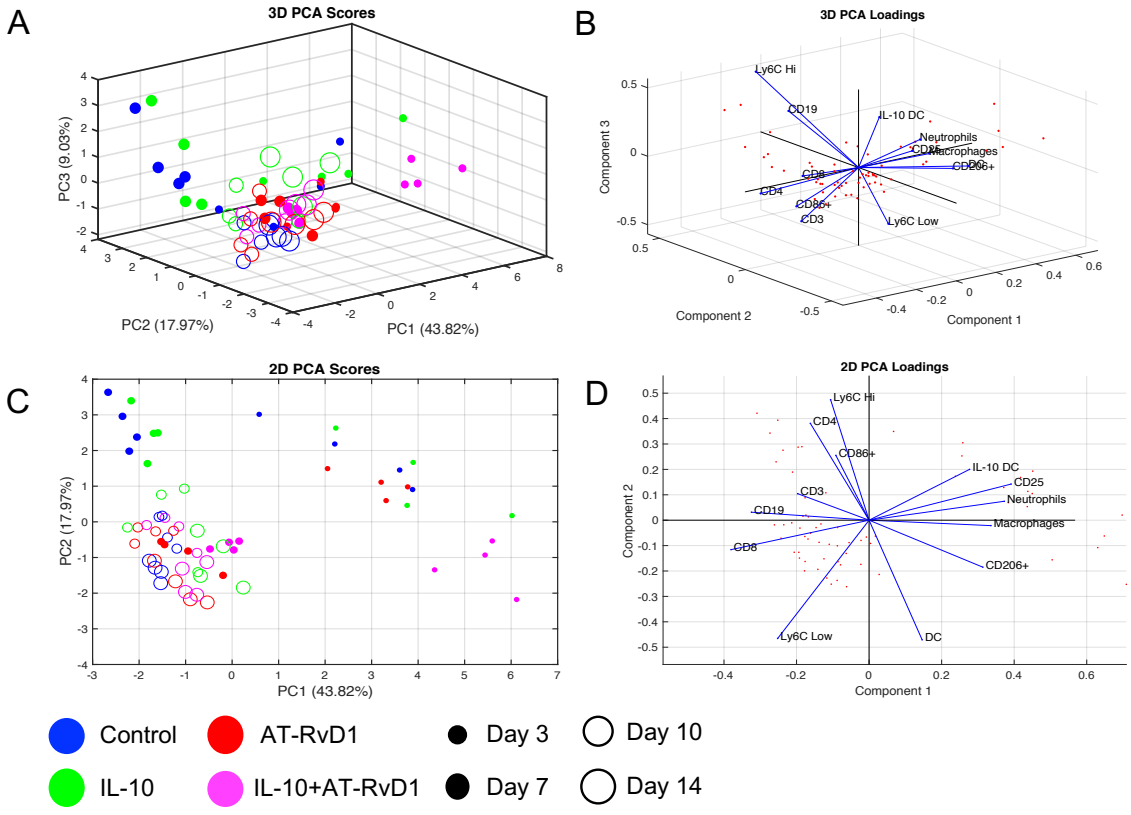

Figure 45. Unsupervised principal component analysis of flow cytometry quantification in allograft skin transplant LN(A) 3D scores plot of immunomodulatory biomaterial treatments over time. (B) 3D loadings (weight coefficients) plot of the 13 input variables in the reduced principal component space. (C-D) Scores and loadings plots reduced to two dimensions. Input variables are: Macrophages(% of cells), $CD206^{+}$ (% of Macrophages), $CD86^{+}$ (% of Macrophages), DC (% of cells), IL-10+ DCs (% of CD11c+), neutrophil (% of CD11b+), $Ly6C^{lo}$ (% of CD11b+), $Ly6C^{Hi}$ (% of CD11b+), B cells (% of cells), T cells (% of cells), CD8+ T cells (% of CD3+), CD4+ T cells (% of CD3+), and

T_{reg} ($CD25^{+}CD4^{+}CD3^{+}$ % of $CD4^{+}CD3^{+}$). N=4 animals per treatment group at each timepoint.

In the blood PCA, there is no discernible clustering whatsoever over time or treatment (Figure 46). This strengthens the argument presented with the syngraft PCA, that the immunomodulation occurring after hydrogel implantation is local in scope and has little influence on the overall systemic immune populations found in the blood or in lymph nodes.

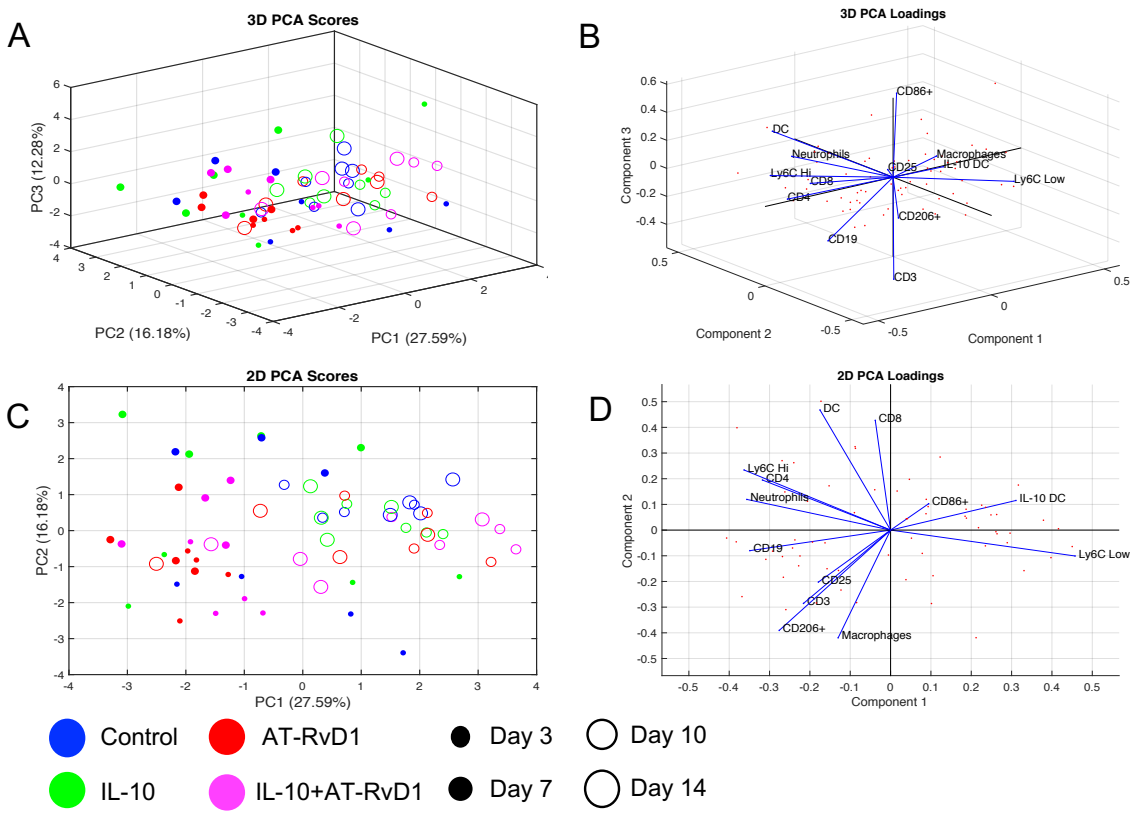

Figure 46. Unsupervised principal component analysis of flow cytometry quantification in allograft skin transplant blood(A) 3D scores plot of immunomodulatory biomaterial treatments over time. (B) 3D loadings (weight coefficients) plot of the 13 input variables in the reduced principal component space. (C-D) Scores and loadings plots reduced to two dimensions. Input variables are:

Macrophages(% of cells), $CD206^+$ (% of Macrophages), $CD86^+$ (% of Macrophages), DC (% of cells), IL-10+ DCs (% of CD11c+), neutrophil (% of CD11b+), $Ly6C^{lo}$ (% of CD11b+), $Ly6C^{Hi}$ (% of CD11b+), B cells (% of cells), T cells (% of cells), CD8+ T cells (% of CD3+), CD4+ T cells (% of CD3+), and T_{reg} ($CD25^+CD4^+CD3^+$ % of $CD4^+CD3^+$). N=4 animals per treatment group at each timepoint**.**

5.2.14 Alloantibody and Complement Deposition After Allograft and Immunomodulatory Hydrogel Treatment

Finally, we wanted to investigate the possible role of anti-donor antibody deposition in the process of skin transplant rejection. We took frozen sections of the skin transplant and surrounding tissue at day 14 and stained the tissue for complement C3c, anti-mouse IgM, and anti-mouse IgG. We also stained syngraft control tissue to serve as a negative indicator for the presence of anti-mouse antibodies. In normal tissue, there is very little complement C3c or anti-mouse antibody staining, because the immune response is able to sense self-antigen and does not deposit antibodies to syngrafted tissue (Figure 47A-D).

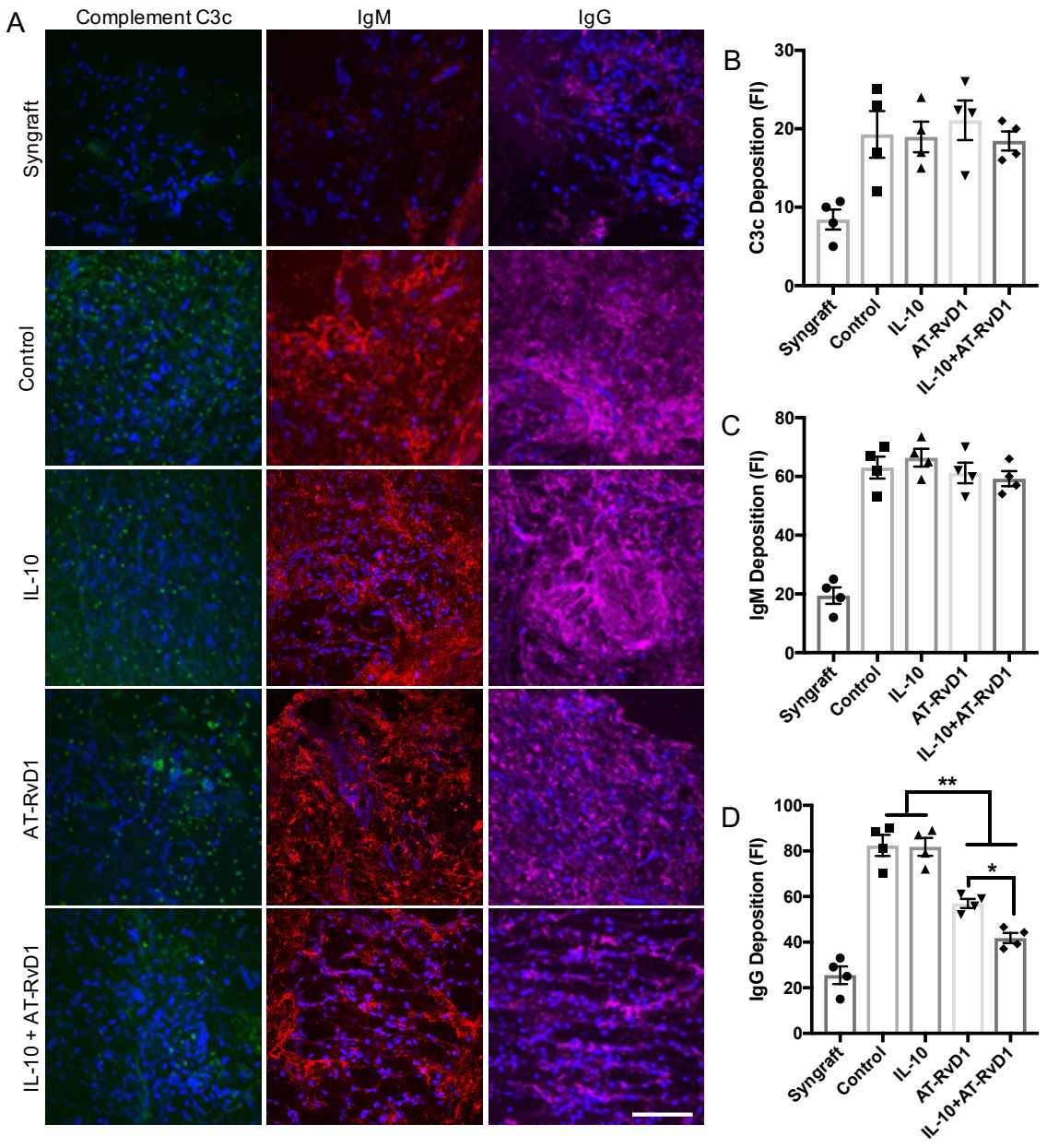

Figure 47. Staining tissue for alloantibody-mediated rejection markers (A) Fluorescence confocal microscopy of skin tissue surrounding transplanted skin stained with markers of humoral immune activation, Complement C3c, IgM, and IgG at two weeks following skin transplant and immunomodulatory hydrogel treatment. (B-D) Quantification of fluorescence intensity of staining using ImageJ. Data presented as mean ± SEM statistical analyses was performed using one-way ANOVA with Tukey's post-hoc test, *p>0.05, **p>0.01, n=4.

However, in the case of allogeneic skin transplant, the Balb/C tissue is recognized as foreign, and the adaptive immune system generates and releases antibodies against these antigens. In mouse to mouse transplants, these antibodies can be detected using anti-mouse secondary antibodies. We see significant increases in complement C3c and IgM deposition across all allograft groups after two weeks (Figure 47B-C). However, in the case of IgG, deposition is significantly decreased in the combination IL-10+AT-RvD1 group compared to all other groups (Figure 47D). This may indicate that rejection to allotransplant in this group is not as severe as the others.

5.3 Discussion

The immune response to allografts is complex and multifactorial. T and B lymphocytes are known mediators of transplant rejection, and much of the field of transplant immunology has focused on modulating the response of the adaptive immune system after allograft. Indeed, the mechanisms of action of the most common immunosuppressive agents prescribed following organ transplantation mainly focus on inhibiting the actions of T cells: calcineurin inhibitors block IL-2 synthesis, anti-proliferative agents like mycophenolate motefil are able to limit lymphocyte proliferation via bloackade of *de novo* purine synthesis, and new immunosuppressive agents like belatacept or abatacept act like CTLA-4 to prevent costimulation of T cells during antigen presentation, thereby decreasing their activity[212, 217]. However, targeting of innate immune cells including mononuclear phagocytes and granulocytes has gained increasing interest due to their ability to play both detrimental and beneficial roles [4]. Neutrophils are recruited to graft tissue in response to ischemia reperfusion injury (IRI) inherent in all transplant procedures[85]. There they can exacerbate graft tissue damage through the

release of metalloproteinases and neutrophil elastase, and actively mediate acute rejection through CD8+ cytotoxic T cell signaling[86-88]. Additionally, while the interaction of neutrophils and cells of humoral immunity is not well-understood, it has been found that neutrophils have the capacity to leave peripheral sites of injury and deliver antigen to lymph nodes[89]. On the other hand, there are subsets of neutrophils that may promote wound healing and tissue repair, and aid in the reperfusion of graft tissue[43]. Mononuclear cell infiltration, including monocytes (MO), dendritic cells (DCs) and macrophages, and the production of pro-inflammatory cytokines such as tumor necrosis factor-alpha (TNF-α), interleukin (IL)-1α, and IL-1β are inherent to the transplant milieu[5]. Macrophages of both donor and recipient origin infiltrate the allograft and proliferate in situ, and comprise 40-60% of cellular infiltrate in acute rejection[90]. Up-regulation of surface MHC class II and increased expression of T cell costimulatory molecules by activated DCs are also implicated in acute rejection. Upon functional maturation, "passenger" DCs in donor tissue migrate to recipient secondary lymphoid organs along chemokine gradients where they are key mediators in alloantigen presentation. Early activation of DCs also leads to allotransplant injury due to accumulation of interferon-γ-producing neutrophils, infiltrating macrophages, CD4+ T cells, B cells, and invariant natural killer T (NKT) cells[91]. Conversely, the phenotypic plasticity of monocyte precursors and DCs in response to microenvironmental signals, the presence of tolerogenic mononuclear phagocyte subsets that coincide with allograft acceptance, and their roles in Treg expansion are evidence that MO and DC subsets are key targets in the quest for transplant acceptance[92, 93]. It was our goal to manipulate this inherent cellular response set off by tissue injury and transplant

to tune the microenvironment surrounding the transplanted tissue and wound to promote integration and healing of the allograft.

We have previously demonstrated that the localized co-delivery of IL-10 and AT-RvD1 from an injectable hydrogel scaffold modulates the recruitment, accumulation, or polarization of pro-regenerative, anti-inflammatory innate and adaptive immune cell subsets in injured tissue. We have also shown that these hydrogels promote vascular network expansion and remodeling. In this study, we aimed to apply these findings to a model of murine skin transplantation to observe how immunomodulatory PEG-MAL hydrogels modulate the immune response after injury when an additional immune stimulus, i.e. an allograft or syngraft, is applied. The skin transplant model is a simple model to study the transplant response, as transplanted allogeneic skin is extremely antigenic and rapidly rejected without intervention over the course of days[218]. Oppositely, syngeneic skin transplants will not be rejected and so the syngraft model can be used to chronicle wound healing and tissue integration. We transplanted syngeneic and allogeneic tail skin onto the backs of C57Bl/6 mice and measured the kinetics of immune cell recruitment into the transplant and surrounding tissue.

The immune response to syngraft transplant proceeds similar to that of normal wound healing. Qualitative observations of macroscopic images of the transplanted tissue area over time show that the syngraft transplant heals and integrates with the tissue over time, with full healing seen across all groups by 14 days. We observed differences in wound and graft contracture between groups, and the control and AT-RvD1-treated syngrafts were noticeably smaller than IL-10-only or IL-10+AT-RvD1 treated syngrafts. This may be due to the ability of IL-10 to reduce scar formation and fibrosis in cutaneous wounds[219]. This

time to healing is accurate for wounds of this size [220]. With delivery of dual-loaded IL-10+AT-RvD1 hydrogels, integration of the graft with host tissue was seen at day 10 post-transplant, whereas there was still healing occurring in other groups. This indicates possible acceleration of the wound healing process following IL-10+AT-RvD1 delivery, however closer analysis of wound closure metrics would be needed to determine the strength of this integration. We also stained frozen tissue sections with H&E to observe tissue morphology and cellular infiltration into the graft area. In syngraft, leukocytes were present in the tissue at all timepoints across all groups. There was no appreciable differences between any treatment groups, meaning that the delivery of immunomodulatory hydrogels does not suppress the immune response after injury, but modulates the recruitment, activation, or polarization of cells found within the injury niche. Given that both pro- and anti-inflammatory responses are necessary for normal wound healing, a complete suppression of the immune response is not desired in this case[64, 67, 221]. When we took similar images of allograft transplants, we saw visible signs of rejection in all groups by day 10, and all allografts were completely rejected by day 14 post-transplant. H&E micrographs of the graft tissue reveal significant immune cell infiltration at all timepoints within all groups. Compared to syngraft, there was marked increase in cellular infiltration, meaning that the immune response to allograft was also not suppressed by hydrogel delivery of immunomodulatory biomolecules. This outcome was not unexpected due to the use of complete MHC-mismatch Balb/c to C57Bl/6 grafts. Skin allograft transplants are extremely antigenic and will be rejected without robust systemic immunosuppression[218]. Future analyses using this model could instead utilize a partial MHC-mismatch, or pair local immunomodulation therapy with traditional systemic IS to try to attain better tissue

integration without rejection. We do believe that early integration of the transplanted tissue was improved with combination IL-10+AT-RvD1 treatment, as evidenced by decreases in the wound size at days 3 and 7, however this early positive response was quickly overshadowed by allograft rejection processes.

This study presents a thorough analysis of the immune response to both syngraft and allograft over different timepoints, treatments, and tissues. We analyzed the immune response after skin transplant at days 3, 7, 10, and 14 in the transplant tissue itself, as well as in blood and the draining lymph nodes. Analysis of blood and draining LNs allows us to draw conclusions about the extent of the immunomodulation occurring after hydrogel treatments. We used principal component analysis as our main analytical tool to look for patterns that emerge between treatment groups over time. When we examined the clustering analysis of both syngraft and allograft LN and blood, we did not see discrimination between treatment groups except for clustering of timepoints. This indicates that any observed changes in the immune response within the tissue is due to local modulation of cell recruitment, proliferation, or polarization. We and others have previously shown that the local delivery of immunomodulatory factors via biomaterial can influence the local immune environment without affecting the systemic immune system as a whole. Local immune modulation is ideal in this context, because systemic immunomodulation, like with systemic IS therapies after transplant, can have unwanted off-target side effects that are detrimental to the host [2]. When we examine the clustering of the transplanted tissue data in both syngraft and allograft, we see clear clusters that emerge between treatment groups. The AT-RvD1 and IL-10+AT-RvD1 samples appear to be closely related over time, separating from the other data due to the influence of

Ly6CLow monocytes and CD206+ M2 macrophages. When we quantified the flow cytometry data over time for each cell subset included in our flow panels, we saw that AT-RvD1 and IL-10+AT-RvD1 treatment increased the proportions of these cell subsets in syngraft and allograft. We and others have shown that these cell subsets are positively correlated with healing outcomes, and in the context of allograft, these cells may enhance graft acceptance due to their ability to signal to and stimulate Treg populations[95, 222]. One notable difference observed between the temporal immune cell recruitment profiles of syngraft and allograft was that the levels of many cells, including neutrophils, monocytes, and lymphocytes seemed to return to baseline levels at around days 10 and 14 in syngraft skin tissue, but that levels of these cell populations remained elevated in allografts. For example, at day 14, the proportion of neutrophils found in syngraft skin tissue was less than 15% of the CD11b+ pool for all groups, whereas neutrophils comprised up to 50% of the cells in this same gate in the allograft skin tissue. This persistent activation of the immune system indicates on ongoing response to the allograft that was not completely ameliorated with immunomodulatory treatment.

We also previously observed expansion of IL-10+ DC and Treg populations following delivery of PEG-MAL hydrogels containing thiolated IL-10. We showed that thiolation slows the release of IL-10 from the hydrogels, allowing it to be released over time. Expansion and activity of these populations is vital to acceptance of transplanted tissue, and cell-based therapies utilizing both IL-10+DCs or Tregs have been pursued in an attempt to enhance allograft transplant acceptance[198, 223-227]. Following syngraft and allograft, we observe increased proportions of these cell types in tissues treated with IL-10, with and without concurrent AT-RvD1 delivery. One marked difference between

syngraft and allograft was that both IL-10+ DCs and Tregs were increased after three days following allograft, whereas these populations were not expanded in syngraft until day 7. One possible explanation could be due to changes in the cytokine milieu following allograft. PEG-MAL hydrogels are protease-degradable, and the stimulus of MHC-mismatch allograft may increase the release and activity of protein-degrading enzymes, leading to earlier degradation of the PEG-MAL hydrogel and subsequent release of IL-10. We observed increased T cell migration to the allografts compared to syngraft. In syngraft, T cells comprised less than 10% of the overall proportion of live cells, with the majority of samples having less than 5% T cells out of total cells. In the allograft, however, T cell levels were doubled compared to syngraft at 14 days, making up 10-15% of the total live cell population. While we saw expansion in T cell numbers following allograft, we did not observe much modulation in the proportions of CD4+ and CD8+ T cells. In fact, these populations comprised a small amount of the total CD3+ T cell pool. There was a large proportion of CD3+ cells that were CD4 and CD8 double negative. It is possible that these CD3+CD4-CD8- T cells are gamma delta T cells, or double negative alpha beta T cells. Both of these T cell populations exist in small proportions during homeostasis but may expand in response to injury or other immune system stimulus, however the roles of these T cells has not clearly been elucidated, but these cells may act to promote transplant rejection [200, 228], and further inquiry is required to determine the exact function and origin of these cells after skin injury and tissue transplant.

Although we observed significant alterations in the recruitment and accumulation of pro-regenerative immune cells that have been shown to promote processes leading to transplant acceptance, the allografts were still rejected after 10-14 days. The increased T

cell infiltration that we see in the allografts may be contributing to this rejection response. While the overall proportions of CD4 and CD8 T cells were unaltered compared to syngraft, the overall increase in total number may promote rejection. One other mechanism that we did not explore fully to explain why rejection persisted is due to humoral immunity. We observed a significant increase in CD19+ B cells in the allograft tissue after dual-loaded IL-10+AT-RVD1 delivery at two weeks, a response that was not seen in syngraft tissue samples. It is possible that this increased recruitment of B cells is a compensatory mechanism activated by the host immune system to deal with the detection of foreign antigen. We stained skin sections for immunoglobulins IgG and IgM, as well as complement C3c, a downstream component of the humoral immune response, and saw significant deposition of IgG, IgM, and C3c compared to syngraft in all allograft groups at two weeks following transplant. B cell responses have been shown to play a role in mediating organ transplant rejection, and the anti-CD20 monoclonal antibody rituximab has been used off-label in kidney transplant immunosuppression to prevent this humoral rejection response [229]. It is not known if AT-RvD1 or IL-10 can promote or prevent B cell actions, so more study is necessary to determine how to ameliorate this response while utilizing local, hydrogel-based immunomodulation. Overall, this study is a promising first step in the exploration of local therapies to improve allograft tissue integration and healing, and future studies should focus on combining this therapy with systemic IS to attain a balance between prevention of rejection and enhancement of wound healing outcomes.

5.4 Methods

5.4.1 Hydrogel Fabrication

Four-arm poly(ethylene glycol) (PEG, 10 kDA molecular weight) end-functionalized with maleimide (>95% purity, Laysan Bio) at 4.5% weight/volume was used for all hydrogel formulations. PEG macromers were functionalized with RGD peptide (GRGDSPC), crosslinked with the cysteine-flanked peptide VPM (GCRDVPMSMRGGDRCG) (AAPPTec) in 0.5M MES buffer, pH 5.5. The final concentration of RGD was 1.0mM. Gels were also loaded with 50ug/mL IL-10, and 4ug/mL AT-RvD1 (Cayman Chemical). The crosslinker concentration was based on the concentration of non-reacted maleimide groups remaining on PEG macromers. For hydrogels used in animal studies, all components were filtered through a spin column after pH measurements and kept under sterile conditions until injection into the animals.

5.4.2 Skin Transplant Graft Experiments

Female C57BL/6 aged 5-7 weeks (Charles River) were transplanted with full thickness tail skin grafts from age- and sex-matched Balb/c or C57Bl/6 mice as previously described[218]. Briefly, donor mice were sacrificed under terminal anesthesia via cervical dislocation. Donors were placed tail-first into a sterile decapicone with the tail exposed. The tail skin was sterilized via three washes with 70% ethanol and chlorhexidine. The tail skin was removed with surgical scissors and kept in ice cold sterile saline until use. Recipient mice were anesthetized with 50uL Ketamine-Xylazine-Saline cocktail (ratio 5:1:4) and shaved and sterilized with via three washes with 70% ethanol and chlorhexidine. A full thickness defect was cut into the dorsal skin of the recipient mouse. Hydrogels were mixed and loaded into a syringe and injected in depots in the defect area. For experiments utilizing soluble IL-10 and AT-RvD1, dosages to match hydrogel dosages were dissolved in 30uL sterile saline and injected underneath the graft area. Skin grafts were cut from

donor tails to fit into the defect area. Wounds were bandaged, and mice were administered sustained-released buprenorphine i.p. (0.1-0.2 mg/kg) and allowed to recover in heated cages. Bandages covering grafts were removed 7 days after graft placement. All mice received standard laboratory diet and water ad libitum throughout the course of the experiment.

5.4.3 Tissue Harvest and Flow Cytometry

To collect samples for flow cytometry analysis, mice were euthanized via CO2 asphyxiation. The skin graft and surrounding tissue was excised, minced, and digested with collagenase type 1-A (3.3mg/ml, Sigma), hyaluronidase type IV-S (1mg/mL, Sigma), and DNASE-I (0.1mg/mL, Sigma) in RPMI in a shaking water bath at 37°C for 90 minutes and further separated with a cell strainer to create a single cell suspension. Peripheral blood was collected via cardiac puncture. From cardiac puncture, 50uL blood was used for flow cytometric analysis. Erythrocytes within blood were lysed with ammonium chloride (StemCell Technologies) and the remaining leukocytes were isolated for flow cytometry analysis. Brachial and axillary lymph nodes were isolated and mashed through a 40 micron cell strainer to create a single cell suspension. Single cell suspensions of skin tissue, lymph nodes, and blood were stained for flow cytometry analysis using standard methods and analyzed on a FACS-AriaIIIu flow cytometer (BD Biosciences). Dead cells were excluded through staining using Zombie Red fixable viability stain (BioLegend). The antibodies used for identifying cell populations of interest were: PE conjugated MerTK (Biolegend), PE-Cy7 conjugated MHC-II (BioLegend), BV605 conjugated CD206 (BioLegend), BV510 conjugated Ly6C (BioLegend), APC-Cy7 conjugated Ly6G (BioLegend), BV711 conjugated CD64 (BioLegend), BV785 conjugated CD19 (BioLegend), APC conjugated

Cd11b (BioLegend), BV421 conjugated CD11c (Biolegend, FITC conjugated CD86 (BioLegend), PerCP-Cy5.5 conjugated CD3 (Biolegend), BV785 conjugated CD8 (BioLegend), BV605 conjugated CD4 (BioLegend), and BV711 conjugated CD25 (BioLegend). Staining using BV dyes was performed in the presence of Brilliant Stain Buffer (BD Biosciences). Cells were stained for intracellular cytokines using PE conjugated IL-10 (BioLegend) and PE-Cy7 conjugated TNF- α (eBiosciences). Positivity was determined by gating on fluorescence minus one controls. Absolute quantification of cell numbers was performed by adding 25μL of AccuCheck counting beads to flow cytometry samples (Thermo Fisher Scientific).

5.4.4 Immunohistochemistry

Skin transplant graft and surrounding tissue, retrieved at the end of the experiments, were flash frozen, cryosectioned, and post-fixed with ice cold acetone. Sections were stained with hematoxylin and eosin (H&E) to observe morphology. Immunofluorescence was also used to assess cell infiltration and response to skin graft. Sections were blocked at RT for one hour in PBS containing 0.4% Triton-X and 5% goat serum. Tissues were stained overnight at 4°C in PBS-Triton-X supplemented with 1% goat serum with FITC conjugated Anti-C3b/c (1:300 dilution, Abcam) primary antibody to detect C3 deposition in the tissue. Alexafluor 568 conjugated Goat anti-rat IgG (1:200 dilution, Abcam) and Alexafluor 647 conjugated goat anti-rat IgM (1:200 dilution, Abcam) were used to detect tissue deposition of IgG and IgM, respectively. Images were acquired with a fluorescence microscope (Zeiss 710 NLO), and all images were captured with identical exposure times and settings in each experiment.

5.4.5 Statistical Analysis

All statistical analyses were performed using Graphpad Prism version 6.0 (La Jolla, CA). Results are presented as mean ± standard error of the mean (SEM). For grouped analyses, one-way ANOVA with Tukey's post-test was used for multiple comparisons. Unless otherwise noted, $p<0.05$ was considered statistically significant.

CHAPTER 6. CONCLUSIONS AND FUTURE DIRECTIONS

6.1 Overall Summary

The work presented in this thesis represents a significant contribution to the fields of biomaterials and regenerative medicine by demonstrating that local delivery of endogenous anti-inflammatory factors can enhance the recruitment and differentiation of immune cell subsets of both the innate and adaptive immune system to enhance post-injury vascularization and tissue repair. This work expands the understanding of the relationship between pro-regenerative myeloid and lymphoid cells, and identifies methods in which this relationship can be manipulated to promote wound healing.

In Aim 1, we explored how biomaterial-mediated delivery of the specialized proresolving mediator AT-RvD1 was able to modulate the recruitment of the earliest cells involved in the immune response after injury. We were specifically interested in subpopulations of macrophages, monocytes, and a recently identified neutrophil population active in early vascular remodeling, CD49d+ neutrophils. We utilized PLGA thin films as a model biomaterial delivery system due to its ease of manufacturing and our prior experience with delivering lipid small molecules from these thin films. We found that delivery of AT-RvD1 via biomaterial to injured tissue was able to modulate neutrophil and monocyte recruitment and phenotype better than a single dose of AT-RvD1 dissolved into saline given at the time of surgery. We also explored macrophage recruitment and found significantly more CD206+ M2 macrophages in the tissue at three days following injury compared to unloaded PLGA films. We observed the beginnings of early vascular remodeling, finding significantly increased expansion of CD31+ capillary networks in

peri-implant areas. In addition, we saw significant recruitment of pro-angiogenic CD49d+ neutrophil subsets following implantation of AT-RvD1-loaded films. For this analysis, we utilized SPADE, an emerging technique to map flow cytometry data based on receptor expression levels that is able to remove the need for manual gating. Ours was the first study to identify a potential method to target and enrich the injured tissue with these pro-angiogenic neutrophils to enhance vascularization around biomaterial implants. The significance of this work lies in our identification of the cell subsets that are modulated by AT-RvD1, and our novel findings that locally delivered AT-RvD1 has the ability to promote the recruitment of these cells in areas of injury.

In aim 2, we demonstrated for the first time the ability to target the recruitment of wound healing pro-regenerative cells from both the innate and adaptive branches of the immune system. Mounting evidence suggests that the wound healing process is driven in part by both branches, and we engineered a hydrogel delivery system to achieve simultaneous *in vivo* release of both AT-RvD1 and IL-10. IL-10 or AT-RvD1 delivery alone from PEG-MAL hydrogels are able to differentially promote the recruitment of pro-regenerative immune cell subsets, but combined delivery of these two factors allows for synergy in their actions and promotes the recruitment of Ly6CLow monocytes, M2 macrophages, IL-10 DCs, and Tregs to injured tissue. Assessment of vascular regeneration parameters revealed that IL-10+AT-RvD1 hydrogels promoted the expansion of vascular networks and arteriolar diameter. Taken together these results indicate that local immunomodulation using combinatorial delivery of bioactive factors can recruit expanded populations of cells positively involved in the wound healing process.

In aim 3, we applied these immunomodulatory PEG-MAL biomaterials to a model of syngeneic or allogeneic skin transplantation. We hypothesized that local modulation of the immune response following transplant would be sufficient to promote grafted tissue integration and wound healing while staving off rejection in the short term. While we did observe significant differences in the local immune response following immunomodulatory hydrogel injection, this local response was unable to overcome the greater systemic rejection response. Although the allogeneic transplants were rejected, we observed early recruitment of Ly6CLow monocytes, and enhanced accumulation of CD25+ Tregs in the allograft and surrounding tissue. Syngraft tissue transplants extended and further confirmed our aim 2 findings, and in the case of IL-10+AT-RvD1 combined delivery, we qualitatively observed earlier wound closure and increased recruitment of pro-regenerative cells to the injury niche.

6.2 Improved characterization of innate and adaptive immune cell function following transplantation and injury and new analysis techniques

While the studies presented here employ well-accepted paradigms to characterize phenotypes of innate and adaptive immune cells, the field of immunology continues to uncover additional layers of heterogeneity and complexity that exist within these cell types. Our growing understanding of the spectrum of cellular phenotypes present *in vivo* means that more sophisticated techniques are necessary to elucidate the origin, activation status, and function of immune cells involved in the response to tissue injury. Neutrophils are now recognized to possess distinct subpopulations along the same vein as monocytes and macrophages, and identification of these cells solely based on CD11b+Ly6G+ flow cytometric staining is likely no longer sufficient to determine their definitive population.

Identification of macrophage polarization status via CD86 or CD206 also does not provide the full story of what functions these cells carry out *in vivo*. Already we know that M2 macrophage polarization can be subdivided into at least three distinct populations *in vitro,* and many more may exist *in vivo*, where complex signaling mechanisms may lead to dual-polarized cells, or intermediate populations. Further characterization of lymphoid cell populations in the response to injury is also necessary. We focused our analysis on CD25+ Tregs due to the growing evidence that these cells are active mediators of wound repair, but additional subpopulations within CD4+ T cells, such as Th1, Th2, and Th17 are involved in the immune response to injury, and we have yet to characterize their recruitment or activity following implantation of immunomodulatory biomaterials. Future studies looking to characterize the immune response to implanted materials and locally delivered immunomodulatory factors could employ high-dimensional, single-cell analytical techniques such as single cell qPCR or highly multiplexed mass cytometry. These techniques allow for a much wider array of markers to be tested compared to traditional flow cytometric analysis, which is limited to 10-15 markers of interest, and could potentially identify novel subpopulations of immune cells involved in inflammation and healing. Analysis of this data could employ emerging dimensionality reduction techniques such as SPADE. We have found that SPADE is able to identify neutrophils at the subpopulation level, but have not yet expanded this analysis to larger datasets.

6.3 Extension of immunomodulatory therapies to other regenerative medicine applications

In the initial characterization of immunomodulatory hydrogels capable of promoting the recruitment of wound healing cells from the innate and adaptive arms of the

immune system, we utilized the murine dorsal skinfold window chamber as our test model. This model provides a significant inflammatory injury and robust immune response, allowing for the use of a multitude of techniques to measure this response and perturbations following immunomodulatory factor delivery. However, due to the size of the wound generated and that the wound area is held under tension, it is unlikely that the skin will heal. Future studies could modulate the size of the defect generated during dorsal window chamber placement to observe closure of full thickness wounds and how immunomodulatory hydrogels are able to influence wound closure. We started to examine wound healing in our use of the syngraft skin transplant model, and we could expand upon our findings by examining metrics of wound healing and tissue integration such as collagen deposition and fibrosis and by measuring tissue tensile strength after healing.

Additionally, future applications of our dual-loaded PEG-MAL hydrogels could be used in the context of other injury models. Any tissue injury is accompanied by an inflammatory response, which provides opportunities for modulating that response to accelerate or enhance repair. We focused on the repair of skin wounds in this work, and it is likely that there exist context dependent immune responses that vary from tissue type to tissue type. Such areas of interest for potential application of our immunomodulatory PEG-MAL hydrogels include muscle regeneration after volumetric muscle defect, promoting cardiac repair after infarct injury, or to direct palatal wound healing and prevent fistula formation after cleft palate repair.

6.4 Further characterization of immune modulation following allotransplant

It was our overall goal in this work to use immunomodulatory biomaterials to promote allograft tissue integration and wound healing following transplant. While we observed the modulation of local recruitment of immune cells after hydrogel treatment, ultimately, all of the allograft skin transplants were rejected over the course of 10-14 days. Skin tissue is one of the most antigenic tissues, and therefore host response to skin alloantigens is swift and robust when the transplanted skin is from an animal with complete MHC mismatch, as is the case with Balb/c to C57Bl/6 transplants. While the use of complete MHC mismatch allows for the study of a rapid rejection response, this model is not clinically relevant, as complete MHC mismatch transplants are exceedingly rare. Instead, future studies could utilize partial MHC-mismatch transplants, which do not exhibit rejection as quickly and may allow for closer study of allograft healing and integration.

Other areas of interest are to expand our analysis of the humoral immune response to immunomodulatory hydrogel treatment and allotransplant. We observed expansion of B cell populations and immunoglobulin deposition in the transplant milieu, but our current experience with the humoral adaptive immune response is limited. Further analysis of this B cell response could identify possible mechanisms that could be exploited to promote allograft healing and integration. Additionally, it is well known that passenger donor immune cells can migrate to host lymph nodes and set off immune response cascades leading to rejection. With the current skin transplant model, we are not able to differentiate host immune cells from tissue resident donor immune cells. It would be beneficial to identify the origins of the cells whose recruitment and activation are modulated via PEG-MAL hydrogels. Transgenic models utilizing CD45.1 and CD45.2 allellic variants would

allow us to identify immune cells originating from the donated tissue versus those host immune cells recruited in response to injury and transplant.

Finally, models of solid organ transplant could also be employed, and these models would allow us to explore wound healing and revascularization following solid organ anastomoses with host vasculature as well as the progression of surgical wound healing. Combinatorial treatments utilizing sliding scale doses of systemic IS and immunomodulatory hydrogels could allow for optimization of regimens that are able to durably prevent transplant rejection while also allowing for early enhancement of transplanted organ integration and surgical wound healing could have the potential to all but eliminate acute complications of systemic IS therapies and improve patient outcomes after transplant.

REFERENCES

[1] P.G. Dean, W.J. Lund, T.S. Larson, M. Prieto, S.L. Nyberg, M.B. Ishitani, W.K. Kremers, M.D. Stegall, Wound-healing complications after kidney transplantation: a prospective, randomized comparison of sirolimus and tacrolimus, Transplantation 77(10) (2004) 1555-61.

[2] R. Girlanda, Complications of Post-Transplant Immunosuppression, in: J.A. Andrades (Ed.), Regenerative Medicine and Tissue Engineering, https://www.intechopen.com/books/regenerative-medicine-and-tissue-engineering/complications-of-post-transplant-immunosuppression, 2013.

[3] A. Zuckermann, M.J. Barten, Surgical wound complications after heart transplantation, Transpl Int 24(7) (2011) 627-36.

[4] P. Abrahimi, R. Liu, J.S. Pober, Blood Vessels in Allotransplantation, Am J Transplant 15(7) (2015) 1748-54.

[5] S.P. Murphy, P.M. Porrett, L.A. Turka, Innate immunity in transplant tolerance and rejection, Immunol Rev 241(1) (2011) 39-48.

[6] T. Gajanayake, R. Olariu, F.M. Leclere, A. Dhayani, Z. Yang, A.K. Bongoni, Y. Banz, M.A. Constantinescu, J.M. Karp, P.K. Vemula, R. Rieben, E. Vogelin, A single localized dose of enzyme-responsive hydrogel improves long-term survival of a vascularized composite allograft, Sci Transl Med 6(249) (2014) 249ra110.

[7] T. Deuse, F. Blankenberg, M. Haddad, H. Reichenspurner, N. Phillips, R.C. Robbins, S. Schrepfer, Mechanisms behind local immunosuppression using inhaled tacrolimus in preclinical models of lung transplantation, Am J Respir Cell Mol Biol 43(4) (2010) 403-12.

[8] National Data - Transplants by Donor Type. <https://optn.transplant.hrsa.gov/data/view-data-reports/national-data/#>, 2017 2017).

[9] A. Rana, A. Gruessner, V.G. Agopian, et al., Survival benefit of solid-organ transplant in the united states, JAMA Surgery 150(3) (2015) 252-259.

[10] A. Mehrabi, H. Fonouni, M. Wente, M. Sadeghi, C. Eisenbach, J. Encke, B.M. Schmied, M. Libicher, M. Zeier, J. Weitz, M.W. Buchler, J. Schmidt, Wound complications following kidney and liver transplantation, Clin Transplant 20 Suppl 17 (2006) 97-110.

[11] S.A. Grim, C.M. Slover, H. Sankary, J. Oberholzer, E. Benedetti, N.M. Clark, Risk factors for wound healing complications in sirolimus-treated renal transplant recipients, Transplant Proc 38(10) (2006) 3520-3.

[12] M.W. Gaber, A.M. Aziz, X. Shang, R. Penmetsa, O.M. Sabek, M.R. Yen, L.W. Gaber, L.W. Moore, A.O. Gaber, Changes in abdominal wounds following treatment with sirolimus and steroids in a rat model, Transplant Proc 38(10) (2006) 3331-2.

[13] D. Kahn, C.W. Spearman, A. Mall, E. Shepherd, G. Engelbrecht, Z. Lotz, M. Tyler, The effect of rapamycin on the healing of the ureteric anastomosis and wound healing, Transplant Proc 37(2) (2005) 830-1.

[14] J.A. van der Vliet, M.C. Willems, B.M. de Man, R.M. Lomme, T. Hendriks, Everolimus interferes with healing of experimental intestinal anastomoses, Transplantation 82(11) (2006) 1477-83.

[15] N. Sikas, G. Imvrios, D. Takoudas, D. Gakis, V. Papanikolaou, Mycophenolate mofetil impairs the integrity of colonic anastomosis, J Surg Res 134(2) (2006) 168-72.

[16] R. Fishel, A. Barbul, H.L. Wasserkrug, L.T. Penberthy, G. Rettura, G. Efron, Cyclosporine A impairs wound healing in rats, J Surg Res 34(6) (1983) 572-5.

[17] T. Hasegawa, K. Sumiyoshi, H. Tsuchihashi, S. Ikeda, A. Nakao, H. Ogawa, FK506 inhibits the enhancing effects of TGF-beta on wound healing in a rabbit dermal ulcer model, J Dermatol Sci 47(1) (2007) 37-40.

[18] A.O. Awojoodu, M.E. Ogle, L.S. Sefcik, D.T. Bowers, K. Martin, K.L. Brayman, K.R. Lynch, S.M. Peirce-Cottler, E. Botchwey, Sphingosine 1-phosphate receptor 3 regulates recruitment of anti-inflammatory monocytes to microvessels during implant arteriogenesis, Proc Natl Acad Sci U S A 110(34) (2013) 13785-90.

[19] A.J. Clover, A.H. Kumar, N.M. Caplice, Deficiency of CX3CR1 delays burn wound healing and is associated with reduced myeloid cell recruitment and decreased sub-dermal angiogenesis, Burns 37(8) (2011) 1386-93.

[20] M. Nahrendorf, F.K. Swirski, E. Aikawa, L. Stangenberg, T. Wurdinger, J.L. Figueiredo, P. Libby, R. Weissleder, M.J. Pittet, The healing myocardium sequentially mobilizes two monocyte subsets with divergent and complementary functions, J Exp Med 204(12) (2007) 3037-47.

[21] A. ElAli, N. Jean LeBlanc, The Role of Monocytes in Ischemic Stroke Pathobiology: New Avenues to Explore, Front Aging Neurosci 8 (2016) 29.

[22] G.Y. Chen, G. Nunez, Sterile inflammation: sensing and reacting to damage, Nat Rev Immunol 10(12) (2010) 826-37.

[23] M.E. Ogle, C.E. Segar, S. Sridhar, E.A. Botchwey, Monocytes and macrophages in tissue repair: Implications for immunoregenerative biomaterial design, Exp Biol Med (Maywood) 241(10) (2016) 1084-97.

[24] D.M. Mosser, J.P. Edwards, Exploring the full spectrum of macrophage activation, Nat Rev Immunol 8(12) (2008) 958-69.

[25] H. Ebaid, Neutrophil depletion in the early inflammatory phase delayed cutaneous wound healing in older rats: improvements due to the use of un-denatured camel whey protein, Diagn Pathol 9 (2014) 46.

[26] J.W. Godwin, A.R. Pinto, N.A. Rosenthal, Macrophages are required for adult salamander limb regeneration, Proc Natl Acad Sci U S A 110(23) (2013) 9415-20.

[27] L. Li, B. Yan, Y.Q. Shi, W.Q. Zhang, Z.L. Wen, Live imaging reveals differing roles of macrophages and neutrophils during zebrafish tail fin regeneration, J Biol Chem 287(30) (2012) 25353-60.

[28] E. Kolaczkowska, P. Kubes, Neutrophil recruitment and function in health and inflammation, Nat Rev Immunol 13(3) (2013) 159-75.

[29] K. Pittman, P. Kubes, Damage-associated molecular patterns control neutrophil recruitment, J Innate Immun 5(4) (2013) 315-23.

[30] K. Kienle, T. Lammermann, Neutrophil swarming: an essential process of the neutrophil tissue response, Immunol Rev 273(1) (2016) 76-93.

[31] T. Lammermann, In the eye of the neutrophil swarm-navigation signals that bring neutrophils together in inflamed and infected tissues, J Leukoc Biol 100(1) (2016) 55-63.

[32] T. Lammermann, P.V. Afonso, B.R. Angermann, J.M. Wang, W. Kastenmuller, C.A. Parent, R.N. Germain, Neutrophil swarms require LTB4 and integrins at sites of cell death in vivo, Nature 498(7454) (2013) 371-5.

[33] T.A. Wilgus, S. Roy, J.C. McDaniel, Neutrophils and Wound Repair: Positive Actions and Negative Reactions, Adv Wound Care (New Rochelle) 2(7) (2013) 379-388.

[34] P. Kruger, M. Saffarzadeh, A.N. Weber, N. Rieber, M. Radsak, H. von Bernuth, C. Benarafa, D. Roos, J. Skokowa, D. Hartl, Neutrophils: Between host defence, immune modulation, and tissue injury, PLoS pathogens 11(3) (2015) e1004651.

[35] V. Brinkmann, U. Reichard, C. Goosmann, B. Fauler, Y. Uhlemann, D.S. Weiss, Y. Weinrauch, A. Zychlinsky, Neutrophil extracellular traps kill bacteria, Science 303(5663) (2004) 1532-5.

[36] S.R. Clark, A.C. Ma, S.A. Tavener, B. McDonald, Z. Goodarzi, M.M. Kelly, K.D. Patel, S. Chakrabarti, E. McAvoy, G.D. Sinclair, E.M. Keys, E. Allen-Vercoe, R. Devinney, C.J. Doig, F.H. Green, P. Kubes, Platelet TLR4 activates neutrophil extracellular traps to ensnare bacteria in septic blood, Nat Med 13(4) (2007) 463-9.

[37] S.K. Jorch, P. Kubes, An emerging role for neutrophil extracellular traps in noninfectious disease, Nat Med 23(3) (2017) 279-287.

[38] E. Kolaczkowska, C.N. Jenne, B.G. Surewaard, A. Thanabalasuriar, W.Y. Lee, M.J. Sanz, K. Mowen, G. Opdenakker, P. Kubes, Molecular mechanisms of NET formation and degradation revealed by intravital imaging in the liver vasculature, Nat Commun 6 (2015) 6673.

[39] C. Nathan, Neutrophils and immunity: challenges and opportunities, Nat Rev Immunol 6(3) (2006) 173-82.

[40] M. Liu, K. Chen, T. Yoshimura, Y. Liu, W. Gong, Y. Le, J.L. Gao, J. Zhao, J.M. Wang, A. Wang, Formylpeptide receptors mediate rapid neutrophil mobilization to accelerate wound healing, PLoS One 9(6) (2014) e90613.

[41] R.M. Devalaraja, L.B. Nanney, J. Du, Q. Qian, Y. Yu, M.N. Devalaraja, A. Richmond, Delayed wound healing in CXCR2 knockout mice, J Invest Dermatol 115(2) (2000) 234-44.

[42] J. Li, Y.P. Zhang, R.S. Kirsner, Angiogenesis in wound repair: angiogenic growth factors and the extracellular matrix, Microsc Res Tech 60(1) (2003) 107-14.

[43] G. Christoffersson, E. Vagesjo, J. Vandooren, M. Liden, S. Massena, R.B. Reinert, M. Brissova, A.C. Powers, G. Opdenakker, M. Phillipson, VEGF-A recruits a proangiogenic MMP-9-delivering neutrophil subset that induces angiogenesis in transplanted hypoxic tissue, Blood 120(23) (2012) 4653-62.

[44] S. Massena, G. Christoffersson, E. Vagesjo, C. Seignez, K. Gustafsson, F. Binet, C. Herrera Hidalgo, A. Giraud, J. Lomei, S. Westrom, M. Shibuya, L. Claesson-Welsh, P. Gerwins, M. Welsh, J. Kreuger, M. Phillipson, Identification and characterization of VEGF-A-responsive neutrophils expressing CD49d, VEGFR1, and CXCR4 in mice and humans, Blood 126(17) (2015) 2016-26.

[45] J.P. Edwards, X. Zhang, K.A. Frauwirth, D.M. Mosser, Biochemical and functional characterization of three activated macrophage populations, J Leukoc Biol 80(6) (2006) 1298-307.

[46] C.Y. Slaney, A. Toker, A. La Flamme, B.T. Backstrom, J.L. Harper, Naive blood monocytes suppress T-cell function. A possible mechanism for protection from autoimmunity, Immunol Cell Biol 89(1) (2011) 7-13.

[47] F. Geissmann, S. Jung, D.R. Littman, Blood monocytes consist of two principal subsets with distinct migratory properties, Immunity 19(1) (2003) 71-82.

[48] R. Goncalves, X. Zhang, H. Cohen, A. Debrabant, D.M. Mosser, Platelet activation attracts a subpopulation of effector monocytes to sites of Leishmania major infection, J Exp Med 208(6) (2011) 1253-65.

[49] L.M. Carlin, E.G. Stamatiades, C. Auffray, R.N. Hanna, L. Glover, G. Vizcay-Barrena, C.C. Hedrick, H.T. Cook, S. Diebold, F. Geissmann, Nr4a1-dependent Ly6C(low) monocytes monitor endothelial cells and orchestrate their disposal, Cell 153(2) (2013) 362-75.

[50] D. Dal-Secco, J. Wang, Z. Zeng, E. Kolaczkowska, C.H. Wong, B. Petri, R.M. Ransohoff, I.F. Charo, C.N. Jenne, P. Kubes, A dynamic spectrum of monocytes arising from the in situ reprogramming of CCR2+ monocytes at a site of sterile injury, J Exp Med 212(4) (2015) 447-56.

[51] L. Arnold, A. Henry, F. Poron, Y. Baba-Amer, N. van Rooijen, A. Plonquet, R.K. Gherardi, B. Chazaud, Inflammatory monocytes recruited after skeletal muscle injury switch into antiinflammatory macrophages to support myogenesis, J Exp Med 204(5) (2007) 1057-69.

[52] R. van Furth, Z.A. Cohn, The origin and kinetics of mononuclear phagocytes, J Exp Med 128(3) (1968) 415-35.

[53] C. Shi, E.G. Pamer, Monocyte recruitment during infection and inflammation, Nat Rev Immunol 11(11) (2011) 762-74.

[54] S. Yona, K.W. Kim, Y. Wolf, A. Mildner, D. Varol, M. Breker, D. Strauss-Ayali, S. Viukov, M. Guilliams, A. Misharin, D.A. Hume, H. Perlman, B. Malissen, E. Zelzer, S. Jung, Fate mapping reveals origins and dynamics of monocytes and tissue macrophages under homeostasis, Immunity 38(1) (2013) 79-91.

[55] M. Nahrendorf, M.J. Pittet, F.K. Swirski, Monocytes: protagonists of infarct inflammation and repair after myocardial infarction, Circulation 121(22) (2010) 2437-45.

[56] S. Gordon, P.R. Taylor, Monocyte and macrophage heterogeneity, Nat Rev Immunol 5(12) (2005) 953-64.

[57] F. Tacke, D. Alvarez, T.J. Kaplan, C. Jakubzick, R. Spanbroek, J. Llodra, A. Garin, J. Liu, M. Mack, N. van Rooijen, S.A. Lira, A.J. Habenicht, G.J. Randolph, Monocyte subsets differentially employ CCR2, CCR5, and CX3CR1 to accumulate within atherosclerotic plaques, J Clin Invest 117(1) (2007) 185-94.

[58] E. Zigmond, C. Varol, J. Farache, E. Elmaliah, A.T. Satpathy, G. Friedlander, M. Mack, N. Shpigel, I.G. Boneca, K.M. Murphy, G. Shakhar, Z. Halpern, S. Jung, Ly6C hi monocytes in the inflamed colon give rise to proinflammatory effector cells and migratory antigen-presenting cells, Immunity 37(6) (2012) 1076-90.

[59] I. Avraham-Davidi, S. Yona, M. Grunewald, L. Landsman, C. Cochain, J.S. Silvestre, H. Mizrahi, M. Faroja, D. Strauss-Ayali, M. Mack, S. Jung, E. Keshet, On-site

education of VEGF-recruited monocytes improves their performance as angiogenic and arteriogenic accessory cells, J Exp Med 210(12) (2013) 2611-25.

[60] L. Denney, W.L. Kok, S.L. Cole, S. Sanderson, A.J. McMichael, L.P. Ho, Activation of invariant NKT cells in early phase of experimental autoimmune encephalomyelitis results in differentiation of Ly6Chi inflammatory monocyte to M2 macrophages and improved outcome, J Immunol 189(2) (2012) 551-7.

[61] C.E. Olingy, C.L. San Emeterio, M.E. Ogle, J.R. Krieger, A.C. Bruce, D.D. Pfau, B.T. Jordan, S.M. Peirce, E.A. Botchwey, Non-classical monocytes are biased progenitors of wound healing macrophages during soft tissue injury, Sci Rep 7(1) (2017) 447.

[62] A. Mantovani, A. Sica, S. Sozzani, P. Allavena, A. Vecchi, M. Locati, The chemokine system in diverse forms of macrophage activation and polarization, Trends Immunol 25(12) (2004) 677-86.

[63] K.L. Spiller, R.R. Anfang, K.J. Spiller, J. Ng, K.R. Nakazawa, J.W. Daulton, G. Vunjak-Novakovic, The role of macrophage phenotype in vascularization of tissue engineering scaffolds, Biomaterials 35(15) (2014) 4477-88.

[64] K.L. Spiller, S. Nassiri, C.E. Witherel, R.R. Anfang, J. Ng, K.R. Nakazawa, T. Yu, G. Vunjak-Novakovic, Sequential delivery of immunomodulatory cytokines to facilitate the M1-to-M2 transition of macrophages and enhance vascularization of bone scaffolds, Biomaterials 37 (2015) 194-207.

[65] M.J. Crane, J.M. Daley, O. van Houtte, S.K. Brancato, W.L. Henry, Jr., J.E. Albina, The monocyte to macrophage transition in the murine sterile wound, PLoS One 9(1) (2014) e86660.

[66] F.O. Martinez, S. Gordon, M. Locati, A. Mantovani, Transcriptional profiling of the human monocyte-to-macrophage differentiation and polarization: new molecules and patterns of gene expression, J Immunol 177(10) (2006) 7303-11.

[67] K.L. Spiller, E.A. Wrona, S. Romero-Torres, I. Pallotta, P.L. Graney, C.E. Witherel, L.M. Panicker, R.A. Feldman, A.M. Urbanska, L. Santambrogio, G. Vunjak-Novakovic, D.O. Freytes, Differential Gene Expression in Human, Murine, and Cell Line-derived Macrophages upon Polarization, Exp Cell Res (2015).

[68] M. Sironi, F.O. Martinez, D. D'Ambrosio, M. Gattorno, N. Polentarutti, M. Locati, A. Gregorio, A. Iellem, M.A. Cassatella, J. Van Damme, S. Sozzani, A. Martini, F. Sinigaglia, A. Vecchi, A. Mantovani, Differential regulation of chemokine production by Fcgamma receptor engagement in human monocytes: association of CCL1 with a distinct form of M2 monocyte activation (M2b, Type 2), J Leukoc Biol 80(2) (2006) 342-9.

[69] J.A. Knipper, S. Willenborg, J. Brinckmann, W. Bloch, T. Maass, R. Wagener, T. Krieg, T. Sutherland, A. Munitz, M.E. Rothenberg, A. Niehoff, R. Richardson, M. Hammerschmidt, J.E. Allen, S.A. Eming, Interleukin-4 Receptor alpha Signaling in

Myeloid Cells Controls Collagen Fibril Assembly in Skin Repair, Immunity 43(4) (2015) 803-16.

[70] N. Mokarram, A. Merchant, V. Mukhatyar, G. Patel, R.V. Bellamkonda, Effect of modulating macrophage phenotype on peripheral nerve repair, Biomaterials 33(34) (2012) 8793-801.

[71] J.R. Krieger, M.E. Ogle, J. McFaline-Figueroa, C.E. Segar, J.S. Temenoff, E.A. Botchwey, Spatially localized recruitment of anti-inflammatory monocytes by SDF-1alpha-releasing hydrogels enhances microvascular network remodeling, Biomaterials 77 (2016) 280-90.

[72] K. Sadtler, K. Estrellas, B.W. Allen, M.T. Wolf, H. Fan, A.J. Tam, C.H. Patel, B.S. Luber, H. Wang, K.R. Wagner, J.D. Powell, F. Housseau, D.M. Pardoll, J.H. Elisseeff, Developing a pro-regenerative biomaterial scaffold microenvironment requires T helper 2 cells, Science 352(6283) (2016) 366-70.

[73] Y. Liu, L. Wang, T. Kikuiri, K. Akiyama, C. Chen, X. Xu, R. Yang, W. Chen, S. Wang, S. Shi, Mesenchymal stem cell-based tissue regeneration is governed by recipient T lymphocytes via IFN-gamma and TNF-alpha, Nat Med 17(12) (2011) 1594-601.

[74] N. Ali, B. Zirak, R.S. Rodriguez, M.L. Pauli, H.A. Truong, K. Lai, R. Ahn, K. Corbin, M.M. Lowe, T.C. Scharschmidt, K. Taravati, M.R. Tan, R.R. Ricardo-Gonzalez, A. Nosbaum, M. Bertolini, W. Liao, F.O. Nestle, R. Paus, G. Cotsarelis, A.K. Abbas, M.D. Rosenblum, Regulatory T Cells in Skin Facilitate Epithelial Stem Cell Differentiation, Cell 169(6) (2017) 1119-1129 e11.

[75] D. Burzyn, W. Kuswanto, D. Kolodin, J.L. Shadrach, M. Cerletti, Y. Jang, E. Sefik, T.G. Tan, A.J. Wagers, C. Benoist, D. Mathis, A special population of regulatory T cells potentiates muscle repair, Cell 155(6) (2013) 1282-95.

[76] W. Kuswanto, D. Burzyn, M. Panduro, K.K. Wang, Y.C. Jang, A.J. Wagers, C. Benoist, D. Mathis, Poor Repair of Skeletal Muscle in Aging Mice Reflects a Defect in Local, Interleukin-33-Dependent Accumulation of Regulatory T Cells, Immunity 44(2) (2016) 355-67.

[77] A. Nosbaum, N. Prevel, H.A. Truong, P. Mehta, M. Ettinger, T.C. Scharschmidt, N.H. Ali, M.L. Pauli, A.K. Abbas, M.D. Rosenblum, Cutting Edge: Regulatory T Cells Facilitate Cutaneous Wound Healing, J Immunol 196(5) (2016) 2010-4.

[78] T.C. Scharschmidt, K.S. Vasquez, H.A. Truong, S.V. Gearty, M.L. Pauli, A. Nosbaum, I.K. Gratz, M. Otto, J.J. Moon, J. Liese, A.K. Abbas, M.A. Fischbach, M.D. Rosenblum, A Wave of Regulatory T Cells into Neonatal Skin Mediates Tolerance to Commensal Microbes, Immunity 43(5) (2015) 1011-21.

[79] X. Zhou, J. Tang, H. Cao, H. Fan, B. Li, Tissue resident regulatory T cells: novel therapeutic targets for human disease, Cell Mol Immunol 12(5) (2015) 543-52.

[80] K.J. Lavine, S. Epelman, K. Uchida, K.J. Weber, C.G. Nichols, J.D. Schilling, D.M. Ornitz, G.J. Randolph, D.L. Mann, Distinct macrophage lineages contribute to disparate patterns of cardiac recovery and remodeling in the neonatal and adult heart, Proc Natl Acad Sci U S A 111(45) (2014) 16029-34.

[81] J. Weirather, U.D. Hofmann, N. Beyersdorf, G.C. Ramos, B. Vogel, A. Frey, G. Ertl, T. Kerkau, S. Frantz, Foxp3+ CD4+ T cells improve healing after myocardial infarction by modulating monocyte/macrophage differentiation, Circ Res 115(1) (2014) 55-67.

[82] F. Carbone, A. Nencioni, F. Mach, N. Vuilleumier, F. Montecucco, Pathophysiological role of neutrophils in acute myocardial infarction, Thromb Haemost 110(3) (2013) 501-14.

[83] Y. Dombrowski, T. O'Hagan, M. Dittmer, R. Penalva, S.R. Mayoral, P. Bankhead, S. Fleville, G. Eleftheriadis, C. Zhao, M. Naughton, R. Hassan, J. Moffat, J. Falconer, A. Boyd, P. Hamilton, I.V. Allen, A. Kissenpfennig, P.N. Moynagh, E. Evergren, B. Perbal, A.C. Williams, R.J. Ingram, J.R. Chan, R.J.M. Franklin, D.C. Fitzgerald, Regulatory T cells promote myelin regeneration in the central nervous system, Nat Neurosci 20(5) (2017) 674-680.

[84] A. Castiglioni, G. Corna, E. Rigamonti, V. Basso, M. Vezzoli, A. Monno, A.E. Almada, A. Mondino, A.J. Wagers, A.A. Manfredi, P. Rovere-Querini, FOXP3+ T Cells Recruited to Sites of Sterile Skeletal Muscle Injury Regulate the Fate of Satellite Cells and Guide Effective Tissue Regeneration, PLoS One 10(6) (2015) e0128094.

[85] Z.V. Schofield, T.M. Woodruff, R. Halai, M.C. Wu, M.A. Cooper, Neutrophils--a key component of ischemia-reperfusion injury, Shock 40(6) (2013) 463-70.

[86] N.D. Jones, M.O. Brook, M. Carvalho-Gaspar, S. Luo, K.J. Wood, Regulatory T cells can prevent memory CD8+ T-cell-mediated rejection following polymorphonuclear cell depletion, Eur J Immunol 40(11) (2010) 3107-16.

[87] Y. Uchida, M.C. Freitas, D. Zhao, R.W. Busuttil, J.W. Kupiec-Weglinski, The protective function of neutrophil elastase inhibitor in liver ischemia/reperfusion injury, Transplantation 89(9) (2010) 1050-6.

[88] M.T. Hardison, F.S. Galin, C.E. Calderon, U.V. Djekic, S.B. Parker, K.M. Wille, P.L. Jackson, R.A. Oster, K.R. Young, J.E. Blalock, A. Gaggar, The presence of a matrix-derived neutrophil chemoattractant in bronchiolitis obliterans syndrome after lung transplantation, J Immunol 182(7) (2009) 4423-31.

[89] C. Beauvillain, P. Cunin, A. Doni, M. Scotet, S. Jaillon, M.L. Loiry, G. Magistrelli, K. Masternak, A. Chevailler, Y. Delneste, P. Jeannin, CCR7 is involved in the migration of neutrophils to lymph nodes, Blood 117(4) (2011) 1196-204.

[90] D.F. LaRosa, A.H. Rahman, L.A. Turka, The innate immune system in allograft rejection and tolerance, J Immunol 178(12) (2007) 7503-9.

[91] A. Bajwa, G.R. Kinsey, M.D. Okusa, Immune mechanisms and novel pharmacological therapies of acute kidney injury, Curr Drug Targets 10(12) (2009) 1196-204.

[92] A.E. Morelli, A.W. Thomson, Tolerogenic dendritic cells and the quest for transplant tolerance, Nat Rev Immunol 7(8) (2007) 610-21.

[93] A. Vishwakarma, N.S. Bhise, M.B. Evangelista, J. Rouwkema, M.R. Dokmeci, A.M. Ghaemmaghami, N.E. Vrana, A. Khademhosseini, Engineering Immunomodulatory Biomaterials To Tune the Inflammatory Response, Trends Biotechnol 34(6) (2016) 470-82.

[94] C.L. San Emeterio, C.E. Olingy, Y. Chu, E.A. Botchwey, Selective recruitment of non-classical monocytes promotes skeletal muscle repair, Biomaterials 117 (2017) 32-43.

[95] L.M. Francisco, P.T. Sage, A.H. Sharpe, The PD-1 pathway in tolerance and autoimmunity, Immunol Rev 236 (2010) 219-42.

[96] C.N. Serhan, N.A. Petasis, Resolvins and protectins in inflammation resolution, Chem Rev 111(10) (2011) 5922-43.

[97] K.J. Ho, M. Spite, C.D. Owens, H. Lancero, A.H. Kroemer, R. Pande, M.A. Creager, C.N. Serhan, M.S. Conte, Aspirin-triggered lipoxin and resolvin E1 modulate vascular smooth muscle phenotype and correlate with peripheral atherosclerosis, Am J Pathol 177(4) (2010) 2116-23.

[98] T. Miyahara, S. Runge, A. Chatterjee, M. Chen, G. Mottola, J.M. Fitzgerald, C.N. Serhan, M.S. Conte, D-series resolvin attenuates vascular smooth muscle cell activation and neointimal hyperplasia following vascular injury, FASEB J 27(6) (2013) 2220-32.

[99] J. Claria, B.T. Nguyen, A.L. Madenci, C.K. Ozaki, C.N. Serhan, Diversity of lipid mediators in human adipose tissue depots, Am J Physiol Cell Physiol 304(12) (2013) C1141-9.

[100] M. Spite, J. Claria, C.N. Serhan, Resolvins, specialized proresolving lipid mediators, and their potential roles in metabolic diseases, Cell Metab 19(1) (2014) 21-36.

[101] V. Chiurchiu, A. Leuti, J. Dalli, A. Jacobsson, L. Battistini, M. Maccarrone, C.N. Serhan, Proresolving lipid mediators resolvin D1, resolvin D2, and maresin 1 are critical in modulating T cell responses, Sci Transl Med 8(353) (2016) 353ra111.

[102] W. Liao, F. Zeng, K. Kang, Y. Qi, L. Yao, H. Yang, L. Ling, N. Wu, D. Wu, Lipoxin A4 attenuates acute rejection via shifting TH1/TH2 cytokine balance in rat liver transplantation, Transplant Proc 45(6) (2013) 2451-4.

[103] B.D. Levy, Q.Y. Zhang, C. Bonnans, V. Primo, J.J. Reilly, D.L. Perkins, Y. Liang, M. Amin Arnaout, B. Nikolic, C.N. Serhan, The endogenous pro-resolving mediators

lipoxin A4 and resolvin E1 preserve organ function in allograft rejection, Prostaglandins Leukot Essent Fatty Acids 84(1-2) (2011) 43-50.

[104] J. Hua, Y. Jin, Y. Chen, T. Inomata, H. Lee, S.K. Chauhan, N.A. Petasis, C.N. Serhan, R. Dana, The resolvin D1 analogue controls maturation of dendritic cells and suppresses alloimmunity in corneal transplantation, Invest Ophthalmol Vis Sci 55(9) (2014) 5944-51.

[105] W. Ouyang, S. Rutz, N.K. Crellin, P.A. Valdez, S.G. Hymowitz, Regulation and functions of the IL-10 family of cytokines in inflammation and disease, Annu Rev Immunol 29 (2011) 71-109.

[106] S. Corinti, C. Albanesi, A. la Sala, S. Pastore, G. Girolomoni, Regulatory activity of autocrine IL-10 on dendritic cell functions, J Immunol 166(7) (2001) 4312-8.

[107] M.A. Boks, J.R. Kager-Groenland, M.S. Haasjes, J.J. Zwaginga, S.M. van Ham, A. ten Brinke, IL-10-generated tolerogenic dendritic cells are optimal for functional regulatory T cell induction--a comparative study of human clinical-applicable DC, Clin Immunol 142(3) (2012) 332-42.

[108] A. Taylor, J. Verhagen, K. Blaser, M. Akdis, C.A. Akdis, Mechanisms of immune suppression by interleukin-10 and transforming growth factor-beta: the role of T regulatory cells, Immunology 117(4) (2006) 433-42.

[109] M. Hara, C.I. Kingsley, M. Niimi, S. Read, S.E. Turvey, A.R. Bushell, P.J. Morris, F. Powrie, K.J. Wood, IL-10 is required for regulatory T cells to mediate tolerance to alloantigens in vivo, J Immunol 166(6) (2001) 3789-96.

[110] J. Claria, J. Dalli, S. Yacoubian, F. Gao, C.N. Serhan, Resolvin D1 and Resolvin D2 Govern Local Inflammatory Tone in Obese Fat, The Journal of Immunology, 2012, pp. 2597-2605.

[111] L.V. Norling, M. Spite, R. Yang, R.J. Flower, M. Perretti, C.N. Serhan, Cutting Edge: Humanized Nano-Proresolving Medicines Mimic Inflammation-Resolution and Enhance Wound Healing, The Journal of Immunology, 2011, pp. 5543-5547.

[112] A. Ortega-Gomez, M. Perretti, O. Soehnlein, Resolution of inflammation: an integrated view, EMBO Mol Med 5(5) (2013) 661-74.

[113] B.D. Levy, Resolvins and protectins Natural pharmacophores for resolution biology, Prostaglandins Leukotrienes & Essential Fatty Acids, Elsevier, 2010, pp. 327-332.

[114] M.J. Zhang, B.E. Sansbury, J. Hellmann, J.F. Baker, L. Guo, C.M. Parmer, J.C. Prenner, D.J. Conklin, A. Bhatnagar, M.A. Creager, M. Spite, Resolvin D2 Enhances Postischemic Revascularization While Resolving Inflammation, Circulation 134(9) (2016) 666-680.

[115] Y.P. Sun, S.F. Oh, J. Uddin, R. Yang, K. Gotlinger, E. Campbell, S.P. Colgan, N.A. Petasis, C.N. Serhan, Resolvin D1 and Its Aspirin-triggered 17R Epimer: STEREOCHEMICAL ASSIGNMENTS, ANTI-INFLAMMATORY PROPERTIES, AND ENZYMATIC INACTIVATION, Journal of Biological Chemistry, 2007, pp. 9323-9334.

[116] G. Tiwari, R. Tiwari, B. Sriwastawa, L. Bhati, S. Pandey, P. Pandey, S.K. Bannerjee, Drug delivery systems: An updated review, Int J Pharm Investig 2(1) (2012) 2-11.

[117] D.P. Vasconcelos, M. Costa, I.F. Amaral, M.A. Barbosa, A.P. Aguas, J.N. Barbosa, Development of an immunomodulatory biomaterial: using resolvin D1 to modulate inflammation, Biomaterials 53 (2015) 566-73.

[118] N. Kamaly, G. Fredman, M. Subramanian, S. Gadde, A. Pesic, L. Cheung, Z.A. Fayad, R. Langer, I. Tabas, O.C. Farokhzad, Development and in vivo efficacy of targeted polymeric inflammation-resolving nanoparticles, Proc Natl Acad Sci U S A 110(16) (2013) 6506-11.

[119] B. Wu, G. Mottola, A. Chatterjee, K.D. Lance, M. Chen, I.O. Siguenza, T.A. Desai, M.S. Conte, Perivascular delivery of resolvin D1 inhibits neointimal hyperplasia in a rat model of arterial injury, J Vasc Surg 65(1) (2017) 207-217 e3.

[120] K.D. Lance, A. Chatterjee, B. Wu, G. Mottola, H. Nuhn, P.P. Lee, B.E. Sansbury, M. Spite, T.A. Desai, M.S. Conte, Unidirectional and sustained delivery of the proresolving lipid mediator resolvin D1 from a biodegradable thin film device, J Biomed Mater Res A 105(1) (2017) 31-41.

[121] A.P. Rogerio, O. Haworth, R. Croze, S.F. Oh, M. Uddin, T. Carlo, M.A. Pfeffer, R. Priluck, C.N. Serhan, B.D. Levy, Resolvin D1 and Aspirin-Triggered Resolvin D1 Promote Resolution of Allergic Airways Responses, The Journal of Immunology, 2012, pp. 1983-1991.

[122] A. Das, D.A. Barker, T. Wang, C.M. Lau, Y. Lin, E.A. Botchwey, Delivery of bioactive lipids from composite microgel-microsphere injectable scaffolds enhances stem cell recruitment and skeletal repair, PLoS One 9(7) (2014) e101276.

[123] A. Das, C.E. Segar, B.B. Hughley, D.T. Bowers, E.A. Botchwey, The promotion of mandibular defect healing by the targeting of S1P receptors and the recruitment of alternatively activated macrophages, Biomaterials 34(38) (2013) 9853-62.

[124] K.A. Wieghaus, S.M. Capitosti, C.R. Anderson, R.J. Price, B.R. Blackman, M.L. Brown, E.A. Botchwey, Small molecule inducers of angiogenesis for tissue engineering, Tissue Eng 12(7) (2006) 1903-13.

[125] L.S. Sefcik, C.E. Aronin, A.O. Awojoodu, S.J. Shin, F. Mac Gabhann, T.L. MacDonald, B.R. Wamhoff, K.R. Lynch, S.M. Peirce, E.A. Botchwey, Selective

activation of sphingosine 1-phosphate receptors 1 and 3 promotes local microvascular network growth, Tissue Eng Part A 17(5-6) (2011) 617-29.

[126] C. Huang, A. Das, D. Barker, S. Tholpady, T. Wang, Q. Cui, R. Ogle, E. Botchwey, Local delivery of FTY720 accelerates cranial allograft incorporation and bone formation, Cell Tissue Res 347(3) (2012) 553-66.

[127] J. Wang, Neutrophils in tissue injury and repair, Cell Tissue Res 371(3) (2018) 531-539.

[128] S.L. Wong, M. Demers, K. Martinod, M. Gallant, Y. Wang, A.B. Goldfine, C.R. Kahn, D.D. Wagner, Diabetes primes neutrophils to undergo NETosis, which impairs wound healing, Nat Med 21(7) (2015) 815-9.

[129] E.A. Liehn, N. Tuchscheerer, I. Kanzler, M. Drechsler, L. Fraemohs, A. Schuh, R.R. Koenen, S. Zander, O. Soehnlein, M. Hristov, G. Grigorescu, A.O. Urs, M. Leabu, I. Bucur, M.W. Merx, A. Zernecke, J. Ehling, F. Gremse, T. Lammers, F. Kiessling, J. Bernhagen, A. Schober, C. Weber, Double-edged role of the CXCL12/CXCR4 axis in experimental myocardial infarction, J Am Coll Cardiol 58(23) (2011) 2415-23.

[130] J. Vinten-Johansen, Involvement of neutrophils in the pathogenesis of lethal myocardial reperfusion injury, Cardiovasc Res 61(3) (2004) 481-97.

[131] M.E. Ogle, L.S. Sefcik, A.O. Awojoodu, N.F. Chiappa, K. Lynch, S. Peirce-Cottler, E.A. Botchwey, Engineering in vivo gradients of sphingosine-1-phosphate receptor ligands for localized microvascular remodeling and inflammatory cell positioning, Acta Biomater 10(11) (2014) 4704-14.

[132] C.W. Hsu, R.A. Poche, J.E. Saik, S. Ali, S. Wang, N. Yosef, G.A. Calderon, L. Scott, Jr., T.J. Vadakkan, I.V. Larina, J.L. West, M.E. Dickinson, Improved Angiogenesis in Response to Localized Delivery of Macrophage-Recruiting Molecules, PLoS One 10(7) (2015) e0131643.

[133] A.R. Reeves, K.L. Spiller, D.O. Freytes, G. Vunjak-Novakovic, D.L. Kaplan, Controlled release of cytokines using silk-biomaterials for macrophage polarization, Biomaterials 73 (2015) 272-83.

[134] M. Bartneck, K.H. Heffels, Y. Pan, M. Bovi, G. Zwadlo-Klarwasser, J. Groll, Inducing healing-like human primary macrophage phenotypes by 3D hydrogel coated nanofibres, Biomaterials 33(16) (2012) 4136-46.

[135] A. Mantovani, S. Sozzani, M. Locati, P. Allavena, A. Sica, Macrophage polarization: tumor-associated macrophages as a paradigm for polarized M2 mononuclear phagocytes, Trends Immunol 23(11) (2002) 549-55.

[136] M. Lech, H.J. Anders, Macrophages and fibrosis: How resident and infiltrating mononuclear phagocytes orchestrate all phases of tissue injury and repair, Biochim Biophys Acta 1832(7) (2013) 989-97.

[137] A. Sindrilaru, T. Peters, S. Wieschalka, C. Baican, A. Baican, H. Peter, A. Hainzl, S. Schatz, Y. Qi, A. Schlecht, J.M. Weiss, M. Wlaschek, C. Sunderkotter, K. Scharffetter-Kochanek, An unrestrained proinflammatory M1 macrophage population induced by iron impairs wound healing in humans and mice, J Clin Invest 121(3) (2011) 985-97.

[138] S. Gordon, F.O. Martinez, Alternative activation of macrophages: mechanism and functions, Immunity 32(5) (2010) 593-604.

[139] S. Krishnamoorthy, A. Recchiuti, N. Chiang, S. Yacoubian, C.H. Lee, R. Yang, N.A. Petasis, C.N. Serhan, Resolvin D1 binds human phagocytes with evidence for proresolving receptors, Proc Natl Acad Sci U S A 107(4) (2010) 1660-5.

[140] M.M. Mircescu, L. Lipuma, N. van Rooijen, E.G. Pamer, T.M. Hohl, Essential role for neutrophils but not alveolar macrophages at early time points following Aspergillus fumigatus infection, J Infect Dis 200(4) (2009) 647-56.

[141] S. Hasegawa, H. Eguchi, A. Tomokuni, Y. Tomimaru, T. Asaoka, H. Wada, N. Hama, K. Kawamoto, S. Kobayashi, S. Marubashi, M. Konnno, H. Ishii, M. Mori, Y. Doki, H. Nagano, Pre-treatment neutrophil to lymphocyte ratio as a predictive marker for pathological response to preoperative chemoradiotherapy in pancreatic cancer, Oncol Lett 11(2) (2016) 1560-1566.

[142] D.D. Benson, M.R. Kelher, X. Meng, D.A. Fullerton, J.H. Lee, C.C. Silliman, C.C. Barnett, Jr., Gender-specific transfusion affects tumor-associated neutrophil: macrophage ratios in murine pancreatic adenocarcinoma, J Gastrointest Surg 14(10) (2010) 1560-5.

[143] A.J. Templeton, M.G. McNamara, B. Seruga, F.E. Vera-Badillo, P. Aneja, A. Ocana, R. Leibowitz-Amit, G. Sonpavde, J.J. Knox, B. Tran, I.F. Tannock, E. Amir, Prognostic role of neutrophil-to-lymphocyte ratio in solid tumors: a systematic review and meta-analysis, J Natl Cancer Inst 106(6) (2014) dju124.

[144] G.M. Barton, A calculated response: control of inflammation by the innate immune system, J Clin Invest 118(2) (2008) 413-20.

[145] C.N. Serhan, J. Savill, Resolution of inflammation: the beginning programs the end, Nat Immunol 6(12) (2005) 1191-7.

[146] C.N. Serhan, Resolution phase of inflammation: novel endogenous anti-inflammatory and proresolving lipid mediators and pathways, Annu Rev Immunol 25 (2007) 101-37.

[147] S. Ueha, F.H. Shand, K. Matsushima, Cellular and molecular mechanisms of chronic inflammation-associated organ fibrosis, Front Immunol 3 (2012) 71.

[148] K.L. Rock, E. Latz, F. Ontiveros, H. Kono, The sterile inflammatory response, Annu Rev Immunol 28 (2010) 321-42.

[149] C. Nathan, Points of control in inflammation, Nature 420(6917) (2002) 846-52.

[150] M. Murakami, T. Hirano, The molecular mechanisms of chronic inflammation development, Front Immunol 3 (2012) 323.

[151] J.M. Anderson, A. Rodriguez, D.T. Chang, Foreign body reaction to biomaterials, Semin Immunol 20(2) (2008) 86-100.

[152] O. Veiseh, J.C. Doloff, M. Ma, A.J. Vegas, H.H. Tam, A.R. Bader, J. Li, E. Langan, J. Wyckoff, W.S. Loo, S. Jhunjhunwala, A. Chiu, S. Siebert, K. Tang, J. Hollister-Lock, S. Aresta-Dasilva, M. Bochenek, J. Mendoza-Elias, Y. Wang, M. Qi, D.M. Lavin, M. Chen, N. Dholakia, R. Thakrar, I. Lacik, G.C. Weir, J. Oberholzer, D.L. Greiner, R. Langer, D.G. Anderson, Size- and shape-dependent foreign body immune response to materials implanted in rodents and non-human primates, Nat Mater 14(6) (2015) 643-51.

[153] S. Chen, J.A. Jones, Y. Xu, H.Y. Low, J.M. Anderson, K.W. Leong, Characterization of topographical effects on macrophage behavior in a foreign body response model, Biomaterials 31(13) (2010) 3479-91.

[154] W.J. Hu, J.W. Eaton, T.P. Ugarova, L. Tang, Molecular basis of biomaterial-mediated foreign body reactions, Blood 98(4) (2001) 1231-8.

[155] J. Chen, S. Shetty, P. Zhang, R. Gao, Y. Hu, S. Wang, Z. Li, J. Fu, Aspirin-triggered resolvin D1 down-regulates inflammatory responses and protects against endotoxin-induced acute kidney injury, Toxicol Appl Pharmacol 277(2) (2014) 118-23.

[156] B. Amulic, C. Cazalet, G.L. Hayes, K.D. Metzler, A. Zychlinsky, Neutrophil function: from mechanisms to disease, Annu Rev Immunol 30 (2012) 459-89.

[157] A. Brill, T.A. Fuchs, A.S. Savchenko, G.M. Thomas, K. Martinod, S.F. De Meyer, A.A. Bhandari, D.D. Wagner, Neutrophil extracellular traps promote deep vein thrombosis in mice, J Thromb Haemost 10(1) (2012) 136-44.

[158] A. Bekler, G. Erbag, H. Sen, E. Gazi, S. Ozcan, Predictive value of elevated neutrophil-lymphocyte ratio for left ventricular systolic dysfunction in patients with non ST-elevated acute coronary syndrome, Pak J Med Sci 31(1) (2015) 159-63.

[159] A. Mantovani, M.A. Cassatella, C. Costantini, S. Jaillon, Neutrophils in the activation and regulation of innate and adaptive immunity, Nat Rev Immunol 11(8) (2011) 519-31.

[160] A. Mocsai, Diverse novel functions of neutrophils in immunity, inflammation, and beyond, J Exp Med 210(7) (2013) 1283-99.

[161] J.V. Dovi, L.K. He, L.A. DiPietro, Accelerated wound closure in neutrophil-depleted mice, J Leukoc Biol 73(4) (2003) 448-55.

[162] M.A. Muhmmed Suliman, A.A. Bahnacy Juma, A.A. Ali Almadhani, A.V. Pathare, S.S. Alkindi, F. Uwe Werner, Predictive value of neutrophil to lymphocyte ratio in outcomes of patients with acute coronary syndrome, Arch Med Res 41(8) (2010) 618-22.

[163] Y. Ozdemir, M.L. Akin, I. Sucullu, A.Z. Balta, E. Yucel, Pretreatment neutrophil/lymphocyte ratio as a prognostic aid in colorectal cancer, Asian Pac J Cancer Prev 15(6) (2014) 2647-50.

[164] S. Poludasu, E. Cavusoglu, W. Khan, J.D. Marmur, Neutrophil to lymphocyte ratio as a predictor of long-term mortality in African Americans undergoing percutaneous coronary intervention, Clin Cardiol 32(12) (2009) E6-E10.

[165] K. Kasuga, R. Yang, T.F. Porter, N. Agrawal, N.A. Petasis, D. Irimia, M. Toner, C.N. Serhan, Rapid appearance of resolvin precursors in inflammatory exudates: novel mechanisms in resolution, J Immunol 181(12) (2008) 8677-87.

[166] M.E. Ogle, J.R. Krieger, L.E. Tellier, J. McFaline-Figueroa, J.S. Temenoff, E.A. Botchwey, Dual Affinity Heparin-Based Hydrogels Achieve Pro-Regenerative Immunomodulation and Microvascular Remodeling, ACS Biomaterials Science & Engineering (2017).

[167] M. Segawa, S. Fukada, Y. Yamamoto, H. Yahagi, M. Kanematsu, M. Sato, T. Ito, A. Uezumi, S. Hayashi, Y. Miyagoe-Suzuki, S. Takeda, K. Tsujikawa, H. Yamamoto, Suppression of macrophage functions impairs skeletal muscle regeneration with severe fibrosis, Exp Cell Res 314(17) (2008) 3232-44.

[168] R. Shechter, O. Miller, G. Yovel, N. Rosenzweig, A. London, J. Ruckh, K.W. Kim, E. Klein, V. Kalchenko, P. Bendel, S.A. Lira, S. Jung, M. Schwartz, Recruitment of beneficial M2 macrophages to injured spinal cord is orchestrated by remote brain choroid plexus, Immunity 38(3) (2013) 555-69.

[169] A. Ariel, C.N. Serhan, Resolvins and protectins in the termination program of acute inflammation, Trends in Immunology, 2007, pp. 176-183.

[170] M. Grunewald, I. Avraham, Y. Dor, E. Bachar-Lustig, A. Itin, S. Jung, S. Chimenti, L. Landsman, R. Abramovitch, E. Keshet, VEGF-induced adult neovascularization: recruitment, retention, and role of accessory cells, Cell 124(1) (2006) 175-89.

[171] F. Zemani, J.S. Silvestre, F. Fauvel-Lafeve, A. Bruel, J. Vilar, I. Bieche, I. Laurendeau, I. Galy-Fauroux, A.M. Fischer, C. Boisson-Vidal, Ex vivo priming of endothelial progenitor cells with SDF-1 before transplantation could increase their proangiogenic potential, Arterioscler Thromb Vasc Biol 28(4) (2008) 644-50.

[172] S.J. Jenkins, D. Ruckerl, P.C. Cook, L.H. Jones, F.D. Finkelman, N. van Rooijen, A.S. MacDonald, J.E. Allen, Local macrophage proliferation, rather than recruitment from the blood, is a signature of TH2 inflammation, Science 332(6035) (2011) 1284-8.

[173] Y.P. Goh, N.C. Henderson, J.E. Heredia, A. Red Eagle, J.I. Odegaard, N. Lehwald, K.D. Nguyen, D. Sheppard, L. Mukundan, R.M. Locksley, A. Chawla, Eosinophils secrete IL-4 to facilitate liver regeneration, Proc Natl Acad Sci U S A 110(24) (2013) 9914-9.

[174] A.C. Bruce, M.R. Kelly-Goss, J.L. Heuslein, J.K. Meisner, R.J. Price, S.M. Peirce, Monocytes are recruited from venules during arteriogenesis in the murine spinotrapezius ligation model, Arterioscler Thromb Vasc Biol 34(9) (2014) 2012-22.

[175] C. Auffray, D. Fogg, M. Garfa, G. Elain, O. Join-Lambert, S. Kayal, S. Sarnacki, A. Cumano, G. Lauvau, F. Geissmann, Monitoring of blood vessels and tissues by a population of monocytes with patrolling behavior, Science 317(5838) (2007) 666-70.

[176] L.M. Carlin, C. Auffray, F. Geissmann, Measuring intravascular migration of mouse Ly6C(low) monocytes in vivo using intravital microscopy, Curr Protoc Immunol Chapter 14 (2013) Unit 14 33 1-16.

[177] J.L. Collison, L.M. Carlin, M. Eichmann, F. Geissmann, M. Peakman, Heterogeneity in the Locomotory Behavior of Human Monocyte Subsets over Human Vascular Endothelium In Vitro, J Immunol 195(3) (2015) 1162-70.

[178] M.C.P. Sok, M.C. Tria, C.E. Olingy, C.L. San Emeterio, E.A. Botchwey, Aspirin-Triggered Resolvin D1-modified materials promote the accumulation of pro-regenerative immune cell subsets and enhance vascular remodeling, Acta Biomater 53 (2017) 109-122.

[179] P.J. Wermuth, S.A. Jimenez, The significance of macrophage polarization subtypes for animal models of tissue fibrosis and human fibrotic diseases, Clin Transl Med 4 (2015) 2.

[180] T. Worbs, S.I. Hammerschmidt, R. Forster, Dendritic cell migration in health and disease, Nat Rev Immunol 17(1) (2017) 30-48.

[181] R.A. Maldonado, U.H. von Andrian, How tolerogenic dendritic cells induce regulatory T cells, Adv Immunol 108 (2010) 111-65.

[182] L. Bae, J.K. Bohannon, W. Cui, M. Vinish, T. Toliver-Kinsky, Fms-like tyrosine kinase-3 ligand increases resistance to burn wound infection through effects on plasmacytoid dendritic cells, BMC Immunol 18(1) (2017) 9.

[183] M. Vinish, W. Cui, E. Stafford, L. Bae, H. Hawkins, R. Cox, T. Toliver-Kinsky, Dendritic cells modulate burn wound healing by enhancing early proliferation, Wound Repair Regen 24(1) (2016) 6-13.

[184] A. Anzai, T. Anzai, S. Nagai, Y. Maekawa, K. Naito, H. Kaneko, Y. Sugano, T. Takahashi, H. Abe, S. Mochizuki, M. Sano, T. Yoshikawa, Y. Okada, S. Koyasu, S. Ogawa, K. Fukuda, Regulatory role of dendritic cells in postinfarction healing and left ventricular remodeling, Circulation 125(10) (2012) 1234-45.

[185] P. Ruiz, P. Maldonado, Y. Hidalgo, D. Sauma, M. Rosemblatt, M.R. Bono, Alloreactive Regulatory T Cells Allow the Generation of Mixed Chimerism and Transplant Tolerance, Front Immunol 6 (2015) 596.

[186] I. Shalev, N. Selzner, W. Shyu, D. Grant, G. Levy, Role of regulatory T cells in the promotion of transplant tolerance, Liver Transpl 18(7) (2012) 761-70.

[187] C.H. Lee, Resolvins as new fascinating drug candidates for inflammatory diseases, Arch. Pharm. Res., 2012, pp. 3-7.

[188] S. Hong, Y. Lu, R. Yang, K.H. Gotlinger, N.A. Petasis, C.N. Serhan, Resolvin D1, protectin D1, and related docosahexaenoic acid-derived products: Analysis via electrospray/low energy tandem mass spectrometry based on spectra and fragmentation mechanisms, J Am Soc Mass Spectrom, 2007, pp. 128-144.

[189] C.S. Wang, C.L. Maruyama, J.T. Easley, B.G. Trump, O.J. Baker, AT-RvD1 Promotes Resolution of Inflammation in NOD/ShiLtJ mice, Sci Rep 7 (2017) 45525.

[190] A. Chaudhry, R.M. Samstein, P. Treuting, Y. Liang, M.C. Pils, J.M. Heinrich, R.S. Jack, F.T. Wunderlich, J.C. Bruning, W. Muller, A.Y. Rudensky, Interleukin-10 signaling in regulatory T cells is required for suppression of Th17 cell-mediated inflammation, Immunity 34(4) (2011) 566-78.

[191] B. Deng, M. Wehling-Henricks, S.A. Villalta, Y. Wang, J.G. Tidball, IL-10 triggers changes in macrophage phenotype that promote muscle growth and regeneration, J Immunol 189(7) (2012) 3669-80.

[192] J. Dagvadorj, Y. Naiki, G. Tumurkhuu, F. Hassan, S. Islam, N. Koide, I. Mori, T. Yoshida, T. Yokochi, Interleukin-10 inhibits tumor necrosis factor-alpha production in lipopolysaccharide-stimulated RAW 264.7 cells through reduced MyD88 expression, Innate Immun 14(2) (2008) 109-15.

[193] D.E. Soranno, H.D. Lu, H.M. Weber, R. Rai, J.A. Burdick, Immunotherapy with injectable hydrogels to treat obstructive nephropathy, J Biomed Mater Res A 102(7) (2014) 2173-80.

[194] D.E. Soranno, C.B. Rodell, C. Altmann, J. Duplantis, A. Andres-Hernando, J.A. Burdick, S. Faubel, Delivery of interleukin-10 via injectable hydrogels improves renal outcomes and reduces systemic inflammation following ischemic acute kidney injury in mice, Am J Physiol Renal Physiol 311(2) (2016) F362-72.

[195] M.J. van Amerongen, M.C. Harmsen, N. van Rooijen, A.H. Petersen, M.J. van Luyn, Macrophage depletion impairs wound healing and increases left ventricular remodeling after myocardial injury in mice, Am J Pathol 170(3) (2007) 818-29.

[196] T. Varga, R. Mounier, A. Horvath, S. Cuvellier, F. Dumont, S. Poliska, H. Ardjoune, G. Juban, L. Nagy, B. Chazaud, Highly Dynamic Transcriptional Signature of

Distinct Macrophage Subsets during Sterile Inflammation, Resolution, and Tissue Repair, The Journal of Immunology (2016).

[197] S. Gordon, A. Pluddemann, F. Martinez Estrada, Macrophage heterogeneity in tissues: phenotypic diversity and functions, Immunol Rev 262(1) (2014) 36-55.

[198] M.P. Domogalla, P.V. Rostan, V.K. Raker, K. Steinbrink, Tolerance through Education: How Tolerogenic Dendritic Cells Shape Immunity, Front Immunol 8 (2017) 1764.

[199] F. Geissmann, M.G. Manz, S. Jung, M.H. Sieweke, M. Merad, K. Ley, Development of monocytes, macrophages, and dendritic cells, Science 327(5966) (2010) 656-61.

[200] F. D'Acquisto, T. Crompton, CD3+CD4-CD8- (double negative) T cells: saviours or villains of the immune response?, Biochem Pharmacol 82(4) (2011) 333-40.

[201] E.A. Phelps, N.O. Enemchukwu, V.F. Fiore, J.C. Sy, N. Murthy, T.A. Sulchek, T.H. Barker, A.J. Garcia, Maleimide cross-linked bioactive PEG hydrogel exhibits improved reaction kinetics and cross-linking for cell encapsulation and in situ delivery, Adv Mater 24(1) (2012) 64-70, 2.

[202] N. Jetten, S. Verbruggen, M.J. Gijbels, M.J. Post, M.P. De Winther, M.M. Donners, Anti-inflammatory M2, but not pro-inflammatory M1 macrophages promote angiogenesis in vivo, Angiogenesis 17(1) (2014) 109-18.

[203] P.J. Murray, J.E. Allen, S.K. Biswas, E.A. Fisher, D.W. Gilroy, S. Goerdt, S. Gordon, J.A. Hamilton, L.B. Ivashkiv, T. Lawrence, M. Locati, A. Mantovani, F.O. Martinez, J.L. Mege, D.M. Mosser, G. Natoli, J.P. Saeij, J.L. Schultze, K.A. Shirey, A. Sica, J. Suttles, I. Udalova, J.A. van Ginderachter, S.N. Vogel, T.A. Wynn, Macrophage activation and polarization: nomenclature and experimental guidelines, Immunity 41(1) (2014) 14-20.

[204] E.H. Choo, J.H. Lee, E.H. Park, H.E. Park, N.C. Jung, T.H. Kim, Y.S. Koh, E. Kim, K.B. Seung, C. Park, K.S. Hong, K. Kang, J.Y. Song, H.G. Seo, D.S. Lim, K. Chang, Infarcted Myocardium-Primed Dendritic Cells Improve Remodeling and Cardiac Function After Myocardial Infarction by Modulating the Regulatory T Cell and Macrophage Polarization, Circulation 135(15) (2017) 1444-1457.

[205] S. Reinke, S. Geissler, W.R. Taylor, K. Schmidt-Bleek, K. Juelke, V. Schwachmeyer, M. Dahne, T. Hartwig, L. Akyuz, C. Meisel, N. Unterwalder, N.B. Singh, P. Reinke, N.P. Haas, H.D. Volk, G.N. Duda, Terminally differentiated CD8(+) T cells negatively affect bone regeneration in humans, Sci Transl Med 5(177) (2013) 177ra36.

[206] F.R. D'Alessio, K. Tsushima, N.R. Aggarwal, E.E. West, M.H. Willett, M.F. Britos, M.R. Pipeling, R.G. Brower, R.M. Tuder, J.F. McDyer, L.S. King,

CD4+CD25+Foxp3+ Tregs resolve experimental lung injury in mice and are present in humans with acute lung injury, J Clin Invest 119(10) (2009) 2898-913.

[207] J. Li, J. Tan, M.M. Martino, K.O. Lui, Regulatory T-Cells: Potential Regulator of Tissue Repair and Regeneration, Front Immunol 9 (2018) 585.

[208] Y. Takeda, S. Costa, E. Delamarre, C. Roncal, R. Leite de Oliveira, M.L. Squadrito, V. Finisguerra, S. Deschoemaeker, F. Bruyere, M. Wenes, A. Hamm, J. Serneels, J. Magat, T. Bhattacharyya, A. Anisimov, B.F. Jordan, K. Alitalo, P. Maxwell, B. Gallez, Z.W. Zhuang, Y. Saito, M. Simons, M. De Palma, M. Mazzone, Macrophage skewing by Phd2 haplodeficiency prevents ischaemia by inducing arteriogenesis, Nature 479(7371) (2011) 122-6.

[209] A. Hamm, L. Veschini, Y. Takeda, S. Costa, E. Delamarre, M.L. Squadrito, A.T. Henze, M. Wenes, J. Serneels, F. Pucci, C. Roncal, A. Anisimov, K. Alitalo, M. De Palma, M. Mazzone, PHD2 regulates arteriogenic macrophages through TIE2 signalling, EMBO Mol Med 5(6) (2013) 843-57.

[210] E. Fung, A. Helisch, Macrophages in collateral arteriogenesis, Front Physiol 3 (2012) 353.

[211] C.E. Bergmann, I.E. Hoefer, B. Meder, H. Roth, N. van Royen, S.M. Breit, M.M. Jost, S. Aharinejad, S. Hartmann, I.R. Buschmann, Arteriogenesis depends on circulating monocytes and macrophage accumulation and is severely depressed in op/op mice, J Leukoc Biol 80(1) (2006) 59-65.

[212] R. Bootun, Effects of immunosuppressive therapy on wound healing, Int Wound J 10(1) (2013) 98-104.

[213] H. Li, B. Shi, Tolerogenic dendritic cells and their applications in transplantation, Cell Mol Immunol 12(1) (2015) 24-30.

[214] P.T. Walsh, D.K. Taylor, L.A. Turka, Tregs and transplantation tolerance, J Clin Invest 114(10) (2004) 1398-403.

[215] B.E. Burrell, Y. Nakayama, J. Xu, C.C. Brinkman, J.S. Bromberg, Regulatory T cell induction, migration, and function in transplantation, J Immunol 189(10) (2012) 4705-11.

[216] N. Romani, B.E. Clausen, P. Stoitzner, Langerhans cells and more: langerin-expressing dendritic cell subsets in the skin, Immunol Rev 234(1) (2010) 120-41.

[217] A.B. Adams, M.L. Ford, C.P. Larsen, Costimulation Blockade in Autoimmunity and Transplantation: The CD28 Pathway, J Immunol 197(6) (2016) 2045-50.

[218] K.R. Garrod, M.D. Cahalan, Murine skin transplantation, J Vis Exp (11) (2008).

[219] I. Kieran, A. Knock, J. Bush, K. So, A. Metcalfe, R. Hobson, T. Mason, S. O'Kane, M. Ferguson, Interleukin-10 reduces scar formation in both animal and human cutaneous wounds: results of two preclinical and phase II randomized control studies, Wound Repair Regen 21(3) (2013) 428-36.

[220] L. Dunn, H.C. Prosser, J.T. Tan, L.Z. Vanags, M.K. Ng, C.A. Bursill, Murine model of wound healing, J Vis Exp (75) (2013) e50265.

[221] S. Nassiri, I. Zakeri, M.S. Weingarten, K.L. Spiller, Relative Expression of Proinflammatory and Antiinflammatory Genes Reveals Differences between Healing and Nonhealing Human Chronic Diabetic Foot Ulcers, J Invest Dermatol 135(6) (2015) 1700-3.

[222] A. Schmidt, X.M. Zhang, R.N. Joshi, S. Iqbal, C. Wahlund, S. Gabrielsson, R.A. Harris, J. Tegner, Human macrophages induce CD4(+)Foxp3(+) regulatory T cells via binding and re-release of TGF-beta, Immunol Cell Biol 94(8) (2016) 747-62.

[223] F. Kryczanowsky, V. Raker, E. Graulich, M.P. Domogalla, K. Steinbrink, IL-10-Modulated Human Dendritic Cells for Clinical Use: Identification of a Stable and Migratory Subset with Improved Tolerogenic Activity, J Immunol 197(9) (2016) 3607-3617.

[224] V.K. Raker, M.P. Domogalla, K. Steinbrink, Tolerogenic Dendritic Cells for Regulatory T Cell Induction in Man, Front Immunol 6 (2015) 569.

[225] Q. Tang, J.A. Bluestone, Regulatory T-cell therapy in transplantation: moving to the clinic, Cold Spring Harb Perspect Med 3(11) (2013).

[226] Q. Tang, K. Lee, Regulatory T-cell therapy for transplantation: how many cells do we need?, Curr Opin Organ Transplant 17(4) (2012) 349-54.

[227] Q. Tang, J.A. Bluestone, S.M. Kang, CD4(+)Foxp3(+) regulatory T cell therapy in transplantation, J Mol Cell Biol 4(1) (2012) 11-21.

[228] I. Puig-Pey, F. Bohne, C. Benitez, M. Lopez, M. Martinez-Llordella, F. Oppenheimer, J.J. Lozano, J. Gonzalez-Abraldes, G. Tisone, A. Rimola, A. Sanchez-Fueyo, Characterization of gammadelta T cell subsets in organ transplantation, Transpl Int 23(10) (2010) 1045-55.

[229] A.N. Barnett, V.G. Hadjianastassiou, N. Mamode, Rituximab in renal transplantation, Transpl Int 26(6) (2013) 563-75.